HAL
open science

# Thermochemical treatment and Spectro-electrochemical characterization of electrodes used in pilot scale vanadium redox flow battery

Ali Hassan

## To cite this version:

Ali Hassan. Thermochemical treatment and Spectro-electrochemical characterization of electrodes used in pilot scale vanadium redox flow battery. Chemical engineering. Université Paul Sabatier - Toulouse III, 2020. English. NNT : 2020TOU30144 . tel-03160698

**HAL Id: tel-03160698**

**https://theses.hal.science/tel-03160698v1**

Submitted on 5 Mar 2021

**HAL** is a multi-disciplinary open access archive for the deposit and dissemination of scientific research documents, whether they are published or not. The documents may come from teaching and research institutions in France or abroad, or from public or private research centers.

L'archive ouverte pluridisciplinaire **HAL**, est destinée au dépôt et à la diffusion de documents scientifiques de niveau recherche, publiés ou non, émanant des établissements d'enseignement et de recherche français ou étrangers, des laboratoires publics ou privés.

# THÈSE

**En vue de l'obtention du**

## DOCTORAT DE L'UNIVERSITÉ DE TOULOUSE

**Délivré par l'Université Toulouse 3 - Paul Sabatier**

---

**Présentée et soutenue par**

**Ali HASSAN**

Le 30 novembre 2020

# Traitement thermochimique et caractérisation spectro-électrochimique des électrodes en feutre de carbone, utilisées dans des cellules pilote d'une batterie à circulation 'tout vanadium'

---

Ecole doctorale : **MEGEP - Mécanique, Energétique, Génie civil, Procédés**

Spécialité : **Génie des Procédés et de l'Environnement**

Unité de recherche :
**LGC - Laboratoire de Génie Chimique**

Thèse dirigée par
**Théo TZEDAKIS**

Jury
**Mme Florence GENESTE,** Rapporteure
**Mme Christine CACHET-VIVIER,** Rapporteure
**M. Philippe BARBOUX,** Examinateur
**M. Pierre CHAMELOT,** Examinateur
**M. Théo TZEDAKIS,** Directeur de thèse

# *Table of Contents*

**Abstract (English)** ..... **1**
**Abstract (French)** ..... **3**
**General introduction** ..... **5**

***Chapter. 1: Bibliography*** ..... ***9***

1.1. Renewable energy resources and importance of storage resources ..... 11
1.2 Why redox flow batteries ..... 18
1.2.1 Iron chromium redox flow battery ..... 20
1.2.2 Bromine/Polysulphide redox flow battery ..... 20
1.2.3 Vanadium/$Br_2$ flow batteries. ..... 21
1.2.4 Zn/bromine redox flow battery (hybrid flow battery) ..... 21
1.2.5 Zinc/cerium non aqueous redox flow battery (non-aqueous). ..... 22
1.2.6 Vanadium/cerium redox flow battery. (non-aqueous) ..... 22
1.3. Why all Vanadium redox flow ..... 23
1.4 Challenges associated with the VRFBs ..... 24
1.4.1 Membranes ..... 25
1.4.2 Electrolytes ..... 26
1.4.3 Electrodes ..... 27
1.4.3.1 Thermal treatments ..... 29
1.4.3.2 Chemical treatments ..... 31
1.4.3.3 Metal doping ..... 33
1.4.3.4 Electrochemical treatments ..... 36
1.5 Conclusion ..... 38

***Chapter:2 Enhancement of the electrochemical activity of a commercial graphite felt for vanadium redox flow battery (VRFB), by chemical treatment with acidic solution of $K_2Cr_2O_7$.*** ..... ***41***

2.1 Introduction ..... 44
2.2. Experimental ..... 45
2.2.1 Materials and chemicals ..... 45
2.2.2 Electrode activation ..... 46
2.2.3 Electrode characterization ..... 46
2.2.4 Half-cell evaluations ..... 48
2.3 Results and discussions ..... 49
2.3.1 Cyclic voltammetry (CV) and optimization of treatment parameters ..... 49
2.3.1.1 Effect of the temperature during activation with $K_2Cr_2O_7$ solution ..... 51
2.3.1.2 Effect of the time during activation with $K_2Cr_2O_7$ solution ..... 52
2.3.1.3 Effect of duration at the temperature of 140 °C ..... 53
2.3.1.4 Best performing electrode ..... 54
2.3.2 Linear sweep voltammetry (LSV) ..... 56
2.3.3 Surface characterization ..... 58
2.3.3.1 *Scanning electron microscopy (SEM)* ..... 58
2.3.3.2 Fourier-transform infrared spectroscopy (FTIR) ..... 60
2.3.3.3 Surface analysis by linear sweep voltammetry (LSV ..... 61
2.3.4 Determination of Adsorption sites. ..... 62
2.3.5 Wettability test ..... 65
2.3.6 Half-cell evaluation ..... 68
2.4. Conclusion ..... 73

**Chapter:3** ***Activation of the electrode for vanadium redox flow battery (VRFB) by electrochemical treatment, chemical treatment and particle doping.*** ..... **75**

3.1 Methods ..... 79
3.1.1 Cyclic voltammetry ..... 79
3.1.2 Linear sweep voltammetry ..... 79
3.1.3 Fourier transform infrared spectroscopy (FTIR): ..... 79
3.1.4 Scanning electron microscopy (SEM): ..... 79
3.1.5 Classical H-shaped half-cell ..... 80
3.1.6 Pilot scale electrochemical reactor ..... 80
3.2 Results and discussion ..... 83
3.2.1 Activation of the electrode by the $H_3PO_4$ ..... 83
3.2.2 Activation of the electrode by KOH ..... 85
3.2.3 Activation of the electrode by an electrochemical treatment with $(NH_4)_2CO_3$ ..... 90
3.2.4 Activation of the electrode with potassium permanganate ..... 92
3.2.5 Linear sweep voltammetry (LSV) for $k^o$ calculations ..... 97
3.2.6 FTIR and SEM analysis ..... 98
3.2.7 Surface free energy quantification of electrode ..... 100
3.2.8 Charge-Discharge cycles ..... 102
3.3 Conclusion ..... 107

***Chapter: 4 Comparative study of the role of $sp^3$ hybridization and different oxygenal groups on the graphite felt electrodes, towards positive half-cell redox couple in vanadium redox flow batteries .... 109***

4.1 Introduction ..... 112
4.2. Principle of plane wave density functional theory calculations (DFT) ..... 113
4.3. Methods ..... 118
4.4 Results and discussion ..... 120
4.4.1 Interaction of the V(IV) with modified electrode surfaces ..... 125
4.4.2 Interaction of the V(V) with modified electrode surfaces ..... 127
4.4.3 Interaction of the $H_2O$ with modified electrode surfaces ..... 129
4.4.4 Correlation between "$sp^3$ hybridization ⇌ oxygenal groups ⇌ $VO^{2+}/VO_2^+$ affinity with electrode" ..... 131
4.5 Conclusion ..... 134

**5. Conclusion and future perspective. ..... 135**

**6. List of publications ..... 142**

**7. References. ..... 143**

# *Abstract of thesis (English)*

Increase of the share of renewable energy in the overall power production can ensure the future energy demand and help to cope with the environmental challenges inherent to the carbon enrich fossil fuels. Due to intermittent nature of these renewable resources, cost competitive and efficient energy storage devices are required. Vanadium redox flow batteries (VRFBs) are promising storage devices for the stationary applications due to its easy scalability, long charge-discharge cycles. The graphite and the graphite felt are low cost electrodes materials used by VRFBs which exhibits low kinetic reversibility of the redox reaction involving the system $V^{(V)}/V^{(IV)}$ in the positive half-cell; this fact is responsible of significant kinetics overpotential decreasing the delivered voltage from the battery.

In this work, different methods (chemical, thermal, electrochemical,) were tried to activate the surface of commercial graphite, expecting to enhance its electro-kinetics activity, specifically for the positive half-cell reaction ($VO^{2+} \rightleftharpoons VO_2^{+}$). The enhancement of the electro kinetic activity of the electrode surface was characterized by the cyclic and linear sweep voltammetry. Besides the surface chemistry and morphology were analysed by the Fourier-transform infrared spectroscopy (FTIR) and *Scanning electron microscopy (SEM).* In another study, the electrode-electrolyte interaction was quantified by contact angle measurements allowing access to the surface free energy determination.

The activation method enables to create different oxygenal groups (C-OH, C=O -COOH) on the graphite surface and to increase the surface area. Both effects lead to i) the increase by 35 % of the current magnitude of the peak obtained by cyclic voltammetry (for the system $VO^{2+}/VO_2^{+}$) and ii) the decrease of the $\Delta E_{peaks}$ of the same system by 300 mV. The density functional theory calculations (DFT) were performed to evaluate the individual catalytic role of the these oxygenal

groups against the redox couple $VO^{2+}/VO_2^{+}$(in the positive electrode). DFT shows that these oxygenal groups increase $sp^3$ hybridization in the structure of the felt, that are facilitating the redox reactions.

The intrinsic heterogeneous electronic transfer constant ($k°$) of $V^{(V)}/V^{(IV)}$ system is enhanced by 2.6 and 6.1 times for the oxidation ($V^{(IV)}\rightarrow V^{(V)}$) and reduction ($V^{(V)}\rightarrow V^{(IV)}$) reactions, respectively. The electrode-electrolyte interaction improves because of the increment of the surface free energy of GF from 13.9 mN/m to 53.29 mN/m. The electrode performance was evaluated in the classical half-cell by charge discharge cycles. The charging voltage decrease from 1.18V to 1.04V and the discharge voltage increase from 0.42V to 0.75V, after the activation of GF.

Proposed activation methods are novel, easy and effective. The charge discharge cycles of VRFB were performed at stack level, into the electrochemical plug flow reactor, by using 100 $cm^2$ GF in each electrolytic section. At a current density of **50** $A.m^{-2}$, there is an improvement of 20 % and 13 % in energy and voltage efficiency (VE) of stack respectively, due to treated electrode.

# *Résumé de la thèse (français)*

La demande croissante d'énergie au niveau mondial fait que les énergies obtenues de ressources renouvelables connaissent un essor important, notamment dans la production globale d'électricité propre (ne générant pas des gaz à effet de serre, tels les combustibles fossiles enrichis en carbone). La nature 'intermittente' de ces ressources renouvelables d'énergie implique l'utilisation des dispositifs de stockage de grande échelle, efficaces et économiquement compétitifs.

Les batteries à circulation, tout vanadium (VRFB) sont des dispositifs de stockage prometteurs pour les applications stationnaires. En effet, l'absence de contamination irréversible de l'électrolyte est l'avantage principal de cette batterie dont le nombre de cycles 'charge-décharge' est théoriquement illimité.

Le graphite et le feutre de graphite sont des matériaux d'électrodes à faible coût utilisés par les VRFB ; cependant le système $V^{(V)}/V^{(IV)}$ (électrode positive) est cinétiquement lent sur ce matériau et introduit une surtension diminuant la tension délivrée par la batterie. Différentes méthodes (chimiques, thermiques, électrochimiques,…) ont été conçues lors de cette thèse pour activer la surface du graphite commercial, càd. améliorer son activité électrocatalytique vis-à-vis de la réaction ($VO^{2+} \rightleftharpoons VO_2^+$) ayant lieu à l'électrode positive. Cette amélioration a été caractérisée par voltammétrie linéaire (état quasi-stationnaire) et cyclique (état transitoire). En outre, la morphologie de l'électrode et son état de surface ont été analysés par infrarouge à transformée de Fourier (FTIR) et par microscopie électronique à balayage (SEM). De plus, l'interaction électrode-électrolyte a été quantifiée par des mesures d'angle de contact qui ont permis de déterminer l'énergie libre de surface.

L'activation de l'électrode a généré différents groupes oxygénés (C-OH, C = O, COOH) sur sa surface, laquelle a par ailleurs augmenté du fait d'une certaine érosion et donc la création d'une rugosité ; ceci s'est traduit par : i) l'augmentation de 35% de l'amplitude du courant du pic obtenu par voltamétrie cyclique (pour le système $VO^{2+}/VO_2^{+}$) et ii) le rapprochement des pics anodique et cathodique ($\Delta E_{pics}$= 300 mV). Les calculs de la théorie fonctionnelle de la densité (DFT) ont été effectués pour évaluer le rôle de ces groupes oxygénés sur la réactivité du système redox $VO^{2+}/VO_2^{+}$(à l'électrode positive). DFT montre que ces groupes d'oxygéne augmente l'hybridation sp3 dans la structure du graphite, ce qui facilite les réactions redox.

La constante de transfert électronique hétérogène intrinsèque (k °) de ce même système redox a augmentée de 2,6 et 6,1 fois pour l'oxydation ($V^{(IV)} \rightarrow V^{(V)}$) et la réduction ($V^{(V)} \rightarrow V^{(IV)}$), respectivement. Par ailleurs l'augmentation constatée de l'énergie libre de surface du feutre de graphite (de 13,9 mN / m à 53,29 mN / m) traduit l'amélioration, par le traitement, des interactions électrode-électrolyte. La performance de l'électrode a été évaluée dans une demi-cellule classique par des cycles de charge/décharge et les résultats ont montré que la tension aux bornes durant la charge diminue (de 1,18 V à 1,04 V) alors que celle obtenue en décharge augmente (de 0,42 V à 0,75 V), après l'activation de GF.

Des cycles charge/décharge ont également été réalisés avec un réacteur électrochimique filtre presse (pile et électrolyseur pour VRFB), ayant une surface géométrique de 100 $cm^2$ de GF dans chaque compartiment électrolytique.

Grace au traitement effectué, le rendement énergétique et la tension aux bornes se sont améliorés de 20% et 13% respectivement, dans le cas d'une électrolyse en mode galvanostatique (50 $A.m^2$), ce qui montre que les méthodes d'activation proposées sont efficaces et en outre faciles à mettre en œuvre.

# *General introduction*

Energy storage devices are an important part of the supply chain of the power energy market. The life cycle, efficiency , maintenance, capital cost are main characteristics of the energy storage systems. The selection of the energy system depends upon the nature of the application, for which it is deployed. Electrochemical energy storage devices are widely used for multiple applications such as energy management, power quality, load leveling and peak shaving. Lead acid, lithium ion, Nickel-cadmium and flow batteries etc. are some examples of electrochemical storage systems. Flow batteries has fundamental advantage over other conventional systems, because of their unique characteristics of detached energy density and power density.

Many flow batteries have been investigated in last few decades such as, vanadium flow battery, Bromine-Polysulphide, Vanadium-$Br_2$, Zinc-cerium and iron-chromium flow battery. Due to long life cycles and stability of the electrolyte, VRFBs are the most mature technologies. This is because of the unique property of the vanadium, that it is available in four different valencies. But there are still multiples challenges associated with it, such as cost of vanadium, toxicity and low solubility. These issues must need to be fixed to make it the cost competitive and viable option.

The stack of the VRFBs, like any other flow battery, is constituted by the electrodes, membrane, current collectors and electrolytes. All the individual components of the stack contribute in the overall ohmic losses of the stack, and consequently influence the overall efficiency of VRFBs. The electrodes are critical component in VRFBs, because the power density of stack depends on it. In addition to that, the electrodes conditioned the overall size of the stack, thus their selection, mainly conditioned by their electro-kinetic activity, is an important factor in the

optimization of the stack. The graphite felt is widely used electrode material in flow batteries, because it is stable in acidic condition, cheap and possess high surface area. However, it shows high kinetic polarization and could also induce electronic ohmic losses; so, it is necessary to activate it before using in the stack.

The effective and facile methods of surface treatment of the graphite felt are studied in this thesis, expecting to use the GF as the positive electrode in the VRFBs. The experiments and calculations will be performed at multiple scale, ranging from molecular to lab pilot level. The brief introduction of each chapter is as follows;

**Chapter 1** presents bibliography and data analysis. In its initial part, the importance of the energy storage devices is discussed in the realm of today power market and its environmental aspects. Then the advantages of the redox flow batteries, more specifically the all vanadium redox flow batteries, are analyzed over other convectional energy devices, and a critical study of multiple challenges associated with all the components of VRFBs was performed and pointed out the low electroactivity of the electrode against the reactions in the posolyte. The detailed bibliography was done regarding the electrode modification for VRFBs, and subsequently defined the scope of thesis

**Chapter 2** contains the first experimental study done. A new activation method is proposed to activate the graphite felt with acidic $K_2Cr_2O_7$ solution, and the optimized parameters of operational conditions are defined for this method. Initial determination of the electrode electroactivity was done by the cyclic and linear sweep voltammetry. Then the performance of the treated electrode was evaluated in a classical half-cell, containing positive electrolyte ($V^{(IV)/}V^{(V)}$), by charge-discharge electrolysis. To investigate the reason behind the improved

performance, that surface characterization was performed with the help of FTIR, SEM, contact angles measurements.

In **Chapter 3** , the GF was tried to activate with different approaches. The objective is to explore multiple options that can provide more effective way to activate the GF for VRFBs, in taking consideration of effectiveness and easiness of the treatments. Activation of GF by electrochemical oxidation was performed in the $(NH_4)_2CO_3$. Moreover, the $KMnO_4$ derived particle are deposited on GF to explore their catalytic ability, against ($V^{(IV)} \rightleftharpoons V^{(V)}$) reaction. The solutions of the phosphoric acid, potassium hydroxide and potassium permanganate are also investigated for GF activation. The electroactivity of the activated GF is evaluated in the pilot scale electrochemical reactor, by charge discharge cycles.

In **chapter 4,** Plane wave density functional theory calculation (DFT) are performed to investigate the reason of the improvement in the electrode kinetic electroactivity. DFT calculations give the insight of the phenomena on the molecular level and can help in exploring the roles of different functional groups of the electrode surface. The software GPAW is used for setting up these simulations. Projected density of states spectra is also analyzed to explore the effect of surface morphological changes, in the electrode activation.

In end, the ***conclusion and the future perspective*** of the theses is briefly discussed

# ***Chapter. 1: Bibliography***

## Chapter. 1: Bibliography

### 1.1. Renewable energy resources and importance of storage resources

Due to industrial growth and modern living lifestyle, the worlds demand of the energy is increasing. In the year of 2018, the increment rate of electricity consumption increase by 2.18 % [1]. Major base load of this demand is coming from the fossil fuel power plants, that are very carbon enriched. The emissions of greenhouse gases ($CO_2$, $NO_x$) from these power plants are inducing serious environmental challenges and disturbing the ecological balance. After industrial revolution until now, the concentration of the $CO_2$ increased up to 47 % in the atmosphere [2]. In EU, the 75 % of greenhouses gases are coming from the energy sector [3]. On the other hand, the depletion of fossil fuels also poses serious question to sustainable meet of huge demand of energy, in the long term. The policy makers, engineers and technologists are extensively looking into different possibilities and alternative energy resources; that can add up magnificent junk of energy into existing installed capacity. Main aspects of all this research that alternatives resources must be environmentally friendly, economical viable and sustainable.

There is huge potential of extraction of the power from the renewable energy resources, specially from wind and solar energy. In future, these resources can arise as fundament key drivers to drift the high carbon economy towards low carbon economy, if underlying technological challenges will be resolved. The European union (EU), USA and china are extensively enhancing the installed energy capacity from wind and solar power sources. For instance, in the year of 2018, the power production in European union (EU) from the solar energy via photovoltaic cells were 3.9 % (127 TWh) of total electricity production, and this sector is providing almost 175000 jobs [4]. For future, the EU set the ambitious targets for

getting 32 % of total energy demand from renewable energy until 2030 and subsequently to reach the stage of complete carbon neutrality before 2050. Big milestone was achieved in the history of EU in the year of 2019, that the power generation from solar and wind energy exceed the power generation from the coal fired plants. The evolution of the renewable energy resources in the EU is shown in the fig A.1. Globally, in the year of 2019, the overall share of the renewable energies in the power production is 10.4 % . But coal is still largest producing the largest junk of the electricity, tough the production decreased by 270 TWh.[5]

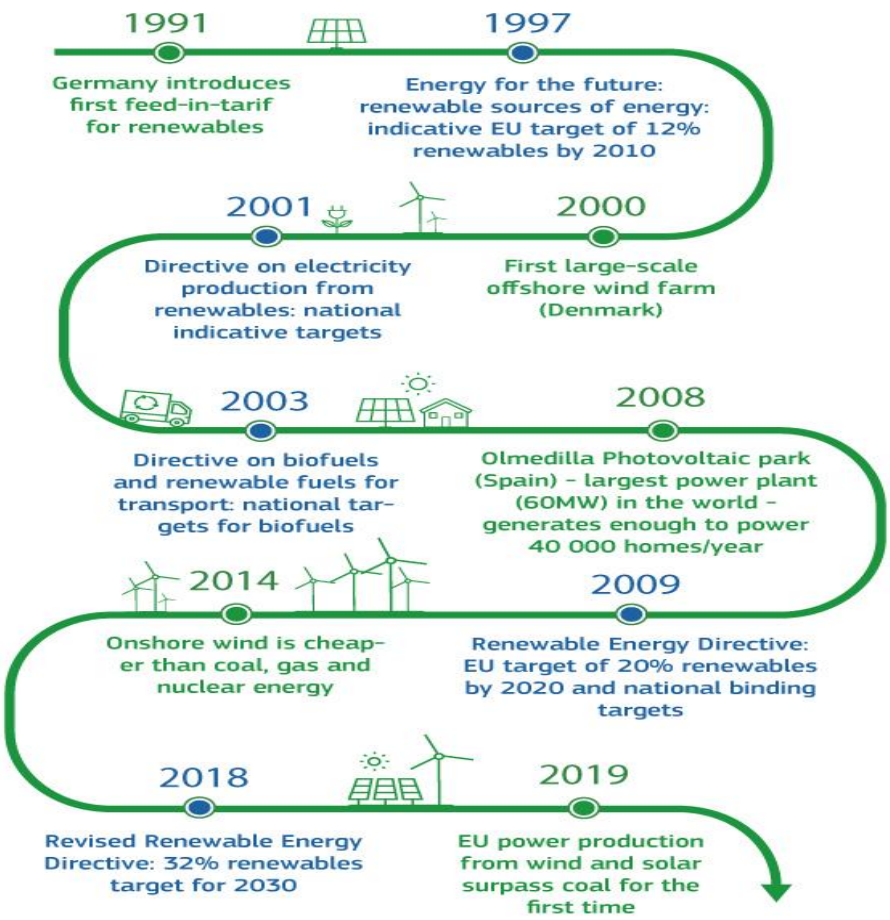


***Fig A.1.*** *The evolution of the renewable energies in the EU (Fig extracted from the reference [3]*

The present infrastructure of the grid system was designed based on resources that generates consistent power, such as coal/gas fired power plants, dams and nuclear power plants etc. As the peak loads are known, so the sudden surges in demand are shaved offed by the dispatchable power generations. The renewable energy such as the solar and wind energy is the intermittent in nature and to increase the share of these resources in energy mix, the smart grid systems are required that can handle the fluctuation in the power generation; and this is possible by installing the relevant energy storage systems. The quality of power is also an import factor, for the power distribution companies. The end users have sophisticated electronic devices, and these are sensitive to the power quality. The energy storage systems can also ensure the quality of the power, during the short duration disturbances in the grid. In addition to that, the frequency regulation to the set condition are also controlled by energy storage systems. The frequency fluctuation is caused by the variable power generation from renewable and changing power load on grid system.

Above mentioned characteristics (grid fluctuation, power quality, frequency regulation) are the grid related issues caused by the variable load/power generations, and important to sort out; but more important factor to increase the share of renewables, is the sustainable power supply from these sources, and to aligned it with power demand. The energy storage devices can ensure the consistency by the load leveling and peak shaving. For instance, the energy can be stored as backup during the peak timings of the sunshine and high wind speed, and this energy could be used to shave off the peak loads in the time of high energy demand. In that way, the storage system brings the more control in the power dispatchment (align with the loads) and make the renewable power generation predicable and market able.

For the time being in European union (EU), the total storage capacity is approximately 5 % of the total power production. Almost similar tread of energy storage is observed globally. The storage energy systems thematically divided into following groups, based on the form of the energy they stored;

1. Mechanical energy storage system ( Flywheel; Pumped hydro etc.)

2- Electrochemical energy storage system ( Li ions battery, lead acid batteries, Flow batteries )

3- Electrical energy storage system ( Supercapacitors)

4- Chemical energy storage system (Fuel cells)

5- Thermal energy storage system

The storage system must meet the following criteria; 1) economical, 2) efficient, 3) low maintenance cost, 4) durable, 5) withstand weather conditions, 6) environmentally friendly; so that the overall supply chain of the power generation remains cost competitive. The choice of suitable energy storage depends upon the application, for which it will be installed. The large-scale application requires the systems, having high energy capacity and discharge time. For example, the compressed air and pumped hydro storage systems can store > 100 MW and their discharge time scale lies between hours and days. The applications like power quality and frequency regulation in the smart grid application usually require the fast response and high specific power. The flywheel and supercapacitor are quite relevant choice in this regard. The response time of both devices are within the seconds., while the specific power varies between the 1000 W/Kg-2000 W/kg. [6,7] The electrochemical devices, such a Lion ion battery, lead-acid battery, fuel cells and metal air battery have the intermediate properties of the both large scale and small-scale storage devices. The power rating of these devices can be increased or decreased by adding/removing the unit cells installed. So, these systems can be used for multiple

application such as bulk energy management, power quality, frequency regulation, load leveling and peak shaving.

Currently, major part of this storage capacity is comprised of the pumped hydro systems . The water is pumped towards the reservoirs at high place and energy is stored in the form of potential energy. On the time of requirement, this water is passed through tunnels and turbine, to convert potential energy into the electricity. In the year of 2017, the energy stored in the pumped hydro systems was 153 GW, while total storage capacity was 159 GW. Rest 4 % of storage capacity lies in the "energy storage systems", as shown in fig A.2. It indicates that other techniques are not matured enough "technically" or "economically", that can be able to handle large scale energy storage, derived from the renewable resources.

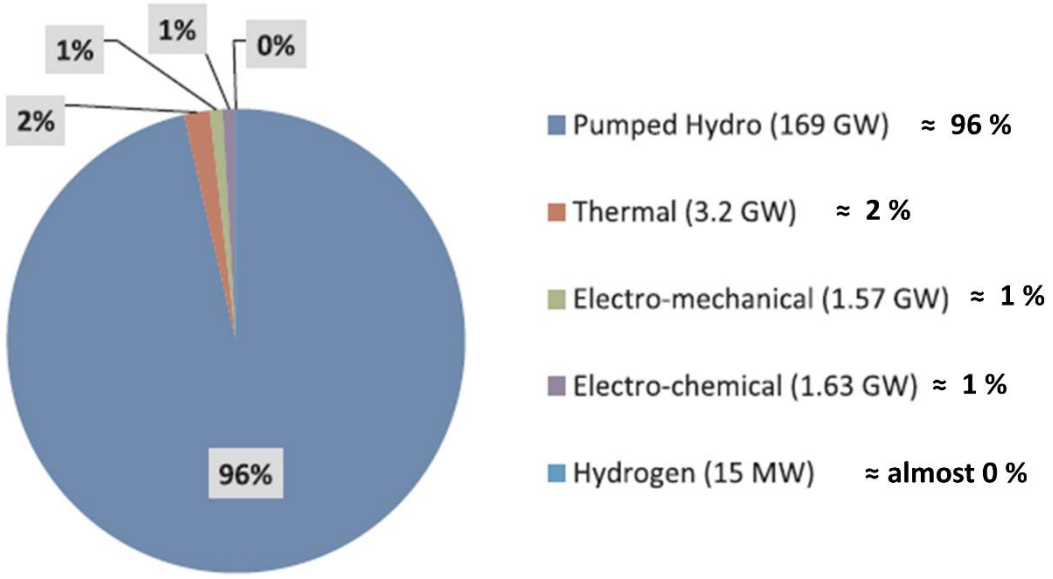


***Fig A. 2****.The percentage share of different energy storage system worldwide (Fig extracted from [7]*

Pumped hydro systems are very dependent on the specific high sites, on which the water reservoirs can be built. Also, these reservoirs capture a lot of the land and not good for the biodiversity. The storage devices should be near to grid station or near the power generation facility to have more distributive grid stations, while the site dependent storage systems pave ways to more centralized systems.

So, the electrochemical energy storage devices are most relevant choice in this regard and could be easily installed next to power generation sites. Different batteries have different pros and cons. For example, Lithium-ion batteries has been successfully commercialized since 1991. These batteries are extensively used into the mobiles, laptops and similar electronic applications. Due to fast response time (< 5 ms), it can also be used for the power quality maintenance. These batteries are also in focus for the mobility application such as hybrid/electric vehicles, due to its high specific energy ( $75 < E_{(W\ h/Kg)} < 200$) and specific power ($0.5 < P_{(KW\ /Kg)} < 2$) [8]. The main disadvantage of lithium ion battery for its use in the renewable integration application, is its high cost. Due to the limited number of charge discharge cycles, the replacement of the devices also induce cost in the power supply. There are also associated risk of the heat up of the battery at high temperature, and it could lead to the explosion in the worst case; because the electrodes of the battery are relatively unstable at high temperature and emitting the oxygenal gases. The renewable energy sites, particularly solar plants, has high temperatures (35 $^{o}$C- 45 $^{o}$C) and any instant temperature rise in battery due to high charging or any fault like that could cause problems.

The lead acid batteries are another option, that are 5 times cheaper than the lithium ion batteries [9,10] ; it consists of the cathode and anode, made up of $PbO_2$ and Pb respectively. The rated

power could vary between 0 to 50 MW; and the discharge rate is in the time scale of seconds to hours. But lead batteries have certain drawback also. Number of charge -discharge cycles are low ( ≈2000), that are very important for large scale stationary applications. [8]. The low energy density (50-90 W h/Kg) is another limitation, that leads towards the problem of the space. The battery operates at lower efficiency at lower temperature; while there are the emissions of the hazardous gases at higher temperature. So the temperate control of these systems may require depending upon the environmental temperature [11]. Due to the lower energy density and lower number of cycles, lead acid battery is not feasible, neither in renewable integration nor in the vehicles. Nickel-cadmium battery is another option for the energy storage; but due to very toxic nature of cadmium, its use is strongly discouraged globally by the health and safety departments. The discarding or dumbing of these Ni-Cd batteries after finishing their lifecycle is also a big problem. There is strict restriction on its use by European union (EU) and it is completely prohibited for the consumer. The characteristics of the Ni-Cd battery is more or less the same like the lead acid batteries; but the price is 2-3 times higher than the lead acid batteries, ($1000/ [12]. These limitations are relatively less in sodium-Sulphur (NaS) batteries. These batteries contain the molten salt of the sulfur and sodium, as electrode and separated by the solid electrolyte of alumina. This battery operating temperature is around 325 $^{o}$C ± 25 $^{o}$ C to keep the salts in the molten form. The promising characteristic of these batteries are its high energy density ($150 < E_{W\,h/L} < 300$) and efficiency, that is around 85 %. The drawback associated with this, is to insure its high operating temperature, its high capital and operating costs [13].

The “electrolyzer- storage system-fuel cell” combinedly form the system to store the energy in chemical form and can convert this energy into the electricity, when provided. The electrolyzer use the electrical energy from renewable sources, to convert the water into the hydrogen and

oxygen. The hydrogen from electrolyzes is stored into the storage tank and can be converted back to electricity by fuel cell. The hydrogen and oxygen are continuously flowed into the fuel cell and reacted to give the electric power and heat. The energy density and the power density of fuel cells are very high ($500 < E_{Wh/L} < 3000$). The main drawback of the fuel cell is its very low efficiency (< 50%). The high capital and hydrogen storage cost, make this regenerative fuel cell system very expensive. [11,14]

## 1.2 Why redox flow batteries

The redox flow batteries are secondary storage devices that convert electrical energy into chemical energy while charging, and vice versa during discharging. The stack ( battery cell) consist of positive and negative half-cell, separated by anionic/cationic exchange membrane., as shown in fig A.3. Each half-cell contains the electrode, where the electrochemical reaction take place.

Two redox couples, having “reasonable” potential gap, are dissolved in the electrolyte stored in two different storage tanks. The electrolyte containing the redox couple with higher potential is called posolyte, while the electrolyte with the lower potential is the negolyte. In the discharge step, the reduction is occurred in the posolyte , while oxidation occur into negolyte. The storage tanks are physically separated from the cell stack.

The flow batteries have the distinguished characteristic to enables to detach energy and power densities, in contrary to conventional energy storage devices and batteries. The conventional batteries stored the electrical energy in the form of chemical energy, and chemical constitute the part of the electrode. So, the electrode is not only providing the base surface for the reaction and

electrode transfer, but also taking part in the reaction and undergoes physio-chemical changes in each charge discharge cycle. This phenomenon could lead towards the fast degradation of the electrodes. Also, the scalability of the conventional batteries is more complicated ; thus, to increase the energy storage capacity, another cell must be introduced. But in the case of flow batteries, the energy is stored outside of stack, in the electrode active material dissolved in the electrolyte. The quantity of dissolved electro-active material determines the energy density of

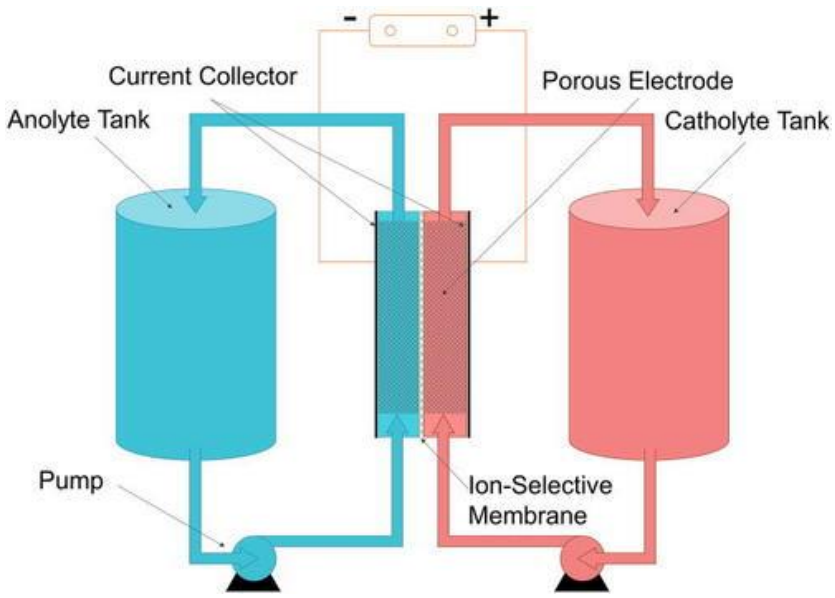


***Fig A.3.*** *The representative diagram of flow cell (fig extracted from the ref: [15])*

the flow cells. The redox reaction take place at the surface electrode during charge-discharge, and power density of the cell is solely depending upon the electrode surface area and its reversibility. So, both properties, “energy density” and “power density” are totally independent of each other. The energy storage capacity of cell could be easily increase by just increasing the storage tank capacity, without changing anything in the stack. Self-discharge of the storage devices is an important factor to be studied; and in case of flow batteries, it is relatively important and induces the need to periodically equilibrating electrolytes. Also, the maintenance of flow batteries is relatively easy. In following section, flow batteries are briefly discussed.

### *1.2.1 Iron chromium redox flow battery*

Iron chromium redox flow battery is the first invented battery, used by the NASA. The positive half-cell electrolyte contains the redox active specie $Fe^{2+}/Fe^{3+}$, while the negative half-cell constituted by the $Cr^{2+}/Cr^{3+}$. The following charge discharge cycles were occurring in both cells. Theocratical cell voltage of Fe-Cr is 1.18 V.

$$Fe^{3+} + e^- \rightleftharpoons Fe^{2+} \qquad E°_{(Fe^{2+}/Fe^{3+})} = +\ 0.77\ V\ vs\ SHE$$

$$Cr^{2+} + \rightleftharpoons Cr^{3+} + e^- \qquad E°_{(Cr^{2+}/cr^{3+})} = -\ 0.41\ V\ vs\ SHE$$

The capital cost Fe/Cr is relatively cheaper (almost 35 $ KW $h^{-1}$) than the vanadium redox flow battery [16]. The electroactivity of the positive half-cell reaction is much faster than the negative half-cell reaction. So, the negative electrode needs to be integrated with some catalyst to remove this limitation. [17–21]

### *1.2.2 Bromine/Polysulphide redox flow battery*

The redox flow reaction of the positive and negative half-cell reaction is as below;

$$3Br^- \rightleftharpoons Br_3^- + 2e^- \qquad E°_{(3Br^-/Br_3^-)} = +\ 1.09\ V\ vs\ SHE$$

$$2S_2^- \rightleftharpoons S_4^{2-} + 2e^- \qquad E°_{(2S_2^-/S_4^{2-})} = -\ 0.265\ V\ vs\ SHE$$

The anolyte is constituted by the X-Br and catholyte is comprised of the X-polysulphide. The charge exchange between both sections is maintained by the counter cation (X) exchange across the cation exchange membrane. The redox active materials are cheaper and have high solubility in the electrolyte. The drawback of this battery is the evolution of the $Br_2$ and $H_2S$ gases at the positive and negative half-cell electrolyte respectively. These gases have foul swell; In addition

to that, the Sulphur can be precipitated in the negative half-cell, leading towards the losses of the active redox species. The sulfur could possibly be agglomerated the fibrous electrode. [18]

### *1.2.3 Vanadium/$Br_2$ flow batteries.*

Vanadium-bromide batteries were introduced by university of new south wales (UNSW) in 2001. The energy density of the V-Br flow battery (35-70 Wh. $L^{-1}$) is almost double than the VRFBs (20-30 Wh. $L^{-1}$)[22].

$$Br_2^- \rightleftharpoons 2Br^- + 2e^- \qquad E^\circ_{(Br_2^-/2Br^-)} = 1.04\ V\ vs\ SHE$$

$$V^{3+} + e^- \rightleftharpoons V^{2+} \qquad E^\circ_{(V^{+2}/V^{+3})} = -0.26\ V\ vs\ SHE$$

The formation of the stench bromine vapors is the main drawback of this battery . This problem could be avoided by the adding different complexing agent in the electrolyte.[23]

### *1.2.4 Zn/bromine redox flow battery (hybrid flow battery).*

Hybrid flow batteries partially share the same characteristics of flow batteries, in which the electrolyte is continuously flowing from the stack, that is stored in the tank outside of stack. But in contrary to flow batteries, the electroactive material of one redox system is stored into the battery as metallic form. In the Zn/Br flow battery, the electrolyte used in both cells are solution of the $ZnBr_2$. In the negative half-cell, the Zn ions from the electrolyte is deposited on the electrode during charging and dissolved back to the electrolyte during discharging. The representative equations are shown below;

$$2Br^- \rightleftharpoons Br_2 + 2e^- \qquad E^\circ = +\ 1.09\ V\ vs\ SHE$$

$$Zn^{2+} + 2e^- \rightleftharpoons Zn \qquad E^\circ = -0.76\ V\ vs\ SHE$$

Though, the energy density of Zn-Br (70 Wh. $L^{-1}$) and OCV (1.8 V) is greater than the VRFBs [24].; but the adsorption of Zn on the electrode (usually graphite felt ) is complicated. Technically there are two different phenomena are involved in this reaction. One step is concerned the adsorption of Zn on the electrode and second step is the electron transfer. The Zn adsorption affinity are limited on the carbon electrodes; and its uniform adsorption on electrode is also questionable [25]

### *1.2.5 Zinc/cerium non aqueous redox flow battery (non-aqueous)*

The redox flow batteries mentioned before, are aqueous redox flow batteries. Different chemistries of non-aqueous redox flow batteries are also discussed by employing the electrolyte, that has wider potential window than water. For example, the Zn/Ce redox couple have the wide potential window gap with the OCP 2.51 V. The representative equations are as follow;

$$Ce^{3+} \rightleftharpoons Ce^{4+} + e^{-} \qquad E° = +1.28 - 1.76\ V\ vs\ SHE$$

$$Zn^{2+} + 2e^{-} \rightleftharpoons Zn \qquad E° = -0.76\ V\ vs\ SHE$$

Instead of water, the organic acid $CH_3SO_3H$ is used as the electrolyte. The low conductivity and its stability are main drawback of this flow battery. [26,27]

### *1.2.6 Vanadium/cerium redox flow battery. (non-aqueous)*

The V-Ce chemistry was proposed for flow batteries, in aqueous, as well as in non-aqueous phase. The theoretical voltage is also high as per following equations.

$$2Ce^{3+} \rightleftharpoons 2Ce^{4+} + 2e^{-} \qquad E° = +1.28 - 1.76\ V\ vs\ SHE$$

$$V^{3+} + e^{-} \rightleftharpoons V^{2+} \qquad E° = -0.26\ V\ vs\ SHE$$

The cell voltage in the aqueous sulphuric acids is high ( 1.8 V), in comparison with the VRFBs (1.26 V), but the solubility of Ce is less than 0.3 mole. $L^{-1}$ [28]. The low solubility of Ce limits the applicability of the Ce-V redox flow battery, despite of its high cell voltage. The solubility of the Ce is increased up to the 0.8 mole. $L^{-1}$ in the mixed organic media of methane sulfonic acid [29], In that way, the theoretical energy density of the V-Ce approaches to the 27.7 Wh $L^{-1}$. But the conductivity and stability of the organic acids is the main drawback.

### 1.3. Why all Vanadium redox flow

In all vanadium redox flow battery, the catholyte and anolyte both consist of the vanadium salt compounds. Vanadium element has unique property to exists in four difference valance states i-e "$V^{(II)}$, $V^{(III)}$, $V^{(IV)}$, $V^{(V)}$", having the required redox potentials to constitute the redox system, so that it can be used in the energy storage application. Prof Skyllas Kazacos from university of new south wales (UNSW) proposed the idea of all vanadium redox flow batteries. The V(II)/V(III) constitutes the negative couple, while the positive half-cell electrolyte contains the V(IV)/V(V) redox system. The respective reactions occurring in both half cells are as below;[30].

<u>Positive electrode</u>: $VO_2^+ + 2H^+ + e^- \rightleftharpoons VO^{2+} + H_2O$ $E°_{(VO^{2+}/VO_2^+)} = 1.00\ V$ *vs SHE;*

<u>Negative electrode:</u> $V^{3+} + e^- \rightleftharpoons V^{2+}$ $E°_{(V^{2+}/V^{3+})} = -0.26\ V$ *vs SHE;*

For the large-scale energy storage applications, the long-life cycles and stability of the electrolyte is important. The electrolyte is stable in the VRFBs, because the same metal ions is used in both half cells. Even if there is some cross contamination between both half cells with the time, there is not any need to change the electrolyte. The regeneration of the electrolyte can be obtained by providing the required charge to the battery at low constant current density. The VRFBs shows

the stable performance over large number of cycles (10000-14000), in comparison with the lithium ion batteries and lead acid batteries. [31].The vanadium redox flow battery has already been successfully commercialized in several countries for multiple application. In 2005, the 4 MW capacity plant was built at Hokkaido japan for storing the energy from wind power plant [22]. The China is building the world largest VRFBs energy storage system, in the wind power plant (Dalian China), having the capacity of the 200 MW [32]. The low energy density of the VRFBs limits its use in the mobile applications, and it is only considered for the stationary applications. As already explained, the lower energy density of flow batteries in the stationary applications could be compensated by increasing the volume of the electrolyte in the storage tanks.

## 1.4 Challenges associated with the VRFBs

There are multiple challenges associated with VRFBs to make it more viable option for stationary energy storage application [33] : 1) The ohmic resistance caused the membrane and the electrolytes. 2) the electronic resistance of the electrode (graphite felt in contact with massive graphite) 3) The cost of the individual components. 4) The kinetic polarization of the reactions on the electrode surface. 5) The mass transfer limitations due to internal geometry, flow rates and the concentration of the electrolyte (causing the pressure drop) [34]. All these factors influence the power density and cost of the stack and it is very important to optimize it [35]. By improving the power and energy densities, the size of the stack required, decreased and consequently all the internal elements (electrodes, membranes, current collectors etc) used are of smaller size. So, the overall cost of stack decrease, and efficiency of the overall VRFBs increased. The bibliographic review of tackling these challenges, related to important components of the stack (membranes, electrolyte and electrode), are as below.

### *1.4.1 Membranes*

Membranes are very important component of the VRFBs, enabling to avoid the cross mixing of both half-cell electrolytes, while allowing the protons transfer for the charge balance for the cationic membrane. It must possess the high mechanical and chemical stability at the variable flowing rates of acidic electrolytes. There are many fluoride and non-fluoride membranes, that are explored by the researchers, in the VRFBs application [36–45]. Among them, some membranes (cationic) enable the $H^+$ transfer, thanks to the $HSO_3^-$ functional groups grafted on the alkyl groups of the polymer. Some other membranes (anionic) allow the $OH^-$ transfer by surface migration via $NH_4^+$ functional groups grafted on the polymer.[45,46] There is the production of $H^+$ on the positive half-cell while charging and vice versa, so it is more general to use the cationic exchange membranes, to exchange $H^+$ ion. Nafion membrane are perfluorinated sulfonic acid cation exchange membranes, having good stability against acidic anolyte and catholyte of VRFBs; also, it ensures high permeability of protons to maintain the charge balance. But these membranes are expensive, and in addition they suffer from a significant permeability loss of the vanadium, causing the self-discharge of battery. [22,47]. To avoid the problems of the vanadium permeability, some researcher did modifications in nafion membranes: for instance, the nafion is successfully modified with polytetrafluoroethene (PTFE) and silica [48] . Qiu et al. modified the nafion membrance with impregnating multiple layers of polyelectrolyte polymers.[49] Similarly, the nafion is modified by $SiO_2$ [50], $TiO_2$ [51] to decrease the vanadium permeation and to increase the proton transfer. All the modified membranes were evaluated at the operational conditions of the vanadium flow cell while charge-discharge, showing better protons ions conductivity and less vanadium permeability. Many researchers fabricate and explored the non-fluorinated membrane also to find the cheaper and more efficient substitute.

The polymers used are sulfonated poly(ether ether ketone) (SPEEK) and poly- benzimidazole, [38,41] but these polymers are susceptible to chemical changes in the acidic environment and lose their efficiency with time. This behaviour leads to the lowering the life cycle of the VRFBs. [52,53]. So currently commercial nafion membrane, even with its higher price, are most widely used membrane in VRFBs.

### *1.4.2 Electrolytes*

The selection of electrolyte and its concentration affects the energy density and the ohmic loses; moreover, it also influences the reaction kinetics on the electrode surface, consequently effecting the energy efficiency. There are certain challenges, that are associated with the electrolytes about the solubility, stability and viscosity. Thee optimum concentration of 3 M -5 M $H_2SO_4$ solution is used as base electrolyte in VRFBs [54], for the concentration of 1.5 M to 2 M vanadium. The solubility of the vanadium salts, specially the $V_2O_5$, is low in the acidic aqueous media and decrease with the increase of the temperature. For the species $V^{2+}$, $V^{3+}$, $V^{4+}$, the solubility increases with increasing temperature and vice versa. At the concentration of 1.5 M, precipitation of V(V) starts over the 40 $^oC$ ; while for the other three vanadium states, "$V^{2+}$, $V^{3+}$, $V^{4+}$", precipitation starts before 10 $^oC$. Thus, for all of four vanadium compounds the solubility remains lower than 1.5 M in the temperature range of 10 $^o$ C to the 40 $^o$ C

To increase the solubility beyond this temperature range (10 $^oC$ - 40 $^oC$), many researchers investigate the addition of some additives[55,56]. Other possibility is to install some heating/cooling device to maintain the temperature of the stack, but this option increases the complexity of the system and introduce additional cost and energy losses. Some researcher investigate the chloride based electrolytes in place of the $H_2SO_4$ for the better solubility of

vanadium; but in the case of HCl, there is the eventual risk of the production of the $Cl_2$ gas [57,58]. Skyllas et al. investigated the addition of the ammonium sulphate and ammonium phosphate in the $H_2SO_4$ solution. The results indicate that the 2 M concentration of the vanadium is stable up to the 45 $^oC$ and battery showed the stable performance around 120 to 150 cycles.[59].

### *1.4.3 Electrodes*

The power density of the (VRFBs) stack highly depend upon electro kinetic activity and active surface area of the electrodes. Many electrodes have been studied for the vanadium redox flow application. The following characteristics is taking under consideration while selecting the electrode material; 1) the fast kinetics against redox reaction over the long time 2) mechanically stable against the flowing conditions. 3) should be chemically stable in the acidic conditions (3 M – 5 M $H_2SO_4$). Also, the positive electrolyte contains $VO_2^+$ in fully charged state and it is strong oxidizer. 4) The cost should be cheap, so that the capital cost of the overall system remains economical.

Generally, carbon based 2-D and 3-D electrodes are used in the VRFBs applications, such as graphite plates, carbon paper, carbon cloth, carbon felt. The other materials are also used such as platinized titanium sheets, carbon nano tubes composite[60–70]. Among these electrodes, graphite felt (GF) is the fibrous 3-D electrode, having highest surface area per unit volume ≈ 22100 $m^2 . m^{-3}$ [71]. The high porosity, good electrical conductivity and low prices also made GF electrodes most popular choice for the VRFBs application. Rest of electrodes have 2-D dimension and have less available area for the redox reactions.

There are few disadvantages associated with the GF. High pressure drops and possible channeling of electrolyte in the porous structure of the felt can affect the loss of efficiency of the stack. The different flow field geometries and channel can eliminate this problem, such as serpentine flow field.[72–74]. The electroactivity of the vanadium reactions is also relatively slow on the GF electrode [75]. The properties of the graphite felt depends upon the starting precursor material; from which they fabricate. Polyacrylonitrile (PAN) and cellulosic rayon are mostly used to synthesis the GF, by the following procedure. 1) The initial precursor in polymerized and oxidized to form carbon fiber. 2) Then it is converted into the polymer felt, subsequently carbonized around 800 $^{o}$C to get the carbon felt. 3) The final graphite felt is obtained by graphitizing the carbon felt at the 1600 $^{o}$C [71,76,77]. Various activation procedures can be used to increase the electroactivity of electrode; such as thermal , electrochemical and chemical treatment. The insertion of the different metal oxides on the electrode surface is also investigated by many researchers. The detailed bibliographic analysis of various activation methods is discussed in the following sections.

The design of the electrochemical reactor depends upon the slowest reaction. Bibliography shows that the kinetics study of both half-cell reactions is widely investigated to determine the rate limiting reaction. Sun et al. proposed the mechanism for both half-cell reaction, as shown in the fig A 4. According to the proposed mechanism, the positive half-cell reaction involves two steps: the proton exchange / $VO^{2+}$ adsorption, and electron transfer step. On the other hand, negative half-cell reaction contains the single electron transfer step. So, positive half-cell reaction seems to be the more complex chain than negative one and act as the rate limiting reaction. Zhong et al. and Gattrell et al. quantitively analyzed the reactions rates on the carbon electrode, that shows the positive half-cell reaction is comparatively slow than the negative half-

cell reaction. [23,75,78]. So, the positive half-cell electrode requires the activation to increase its electroactivity, so that the kinetics polarization of the reaction on the electrode surface decreased. In the following sections, bibliography of concerned different treatments, are critically analyzed.

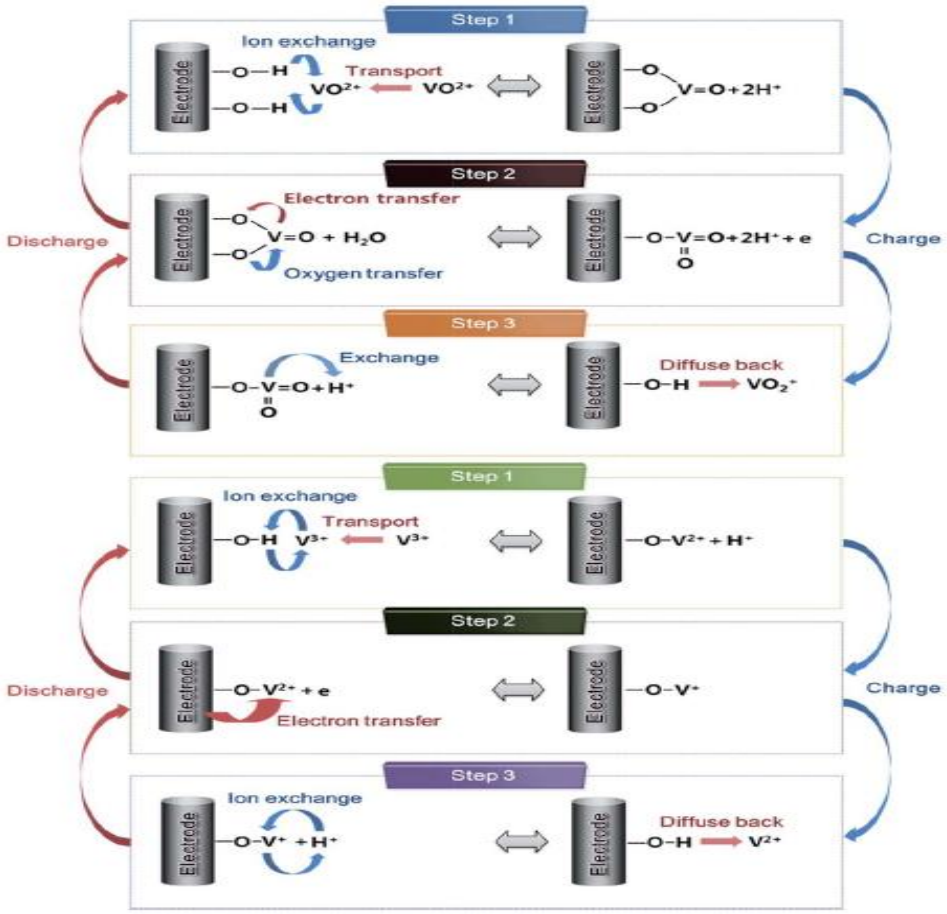


***Fig A.4.*** *The mechanism of both half cells on the electrode surface (fig extracted from the ref:*[79]*)*

### *1.4.3.1 Thermal treatments*

Skyllas et al. [80] investigated the thermal treatment effect on the graphite felt (GF) for VRFBs. The electrode was heated at the different temperatures (200 $^{o}$C - 600 $^{o}$C) and for different durations (10 h -50 h), to find the optimized conditions, at which the electrode shows the better performance. The activation at 400 $^{o}$C for 30 hours in the air, showed improved kinetics of the

electrode. As the temperature increase beyond 400 $^{o}$C, the weight loss is too pronounced because of the burning of the surface. i.e. from 1.06 % to 11.02 %. X. Wu et al. [81] treated the graphite felt with the microwaves, that increased the voltage efficiency by 3 %. In another study, Chen-Hao Wang et al. [82] proposed the activation method by the steam at 700 $^{0}$C. The resulted energy efficiency increased by the 5 %. The steam at high temperature undergoes the reforming reaction and insert the roughness and the oxygenal functional groups.

Min-Sik Park et al. [83] applied oxygen plasma and Gamma-ray irradiation in two different experiments to investigate the effect on the surface morphology of the carbon felt and their activation against $VO^{2+}/VO_2^{+}$ redox couple. The thermal treatment and oxygen plasma treatment change the surface morphology of the carbon felt, but the Gamma-ray irradiation do not have visible effect on the surface morphology. The oxygen plasma alone has limited penetration in the porous structure of the carbon felt and has a non-uniform surface effect. The Gamma-ray irradiation change the surface chemistry of the carbon felt, by converting the already present carboxyl and carbonyl group on the felt surface, into the phenolic group; without changing the physical structure of the carbon felt. Specifically, this treatment breaks the C=O bond and creates the free radical on the surface and enables grafting of the phenolic group on the surface. The overall cell energy efficiency was improved by 7 %.

Chen-Hao Wanget et al. [84] employed a constant flow of $CO_2$ at high temperature of 1000 $^{o}$ C in tubular furnace, to activate the graphite felt by the VRFBs. The C=C bond is converted to the C-O, C=O and the C-OH. Tao Liu et al. [67], used the same treatment procedure (by $CO_2$) for the activation of the carbon paper; they chooses higher operational temperatures i-e 1000 $^{o}$C-1500 $^{o}$C.

### *1.4.3.2 Chemical treatments:*

M. Skyllas-kazacos *et al.* [85] investigated the activation the graphite felt in the 98% concentrated $H_2SO_4$ . The dipping of the graphite felt into the acid at room temperature for one day, did not alter the surface of the electrode, and the resulted GF did not showed any improvement against redox reactions. The effect of different concentration of $H_2SO_4$, from 50 % to 98 %, was studied at their boiling points (≈ 300$^o$ C) up to 15 h. The concentration below the 90% has not any impact on the electrode, while the heating in 98 % $H_2SO_4$ at its boiling point for 5h successfully activate the electrode. The weight losses start by $H_2SO_4$ treatment even after 1-hour but become very pronounced effect after 10 hours. For the same duration, the 70 % $HNO_3$ treatment was also applied on the GF at its boiling point. Though, the activation performance is better than the untreated electrode, but it is lower than the $H_2SO_4$. [85]. Possible reason of this different performance is concentration of the both acids e-y the $H_2SO_4$ used was 98%, while $HNO_3$ used was 67 %.

Lu Yue et al. [86] used both acids ($H_2SO_4$ 98 % + $HNO_3$ 67 %) in the different proportions. The mixed acids show better treatment, than the treatment with the individual nitric acid and Sulphuric acid. Because when the mixed acid applied for the oxidation, the nitric acid starts acting as the oxidant and sulphuric acid starts catalysing the process. This synergetic phenomenon enhanced to maximum extent when the ratio of the sulphuric acid and the nitric acid used in ratio of 3:1 (V/V).

Chao Gao et al. [87] exploited the highly oxidative power of Fenton reagent to activate the graphite felt. The Fenton reagent is widely used in the advanced oxidation processes in rectification of the organic pollutants from the wastewater. The hydroxyl radicals are produced

by the decomposition of $H_2O_2$ in the presence of the iron catalyst. The C=C and the C-H bonds on edge of the graphitic structure was oxidized, the C-H bond convert to C-OH, the C=C bond was converted to the C-C-OH. Upon further oxidation the -OH groups further oxidized to the C=O.

X. Wu et al. [88] activated the graphite felt by modified Hummers method. The hummers process has series of interconnected chemical steps, and even minor deviations from the operational parameters, may lead to structural damage of the electrode or coverage of the surface with different proportion of the functional groups. Jingyu Xi et al. [89] created the micropores and oxygenic groups on the graphite felt by KOH pyrolysis at high temperature in inert environment. The micropores are created in the range of 2 nm. The oxidation of the graphite felt is because of the reduction of the hydroxide. The proposed reaction for the KOH enabling the creation of micropores are as follows ($6KOH + 2C \rightarrow 2K + 3H_2 + 2\ K_2CO_3$) [90]. Some part of the carbon is consumed in the formation of the K metallic, create the new surface by creating flakes on the carbon surface. The mesopores are formed due to the intercalation of the metallic K in the graphene layers. The overall fibrous structure could be destroyed by severe experimental conditions. All the experiments were done in the nitrogen environment, because the carbonization of these reactions is occurred usually above 600 $^0$C and at this temperature, the felt would be burned in the presence of the air.

The role of nitrogen groups on electrode were also studied by several researchers. Yuyan Shao et al. [91] developed the mesoporous carbon with nitrogen doping and insert it on the base carbon electrode material. The nitrogen doped content showed the positive effect in catalysing vanadium redox reactions. The nitrogen groups that doped on the surface was pyridinic-N, Pyrrolic-N, quaternary nitrogen (graphitic nitrogen) and N-oxides of pyridinic-N. Graphitic nitrogen is the

compound that is pinched in the graphene layer and replace one carbon atom from the graphene structure. Carbon atoms near to nitrogen atoms contains high positive charge density due to the electronic affinity of nitrogen atoms. These adjacent carbon atoms act as active sites to enhance the redox reaction. The induction of the nitrogen compounds creates charge delocalization in the structure. This delocalization improves the adsorption of the V-O complexes on the surface and facilitate the $VO^{2+}/VO_2^{+}$redox couple. The procedure of nitrogen doping on carbon nanomaterials require high temperature i-e 850 $^0$C . Tao Wu [92] doped the nitrogen directly on the graphite felt to avoid these limitations. The doping was done by heating the felt at 180 $^o$C in 25% ammonia for the 15 hours, in the airtight closed autoclave. The inherent oxygen groups on the bare graphite felt was converted to the nitrogen compounds like amide groups. The $NH_3$ reaction does not affect the morphology of the electrodes. After treatments, carbon fibres become more smother than the untreated carbon, because of the cleansing effect of the ammonia. The hydrophilicity and absorptivity of the treated samples were improved, in comparison with the untreated felt; that clearly indicate the nitrogen affinity towards vanadium species. Because the ammonia does not affect the surface area of the graphite felt, so all the hydrophilicity and absorptivity were caused by the nitrogen compounds.

#### *1.4.3.3 Metal doping*

M. Skyllas-kazacos *et al.* [61] investigated the electro catalytic activity and reversibility of the glassy carbon , graphite fibers and residual graphite fiber oxide to use as electrode in the vanadium redox flow batteries. They also impregnated different metallic cations i-e $Pt^{+4}$, $Pd^{+2}$, $Au^{+4}$, Mn, $Te^{+4}$, $In^{+3}$ and $Ir^{+3}$ on the residual graphite fiber oxide to have better electrochemical active electrode materials. The rGO fiber impregnated with Pt showed the same electrochemical behaviour towards vanadium redox reactions as the $Pt^{+4}$ itself. The reversibility of electrode is

significantly improved due to the Pt metal active sites (PtO / $PtO_2$) on the electrode. The $Te^{+4}$, $In^{+3}$ and $Ir^{+3}$ showed better performance as compared to the Pt, Pd. Among all these metals, the $Ir^{+3}$ impregnated electrode showed best performance. The peak current of CV current increased by 10% , but the formation of $O_2$ and $H_2$ bubbles is the main draw back

W.H. Wang *et al.* [68] investigated the $IrO_2$ modified carbon felt by the reduction of the $H_2IrCl_6$. The results indicate the improved electronic conductivity, because Ir deposition improves the fibre to fibre contact,. The main drawback of this treatment is that it is too lengthy and complicated process. It almost required 35 hours to treat the electrode. Young-Jun Kim et al. [93] investigated the effect of $Mn_3O_4$ nanoparticles on the Carbon felt. The effect of the $Mn_3O_4$ is more pronounced towards $VO^{2+}/VO_2^{+}$ than the $V^{2+}/V^{3+}$ couple.

Cristina Flox et al [65] investigated the hydrazine treated graphene supported bimetallic nano-$CuPt_3$ on inert material to use as positive electrode for VRFBs. The base material was prepared by injecting hydrazine treated graphene oxide on the inert material. To enhance the electrochemical activity of this material, the $CuPt_3$ particles were impregnated on graphene oxide base electrode. Hydrazine treated Graphene supported monometallic Cu nanoparticles and mono metallic Pt were also investigated separately for the comparison purpose, but the bimetallic particles $CuPt_3$ showed better performance than the both individual metals. The -OH groups on the bimetallic nanoparticles are believed to be the reason of this enhancement. The control of the particle size distribution is difficult to be achieved in this treatment. The durability and stability of these particles with the flow of the electrolyte could also limit the performance of the electrode: the costly platinum metal increases the overall cost of the electrode and the presence of the Cu particles makes the electrode less stable in the acidic conditions.

T.S. Zhao et al. [94] deposited the Copper sulphate nanoparticles on the graphite felt to use it as the negative electrode in the VRFBs. The $Cu^{2+}$ nanoparticles are introduced into the negative electrolyte in the form of the $CuSO_4$. The standard potential of the $Cu/Cu^{2+}$ is in between the potential of the $VO^{2+}/VO_2^{+}$ and the $V^{3+/}V^{2+}$. Before the system approaches the $V^{3+/}V^{2+}$reduction potential, the $Cu^{+2}$ reduces and electrodeposits on the graphite felt. Then metallic copper is oxidized back into the $Cu^{2+}$ ions before the system approaches the potential of the $VO^{2+}/VO_2^{+}$. This indicates that the Cu particles could only affect the kinetics in the electrodeposited form, not in the ionic form. The Columbic efficiency of the cell increase with the increase of the $Cu^{+2}$ concentration up to 0.005M; consequently, affects the kinetics of $V^{3+}/V^{2+}$. This is because copper consumes some factor of the flowing current. The Voltage efficiency of the cell also stop increasing further after the 0.005M. This phenomenon arises, because the Cu nanoparticles agglomerates and loses its nano size distribution and converted to the micro particles on the electrode. That clearly indicate the limitation of the stability of the nanoparticles on the graphite felt. Moreover, the $Cu^{2+}$ in the electrolyte also subject to number of the side reactions in the cells.

Wei Wang et al [95] investigated the graphite felt doped by bismuth nano particles.The results showed that the $V^{3+}/V^{2+}$ couple kinetics is more sluggish than the $VO^{2+}/VO_2^{+}$ in the presence of the HCl solution electrolyte, contrary to the $H_2SO_4$ solution electrolyte, where main limitation comes from the $VO^{2+}/ VO_2^{+}$ redox couple. Bismuth standard reduction potential is in between the $VO^{2+}/VO_2^{+}$ and $V^{3+}/V^{2+}$. So, before reduction of the $V^{3+}$ to $V^{2+}$, the $Bi^{3+}$ electrodeposits on the electrode as Bi metal and act as the catalyst for the vanadium reactions. During the reverse polarisation, Bi oxidized back to the $Bi^{3+}$ ions before the oxidation of the $VO^{2+}/VO_2^{+}$ couple and does not participate in the positive cell reaction.

Wei Wang et al [96] investigated the $Nb_2O_5$-based nanorods loaded on the Graphite felt used as positive and negative electrodes. The treatment time is approximately 50 hours and that make this process less attractive. Moreover, to control the particle size distribution, the great care and precise control of the parameter are necessary.

Haipeng et al. [97] investigated the $ZrO_2$ nanoparticles on the graphite felt for the positive and negative electrodes in the vanadium redox flow batteries. The $ZrO_2$ decrease the kinetic polarization overpotential of the $VO^{2+}/VO_2^{+}$and $V^{3+}/ V^{2+}$ redox couples on the GF. The abundance of oxygen groups on the surface of the $ZrO_2$ contributed mainly towards this improvement. The process of the impregnation of $ZrO_2$ nanoparticles on the GF, took place in temperature environment of 400 $^{o}$C-500 $^{o}$C for 12 h. Zoraida Gonzalez et al.[98] modified the graphite felt with the graphene oxide by the electrophoretic deposition and used it as the positive electrode for the VRFBs. Graphene have good electronic conductivity and high mechanical stability. The graphene deposited on the fibre, improves the electronic conductivity between different fibres.

#### *1.4.3.4 Electrochemical treatments*

Skyllas et al. [99] applied the anodic and cathodic electrochemical treatment on the graphite felt of different thickness and different types (PAN and rayon based) in $H_2SO_4$ acidic media, from 50 min to 180 min. As the oxidation proceed, the lower oxygen groups like -OH start oxidizing to the higher oxidation groups like C=O, -COOH and COOR. The oxygen content up to 22 %, increase the electrical resistivity of the cell. Upon more oxidation, the oxygen groups were transformed to CO and $CO_2$. Xinping Qiu et al. [100] electrochemically oxidized the graphite felt in the 1M $H_2SO_4$ solution. The Graphite felt impregnates with 34 % oxygenic content when

oxidized at the 560–840 mAh $g^{-1}$ and exhibits the improved results than the bare electrode. The voltage and energy efficiency were 5% higher than the untreated electrode. There were some effects on the morphology of the electrode, but it was not too pronounced. LI Xiao-gang et al.[101] activated the graphite felt by the electrochemical oxidation in the 1 mole/L $H_2SO_4$ solution. SEM images showed that the electrochemical oxidation forms some solid particles on the fibres, that is supposed to be some corrosion of the graphite. The -COOH group formed due to the oxidation, is supposed to catalyse the reaction.

Yue men et al [69] exploit three acids (citric acid, oxalic acid and ethylene diamine tetra acetic EDTA) to treat the carbon felt electrochemically. The surface morphology was not affected by the treatment, which just incorporates the oxygen groups on the surface. The columbic and voltage efficiencies were decreased by using the treated electrode. As the surface morphology of the electrode is not changed, while the surface chemistry changed due to the functionalizing by oxygenal groups; so probably these groups are fabricated on the Basel plane and unstable. Kim et al. applied coupled treatment of corona discharge and hydrogen per oxide ($H_2O_2$) to integrate the oxygenic contents on the surface of the carbon felt. The treatment only with $H_2O_2$ neither effects the surface morphology nor the surface chemistry. Moreover, the coupled treatment of corona discharge and the $H_2O_2$ also did not affect the surface morphology significantly. It effects only the surface chemistry of the carbon felt. Corona discharge create free radicals on the surface. These free radicals are too reactive that it can easily react with $H_2O_2$ and converted to the oxygenic groups. [102]. The resulted electrode showed 7 % improvement in the energy efficiency of VRFBs.

## 1.5 Conclusion

The extensive bibliography is done in this chapter, to identify the challenges regarding the vanadium redox flow batteries. The critical analysis of the bibliography shows;

- There is huge scope of renewable energy resources in the future power market. But to integrate the renewable energy into the grids, the efficient and economical storage system with long life cycles are important. EU has the target to obtained 32 % of total power from renewable until 2030.
- Flow batteries is preferable option for this purpose, over the other conventional batteries (Li ions battery, lead acid batteries etc.), because of its detached power and energy densities.
- Among flow batteries, VRFBs have the advantage of employing same metals ions in both half cells, that ensure its electrolyte stability and life cycle. But there are multiple challenges associated with its membranes, electrolytes and electrodes.
- The electrodes are one of the key components in the VRFBs, because the power density of stack depends upon its kinetic activity. Mostly graphite electrode is used in the VRFBs because of its high available surface area, low cost and stability in high acidic electrolytes. But low kinetic activity against the vanadium reactions, is its draw back.
- The positive half-cell reaction of VRFBs is comparatively slow than the negative half-cell reaction and acting as the limiting reaction. Following activations methods are found in the bibliography to treat the GF to use it as positive electrode in VRFBs e-g electrochemical oxidation, metal oxide fabrication on electrode surface, chemical and thermal treatments. But mostly methods are complicated, long and operationally difficult.

In this thesis, various novel, effective , operationally easy and time efficient methods are proposed to activate the GF, to be used as positive electrode in VRFBs. For this purpose, following tools are used: cyclic voltammetry, linear sweep voltammetry, scanning electron microscopy, FTIR, contact angle measurements. Sequentially, the performance of the electrodes is evaluated in half-cell and pilot scale reactor. In end, the density functional theory (DFT) calculations are performed to understand the phenomena at molecular level.

# ***Chapter:2 Enhancement of the electrochemical activity of a commercial graphite felt for vanadium redox flow battery (VRFB), by chemical treatment with acidic solution of $K_2Cr_2O_7$.***

# **Chapter:2** *Enhancement of the electrochemical activity of a commercial graphite felt for vanadium redox flow battery (VRFB), by chemical treatment with acidic solution of $K_2Cr_2O_7$.*


***Abstract*:**

The novel thermal-chemical activation method is proposed to prepare the graphite felt with highly functionalized surface and enhanced active surface area, to be used as the positive half-cell electrode for the vanadium redox flow batteries (VRFBs). The prescribed treatment consists of boiling the felt within $K_2Cr_2O_7$ solution in 5 M $H_2SO_4$, at different temperatures and time durations. It is time efficient, effective and durable. The Cyclic voltammetry analysis enable to optimize the operating conditions i.e. boiling at 140 °C for 2 h. The activation treatment creates different surface oxygen functional groups, as characterized by FTIR, that act as catalytic sites towards the positive half-cell redox couple reaction ($VO^{2+} \rightleftharpoons VO_2^+$). Moreover, the improvement of various other properties of the graphite felt, resulting from the activation are also quantified, such as the surface roughness of fibers, the wettability towards electrolyte, the adsorption affinity against the vanadium and the surface energy of the graphite felt. The improved reversibility of $VO^{2+}/VO_2^+$ redox couple reaction against graphite felt is also evaluated and confirmed by the increase of intrinsic heterogeneous electronic transfer constant by 2.2 and 5.5 folds for the oxidation and reduction reactions, respectively. The performance evaluation of electrode at stack level by charge-discharge cycles, shows the improvement of the voltage efficiency and faradaic yield, as well as, the consistency of the performance over three cycles (~16 h).

## 2. 1 Introduction

The renewable energy recourses are acquiring a lot of attention due to huge pressing concerns about environmental issues and exhausting conventional power sources. Intermittent nature of the renewable energy induce limits on the practical and commercial viability [103,104]. A possibility to overcome limitations is their association to systems, named redox flow batteries, able to store important quantities of electroactive materials and consequently important quantities of energy [105]. For instance, vanadium redox flow batteries are successfully commercialized in certain countries with significant energy density in the range of 20-40 Wh/kg. Lithium ion redox flow batteries, theoretically offer 80-180 Wh/kg energy density, yet not commercially available. In recent times, various redox flow batteries have been investigated due to their large capacities, relatively economical costs, long life cycles and flexible operations i.e. Fe/Cr [16]; Sodium polysulfide/$Br_2$ [106]; V/$Br_2$ [107] and all vanadium redox flow batteries (VRFBs) [108]. The VRFBs was initially proposed by Skyllas-Kazacos [60,61] and appears to be a promising and viable option due to the 1) employment of the same metal ions in both electrolytic compartments, 2) a long electrolyte stability and 3) a minimized self-discharge phenomena [31,42,54,105,109]. The positive and negative half-cell reactions are described by the Eq. (B.1) and (B.2) respectively. The theoretical overall cell voltage (ΔE°) is 1.26 V.

<u>Positive half-cell reaction</u>: $VO_2^+ + 2H^+ + e^- \rightleftharpoons VO^{2+} + H_2O$ $E°_{(VO^{2+}/VO_2^+)}$ = *1.00 V vs SHE;* (B.1)

<u>Negative half-cell reaction:</u> $V^{3+} + e^- \rightleftharpoons V^{2+}$ $E°_{(V^{+2}/V^{+3})}$ = *-0.26 V vs SHE;* (B.2)

The selection of the electrode's material of VRFBs is critical in overall battery design, as it could exhibit high activation overpotentials for both redox couples. Besides, it should have high active

surface area, low cost and good mechanical resistivity and chemical stability against acids [79]. Various carbon based materials were investigated like graphene oxide, graphite fibers, carbon paper, glassy carbon, graphite felt, carbon felt, multiwalled carbon nanotubes, etc. by different research groups [61,63–65], but most often they exhibit low electrocatalytic activity and poor kinetic reversibility for the vanadium redox couples. A lot of efforts have been done so far to improve the electrochemical performance of a carbon-based electrodes, such as chemical or thermal treatment, electrochemical oxidation, doping of the chosen electrode by various metal or metal oxides (Pt, Pd, Au, Ir, Mn, Cu, Bi, Zr……..) [65,68,80,84,91,93–95,97,100,110–113]

The poly acrylonitrile (PAN) based graphite felt (GF) is widely used as electrode material in the vanadium redox flow batteries, due to highly resistive surface against acidic conditions, having low price and large specific surface area [77,82,101,110]. However, its electroactivity against the vanadium redox system appears to be poor and limit its applicability [17].

The present study focuses on the use of coupled thermal and chemical treatment, expecting to modify the surface of the GF to be used as positive half-cell electrode in VRFBs. The study also quantifies the enhancement of the electrode activity in terms of the kinetic constant and the number of the created adsorption sites. A strong oxidizing agent i.e. potassium dichromate $K_2Cr_2O_7$ in sulfuric acid solution, is used to modify the electrode surface functionalities.

## 2.2 Experimental

### *2.2.1 Materials and chemicals*

Poly acrylonitrile (PAN) based graphite felt (GF) of 3 mm thickness and platinum wire (0.125 mm, 99.95 %) is provided by Goodfellow Cambridge Ltd. France. $VOSO_4$. $5H_2O$ and $K_2Cr_2O_7$ are purchased from VWR international, France. The Nafion membrane (N 424) is provided by

the Ion power Inc. USA. The sulfuric acid (95-97%) is purchased from the Sigma-Aldrich Co. France.

### *2.2.2 Electrode activation*

As received GF is thoroughly cleansed with distilled water in sonicator for 30 minutes. Then it is dried in the oven for 15 hours at 50 °C and used as reference material for further use named as untreated-GF. Untreated GF is heated at 400 °C for 5 h in the muffle furnace to burn away any greasy layer or impurities, adsorbed on its surface and then it is cut into six different pieces with dimension of 7 cm × 7 cm each. These pieces are treated as following : the GF is heated in a solution of $K_2Cr_2O_7$ (40 g/L) in 5 M $H_2SO_4$, at different temperatures ($100 < T_{(°C)} < 160$) and for various duration ($2 < t_{(h)} < 8$), under reflux conditions. In the following sections, the GF electrodes are named as: "oven temperature-Cr-duration of treatment in hours-GF"; thus the "140°C-Cr-5hrs-GF" indicates that the piece of GF is heated into the acidic solution of the dichromate at 140 °C for 5 h.

The expected general reaction while the activation of GF surface can be schematically written as;

$$Cr_2O_7^{2-} + \kappa\,(\text{-C-})_{groups} + \kappa/2\,O_2 + 14\,H^+ \rightarrow 2Cr^{3+} + 7\,H_2O + \kappa\,(\text{-C-O-})_{groups} \qquad \text{(B.3)}$$

After treatment, all the samples are thoroughly rinsed with deionized water to remove all the residues of $Cr^{(III)\ or\ (VI)}$ and $H_2SO_4$, remained on the electrode surface during the activation process, followed by drying for 10 h at 50 °C in the oven for further use.

### *2.2.3 Electrode characterizations*

The electrochemical activity of the GF is characterized by voltammetry; the experiments are performed in a classical three electrodes cell of 25 $cm^3$ capacity, containing the acidic solution of

the vanadium. A piece of treated GF, having a certain surface delimited by a layer of glue, is used as working electrode; thin platinum wire (0.125 mm) inserted into the top side of the GF, act as current collector. The Saturated calomel electrode (SCE), immersed into a Luggin capillary and a platinum foil (~3 $cm^2$) are used as reference and counter electrodes, respectively.

Two kinds of voltammetry curves are plotted:

*i)* *Cyclic voltammetry (CV) at the transient state*: The CV is performed using the Potentiostat workstation from OrigaLys ElectrochemSAS France, with operational parameters as; potential window: 0 V to 1.6 V; scan rate: 10 mV/s; GF of 1 $cm^2$ geometrical area, immersed within unstirred solution of 0.05 M $VO^{2+}$ + 2 M $H_2SO_4$

*ii)* *Linear sweep voltammetry (LSV) at the steady state:* I=*f*(E) curves are plotted using the Potentiostat workstation from Metrohm-Autolab pgstat 30, with operational parameters as; Scan rate: 1 mV/s, GF with 2.25 $cm^2$ geometrical area, immersed in a stirred solution at 350 RPM.

Two different solutions are used for linear sweep voltammetry (LSV):

- 0.5 M $VO^{2+}$ is prepared by commercial salt of $VOSO_4$ dissolved in 3M $H_2SO_4$, aiming to study the oxidation of $VO^{2+}$ to $VO_2^+$.
- 0.43< $VO_2^+{}_{(M)}$<0.46 + 3 M $H_2SO_4$ solution was obtained after a preparative electrolysis of $VO^{2+}$ 0.5 M in 3 M $H_2SO_4$, (section 2.3.6) in order to investigate the reduction of $VO_2^+$ to $VO^{2+}$.

The morphology of the untreated and treated GF surfaces is characterized by the scanning electron microscopy (SEM) on Phenom XL (Thermo Fisher Scientific, USA) at an acceleration voltage of 10 kV. The surface functionalities are analysed by the Fourier transform infrared spectroscopy (FTIR) on Thermo Nicolet 6700 (Thermo Fisher Scientific, USA). The 2.6 mg of GF sample is grinded, and the resulting powder is mixed with 250 mg dried potassium bromide

and compressed under a force of 10 ton to form the disk of 13 mm diameter for the analysis. In addition to FTIR analysis, the surface functionalities are also analysed by the linear sweep voltammetry.

The high magnification digital camera is used to evaluate the hydrophilicity of GF electrodes as well as their surface energy, expected to control the electrolyte accessibility.

### *2.2.4 Half-cell evaluations*

As the purpose of the present study is to investigate the performance enhancement of the graphite felt towards the $VO^{2+}/VO_2^+$ reactivity on the positive electrode, the half-cell is preferred against the complete cell, in order to minimize any kind of ohmic drop from other parts of battery stack.

The charge-discharge cycles are performed in a classical H-shaped cell. A rectangular band of GF with 2.25 cm² geometrical surface area is used as positive electrode. The negative electrode is a platinum foil (~3 $cm^2$). The anolyte contains 0.5 M $VO^{2+}$ in 3 M $H_2SO_4$, while 3 M $H_2SO_4$ solution constitutes the catholyte.

A saturated calomel electrode (SCE) immersed into a Luggin capillary is introduced in the positive electrode compartment of the half-cell and used as reference electrode, to follow the potential of the working electrode. The electrolytic compartments are separated by a nafion membrane and clamped between two gaskets to avoid leakages. The electrolyte in the positive electrode compartment is continuously stirred with magnetic bar at 350 RPM. There is no mechanical stirring of the solution in the compartment of the counter electrode, except the convection created by the $H_2$, produced from the proton reduction during electrolysis. Galvanostatic electrolysis were performed for charge/discharges cycles, starting by the oxidation

of the $VO^{2+}$ solution. The magnitude of the applied current is 0.15 A/ 2.25 cm² (i.e. 660 A/m²) and the electrolysis is stopped immediately as the electrode potential reaches 1.65 V/SCE, to avoid the oxidation of water. For the reduction of the electrogenerated $VO_2^+$, the same magnitude of the current (-0.15 A) is applied, and as the electrode potential reaches 0.75 V/SCE, this current is immediately decreased to -0.1 A. The electrolysis is stopped when the electrode potential reaches 0.7 V/SCE to avoid any reduction of $V^{(IV)}$ to $V^{(III)}$. Periodically aliquots are taken to monitor the concentration of the $V^{(IV)}/V^{(V)}$ by UV/Visible spectroscopy (UV/VIS LAMBDA 365 Spectrophotometer). The Faradic yield of the electrode is calculated by the Eq. (B.4)

$$Faradic\ yield = \frac{\text{Theoretical charge required for the achieved conversion}}{\text{Actual charge provided for the achieved conversion}} * 100 \qquad \text{(B.4)}$$

## 2.3 Results and the discussions

### 2.3.1 Cyclic voltammetry (CV) and optimization of treatment parameters

Cyclic voltammetry is performed to evaluate the electrocatalytic activity of the different samples of GF and to find the optimal operating conditions of the treatment, that provide the best reversibility of the redox system $VO^{2+}/VO_2^+$ against these treated electrodes.

In the analysis of the CV curves, the following performance parameters are compared; 1- anodic peak current (*Ia*), 2- cathodic peak current (*Ic* ) 3- anodic to cathodic peak current ratio *(Ia / Ic)*, 4- difference between the anodic and cathodic peak potentials *($\Delta E_{a/c} = E_a - E_c$ )*. The individual peak currents correspond to the available surface area for the reactions, so any increment of the current observed, could be linked to the increase of available surface area of the electrode. The

reversibility of the reactions on the electrode improves with the decrease of $I_a$ / $I_c$ and $\Delta E_{a/c}$, and vice versa [98].

Following general remarks concern all the cyclic voltammograms of this section 2.3.1:

i) All the CV experiments are started with the solution of $VO^{2+}$ in the anodic side. Curves exhibit one signal in the range of 1.1 V to 1.3 V, attributed to one electron oxidation of the $VO^{2+}$ to $VO_2^+$. There is not any well-defined reduction peak observed on the untreated GF; the reverse cathodic curve contains two successive shoulders. Conversely, for all the treated electrodes, reduction curve exhibits a single and well resolute signal, attributed to the reduction $VO_2^+ \rightarrow VO^{2+}$.

For the untreated electrode, the anodic amount of charge appears to be the same (±15%) as the cathodic amount of charge.

The cathodic peak obtained with the treated electrode is located at the same potential (0.5/0.6 V) like the first shoulder obtained with the untreated electrode, it represents the $VO_2^+ \rightarrow VO^{2+}$ reaction. The oxidation of the vanadium (IV), i.e. $VO^{2+}$ leads to the vanadium (V) i.e. $VO_2^+$ of which a part is adsorbed on the graphite (this will be confirmed in the next sections). This part increase if the graphite is activated by the treatment. Thus, when $VO^{2+}$ is oxidized, a part remains adsorbed on the fibbers and the rest leaves the electrode and disperses into the solution, because the low potential scan rate 10 mV/s.

The second observed shoulder, located in the potential range of 0.2 to 0.3 V, is attributed to the reduction of $V^{(IV)}$ to $V^{3+}$. A part of the $V^{(IV)}$ is produced by the reduction of the $V^{(V)}$, but the main reduced quantity of $V^{(IV)}$ arrives by diffusion from the solution during the reverse scan because of the low potential scan rate. Note that, this second shoulder at 0.2 V is also observed if the solution of $VO^{2+}$ is directly submitted to the reduction on the untreated electrode. Besides, the

treatment of the graphite felt appears to decrease its affinity against the reduction of the of $VO^{2+}$, certainly because the saturation of the fibber surface of the felt by the adsorption of the $V^{(V)}$.

ii) The curves of treated electrodes show higher anodic and cathodic peak currents as compared to the untreated electrode; a possible explanation could be the increase of the available surface area of the fibers, typically due to the enhancement of the roughness of the electrode.

iii) The anodic to cathodic peak current ratio ($I_a$ /$I_c$) observed for all curves is always higher than 1. Theoretically, the unity value of the ratio means that: a) all the anodic current is used for the $V^{(IV)} \rightarrow V^{(V)}$, b) all the electrogenerated $V^{(V)}$ is retained/adsorbed/ at the fibers surface and c) all the electrogenerated $V^{(V)}$ is reduced back to $V^{(IV)}$. This correspond to the condition of the reversibility.

In the following section, the effect of activation of the graphite felt with $K_2Cr_2O_7$ solution at different temperature and durations are investigated; and find the most optimized parameters of the treatment.

*2.3.1.1 Effect of the temperature during activation with $K_2Cr_2O_7$ solution*

The duration of activation was fixed at 2 h and samples were heated at different temperatures i-e 100 °C , 140 °C and 160 °C. Fig. B.1 is showing the voltammograms of these samples and compared with the untreated electrode. The observed peak current ratios *($I_a$/$I_c$ )* and potential differences *($\Delta E_{a/c}$)* are 1.42, 1.23, 1.33, and 0.69 V, 0.61 V, 0.70 V at the temperatures of 100 °C, 140 °C and 160 °C, respectively. These results show that the 2 h treatment at 140 °C appears to be most suitable, as it leads to the lowest current ratio ($I_a$ /$I_c$= 1.23) and the lowest peaks potential difference ($\Delta E_{a/c}$ =0.61 V), in comparison with 2.1 and 0.99 V for untreated GF, respectively

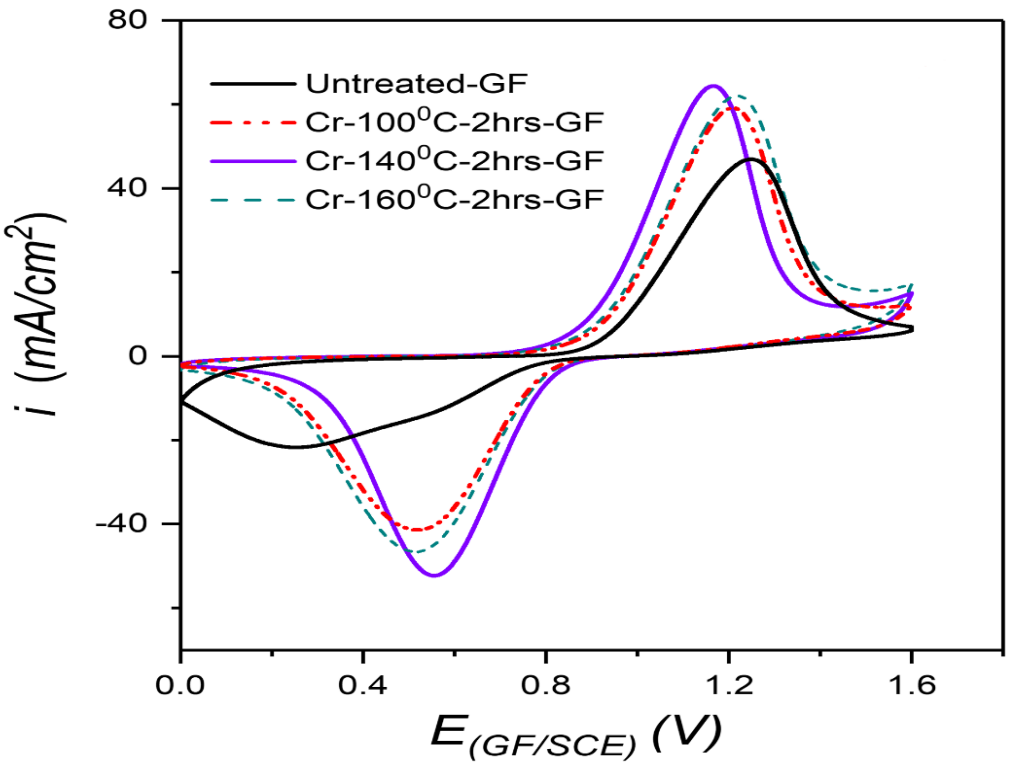


***Fig. B.1:*** *Voltammograms of GF treated at 100 °C , 140 °C and 160 °C for 2 h in acidic $K_2Cr_2O_7$; under unstirred conditions in 0.05 M $VO^{2+}$ + 2 M $H_2SO_4$; r = 10 mV/s; $S_{GF}$=1 cm²; CE = Pt mesh of ~3 cm². (Effect of temperature at 2 h )*

It is important to note that for temperatures higher than 140 °C, the performance of the graphite felt seems to deteriorate. Possibly at higher temperature of activation, the surface oxygen groups could be oxidized to various products including CO, $CO_2$. Moreover, graphite felt can also be exfoliated and subsequently dissolved in acidic solution at high temperature, thus providing graphene or graphene oxide [114]. Very strong oxidation conditions can also rapture the overall fibrous structure of the graphite felt.

*2.3.1.2 Effect of the time during activation with $K_2Cr_2O_7$ solution*

The duration of the activation is also an important parameter in the activation of GF. Fig. B.2 shows the effect of treatment duration, from 2 to 8 h under isothermal conditions of 100 °C. The

improvement of the electroactivity of the GF is observed until 5 h and then starts decreasing for longer durations. At 100 °C, the best performance is obtained at 5 h treatment by 100 °C-Cr-5hrs-GF *($I_a$ /$I_c$=1.4; $\Delta E_{a/c}$=0.66 V)*. Even though, this performance is slightly lower than 140 °C-Cr-2hrs-GF *($I_a$ /$I_c$=1.23; $\Delta E_{a/c}$=0.61 V)*. It seems that 140 $^o$ C is better temperature line than the 100 $^o$ C. So, the effect of the duration at 140 $^o$ C will be further investigated in next section.

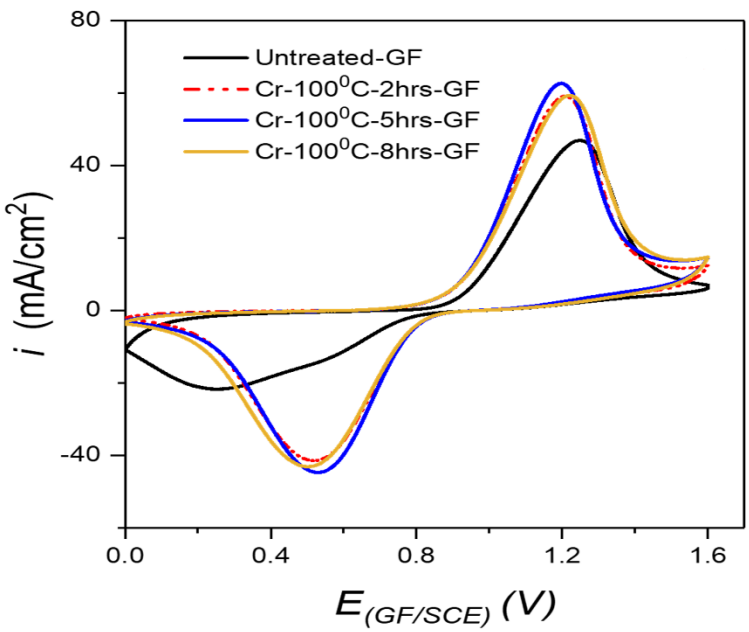


***Fig. B.2:*** *Voltammograms of treated GF (in acidic $K_2Cr_2O_7$) for 2 h, 5 h and 8 h at 100 °C; under unstirred conditions in 0.05 M $VO^{2+}$+ 2 M $H_2SO_4$; r = 10 mV/s; $S_{GF}$=1 cm²; CE = Pt mesh of ~3 cm². (Effect of duration at 100 °C )*

*2.3.1.3 Effect of duration at the temperature of 140 $^o$ C*

As discussed above, that the activation of the electrode at 140 $^o$ C (2 h) is relatively better than the samples prepared at 100 $^o$ C among all durations (2 h, 5 h, 8 h). So, the effect of the time is explored at 140 $^o$ C. Two different samples are prepared by heating the felt at 140 $^o$ C for the duration of 2 h and 5 h. The voltammograms of both samples are compared in the fig B.3. As the duration of the activation exceeds from 2 h, the performance of the electrode deteriorates. The

$\Delta E_{a/c}$ *and* $(I_a / I_c)$ increase from the 0.61 V → 0.80 V, and from 1.38 V→ 1.45 V respectively, when the duration of activation increase from 2 h to 5 h at 140 °C

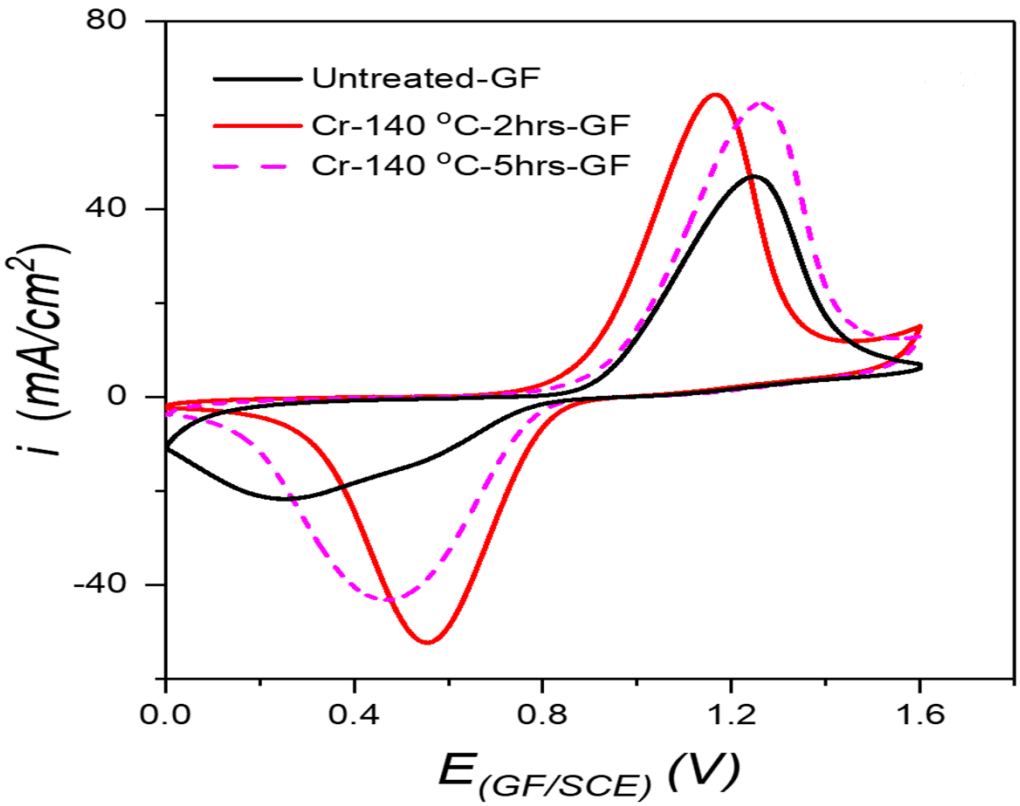


***Fig. B.3:*** *Voltammograms of treated GF (in acidic $K_2Cr_2O_7$) for 2 h and 5 h at 140 °C; under unstirred conditions in 0.05 M $VO^{2+}$ + 2 M $H_2SO_4$; r = 10 mV/s; $S_{GF}$=1 cm²; CE = Pt mesh of ~3 cm². (Effect of duration at 140 °C ).*

<u>*2.3.1.4 Best performing electrode*</u>

In previous section, the activation of the GF by the acidic solution of $K_2Cr_2O_7$ were analyzed at 100 ° C, 140 ° C, 160 ° C for different durations of time at 2 h, 5 h and 8 h. The following performance parameters of all the voltammograms are extracted and compared in fig B.4.

The electrode heated at 140 ° C in the acidic $K_2Cr_2O_7$ solution for 2 hours have highest anodic and cathodic peak currents; while it shows lowest values of $I_a / I_c$ *(1.23) and* $\Delta E_{a/c}$ *(0.61 V).* To conclude, the boiling of the electrode into a solution of $K_2Cr_2O_7$ + $H_2SO_4$ at 140 °C for 2 h under

reflux conditions, provides the best results in the terms of the oxidation of $V^{(IV)}$ and the reduction of $V^{(V)}$. The proposed activation procedure is time efficient, economical and easy. This electrode will be named as "140 °C-Cr-2hrs-GF" onward in this chapter

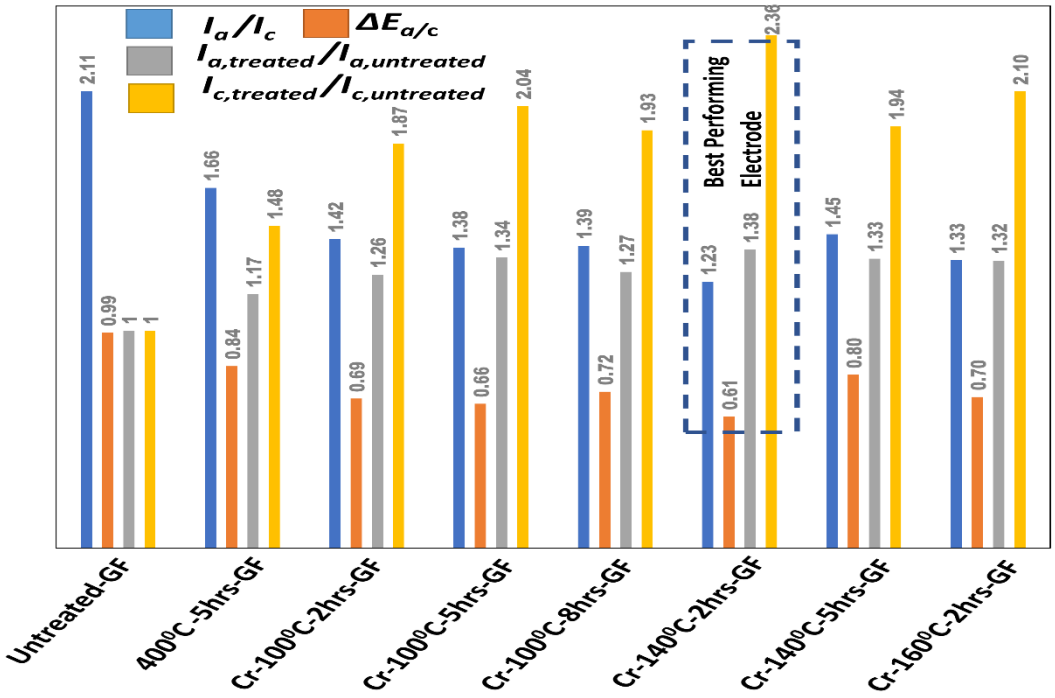


***Fig. B.4:*** *Comparison of $I_a/I_c$, $I_{a,treated}/I_{a,untreated}$, $I_{c,treated}/I_{c,untreated}$ and $\Delta E_{a/c}$ between different treated graphite felt samples and untreated-GF.*

The voltammogram of the treated electrode "140 °C-Cr-2hrs-GF" is compared with the untreated electrode and heat-treated electrode (400 °C for 5 hrs), as shown in the fig. B.5. This electrode will be characterized by various techniques in next sections such as linear sweep voltammetry (LSV), scanning electron microscopy (SEM), fourier-transform infrared spectroscopy (FTIR). The quantification of the adsorption sites and surface free energy of the electrode (140 °C-Cr-2hrs-GF) will also be quantified further in the text. The performance of the electrode, as positive half-cell will also be evaluated in the classical half-cell.

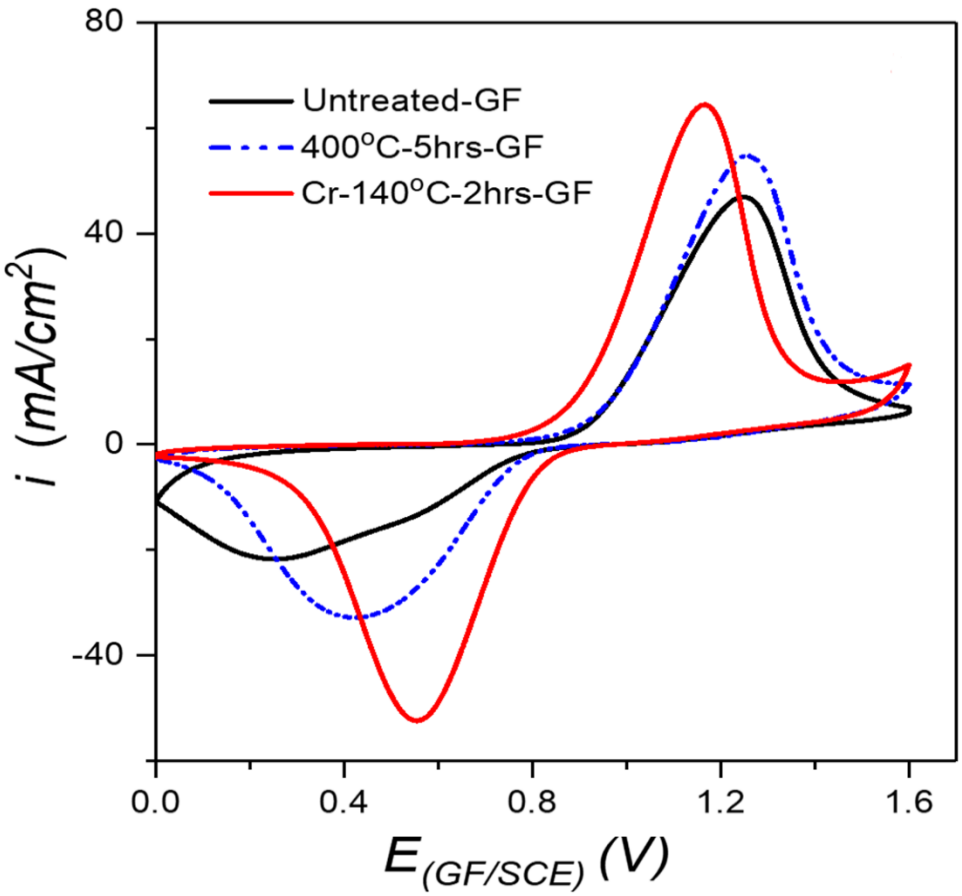


***Fig. B.5:*** *Voltammograms of untreated- GF, 400 °C-5h-GF and Cr-140 °C-2hrs-GF; under unstirred conditions in 0.05 M* $VO^{2+}$ *+ 2 M* $H_2SO_4$*; r = 10 mV/s;* $S_{GF}$*=1 cm²; CE = Pt mesh of ~3 cm².*

### 2.3.2 Linear sweep voltammetry (LSV)

In order to quantify the enhancement of the electrochemical activity of the graphite felt after treatment and to determine the corresponding kinetic parameters, linear sweep voltammetry is performed at the steady state for both, Cr-140°C-2hrs-GF and untreated GF. The examined potential range of the positive electrode of the battery corresponds to 0.7< $E_{\oplus\, in\, V/SCE}$<1.2. Fig. B.6 clearly indicates that the treatment by the dichromate has positive effect on the kinetics of both oxidation and reduction reactions.

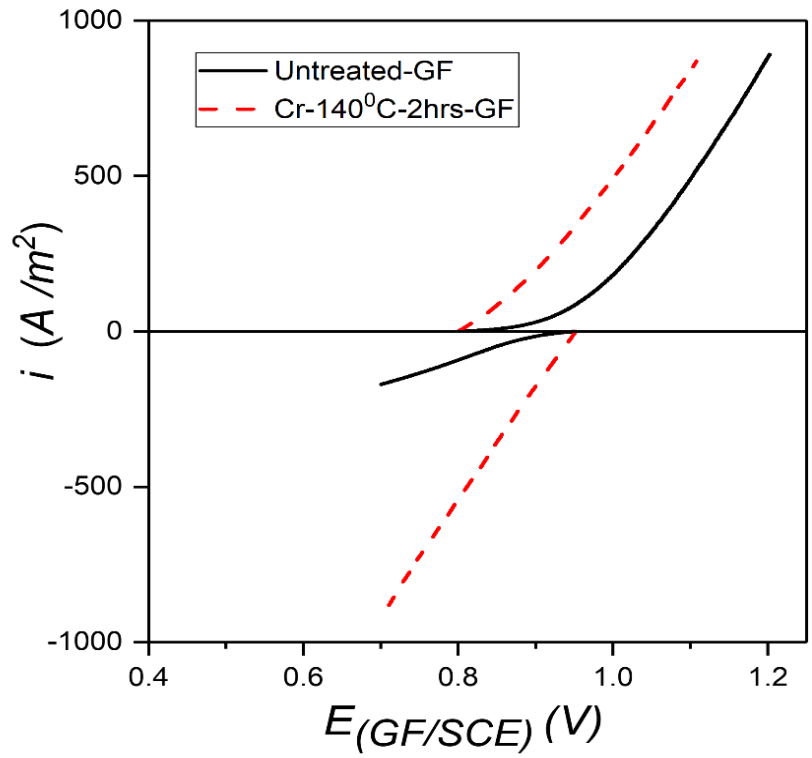


***Fig. B.6:*** *Comparative current-potential curves obtained at the steady state, on Cr-140 °C-2hrs-GF and untreated-GF electrodes for vanadium redox system.* $S_{GF}$*= 2.25 cm²; r= 1 mV/s; CE= Pt ~3 cm; electrolyte: 3 M* $H_2SO_4$*; stirring: 350 RPM; Oxidation: 0.5 M of commercial* $VO^{2+}$*; Reduction: 0.43 M - 0.46 M solution of* $VO_2^+$ *obtained by electrolysis.*

The logarithmic analysis of the curves in electronic transfer limited region i.e. for η≤|0.1 V|, enables to determine the kinetic parameters i.e. the intrinsic heterogeneous electronic transfer constant $k°_{an\ or\ cath.}$, $\alpha$ or $\beta$ by Eq. (B.5) and (B.6).

$$I = n\,F\,S\,k°\,C_{bulk}\,exp\frac{(+\alpha\ or-\beta)nF}{RT}(E_{I\neq o} - E_{I=o}) \qquad (B.5)$$

$$\eta = -\frac{RT}{(+\alpha\ or-\beta)nF}ln(nFSk°C_{bulk}) + \frac{RT}{(+\alpha\ or-\beta)nF}ln\,I = a + b\,log\,i \qquad (B.6)$$

Where:

- *I, n, S, F* and *k°* are respectively the current, the electrons exchanged number, the surface area, the faradic constant and the intrinsic heterogeneous electronic transfer constant;

- $\alpha$ and $\beta$ represent respectively the anodic and cathodic electronic transfer coefficients;

- $E_{I\neq o} - E_{I=o}$ is the overvoltage η.

The table B.1 gives the results of the logarithmic analysis of the *I/E* curve of fig. B.6.

| Electrode used | Reaction involved | α | $\beta$ | $k°$ µm/s (this study) | $k°$ µm/s [115] |
|---|---|---|---|---|---|
| Untreated | $VO^{2+} \rightarrow VO_2^+$ | 0.1 | - | 1.7 | 0.18 |
| Treated | | 0.15 | - | 3.8 | 0.245 |
| Untreated | $VO_2^+ \rightarrow VO^{2+}$ | - | 0.1 | 0.92 | 0.10 |
| Treated | | - | 0.12 | 5.06 | 0.15 |

***Table B.1*** *Kinetic parameters of the $VO_2^+/VO^{2+}$ system on treated and untreated GF electrodes.*

Compared to the untreated electrode, the treatment increases the intrinsic heterogeneous electronic transfer constant $k°$ of $VO^{2+} \rightleftharpoons VO_2^+$, 2.2 folds for the oxidation reaction and 5.5 folds for the reduction reaction. Two facts could explain this behavior: i) the increase of the interfacial concentration of the C-oxygen groups and hence the improvement of the vanadium affinity towards the GF; ii) the creation of more than one type of carbon oxygen groups on the GF surface, which can also contribute to the increases in the rate of vanadium oxidation and reduction reactions.

### 2.3.3 Surface characterization

2.3.3.1 *Scanning electron microscopy (SEM)*

The effect of the treatment on the roughness of the GF is examined by the scanning electron microscopy (SEM). Fig. B.7 shows the images of the untreated-GF *(a, b, c*), 400 °C-5hrs- GF (d,e,f) and Cr-140 °C-2hrs- GF *(g,h,i)*, at different magnifications. The untreated GF (a ,b, c) and

400 °C-5 h-GF (d, e, f) have relatively smooth surfaces. It indicates that the treatment at 400 °C neither affect the overall fibrous structure of the felt significantly nor its surface roughness. The treatment, in presence of the dichromate, creates more roughness on the fibers and enhances their specific surface area available for vanadium adsorption, as shown in fig. B.7. g, h, i. The overall fibrous structure of the GF seems not be affected by the activation procedure as there could not be seen any fragments of fibers.

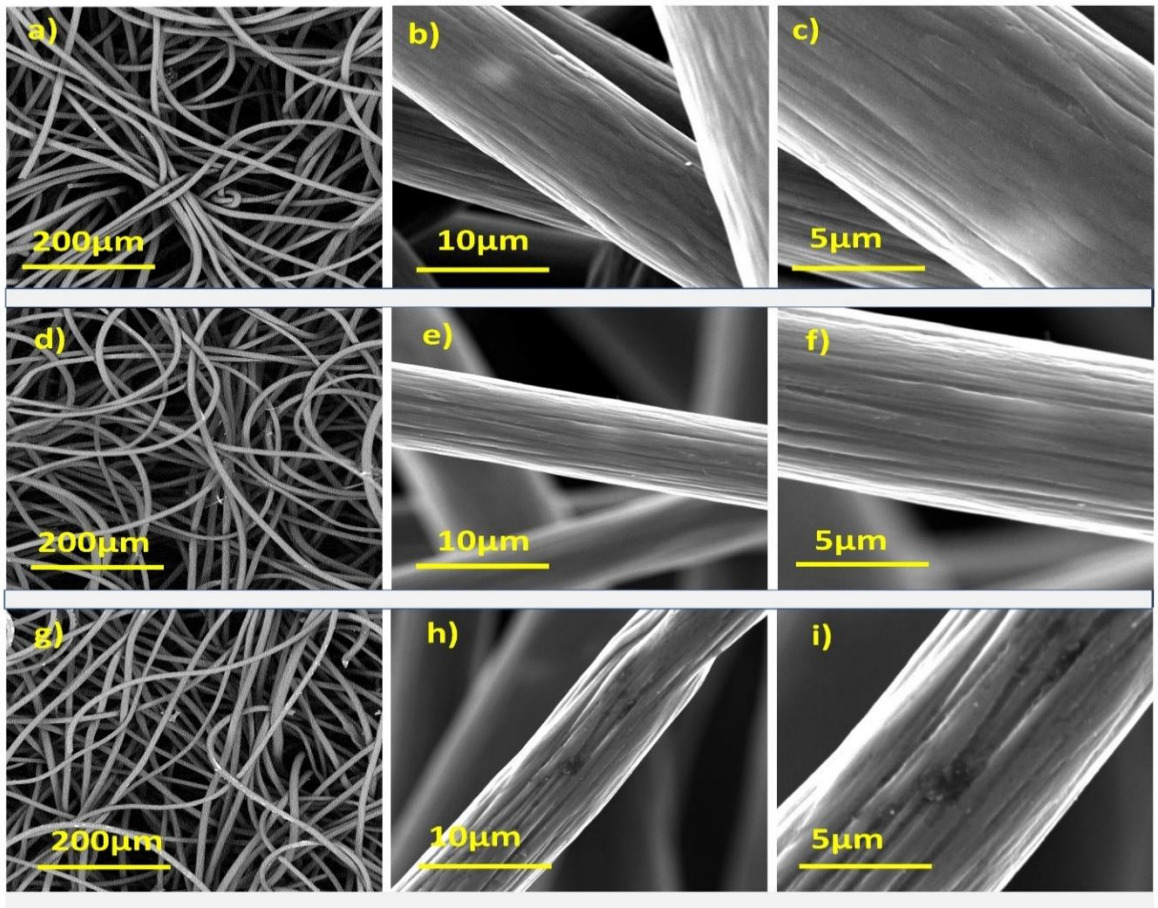


***Fig. B. 7.*** *Various magnification images obtained by scanning electron microscopy (SEM) for different graphite felt samples, at acceleration voltage of 10 kV. Untreated-GF(a, b, c); 400 °C-5h-GF (d, e, f); Cr-140 °C-2hrs-GF: (g, h, i).*

2.3.3.2 *Fourier-transform infrared spectroscopy (FTIR)*

Fourier-transform infrared spectroscopy (FTIR) is used to characterize the presence of oxygen groups and their chemical nature on the felt. The spectrum of the treated electrode shows various peaks (fig B.8). The peaks at 3440 $cm^{-1}$ and 1450 $cm^{-1}$ represent the stretching vibrations of hydroxyl group (-OH). The intensity of the peaks at 3440 $cm^{-1}$ and 1450 $cm^{-1}$, enhanced as compared to the untreated sample, indicates the increment of hydroxyl groups [81]. Besides, the magnitude of the peak at 1628 $cm^{-1}$, assigned to the hydroxyl group in enol (-C=C-OH) [87],

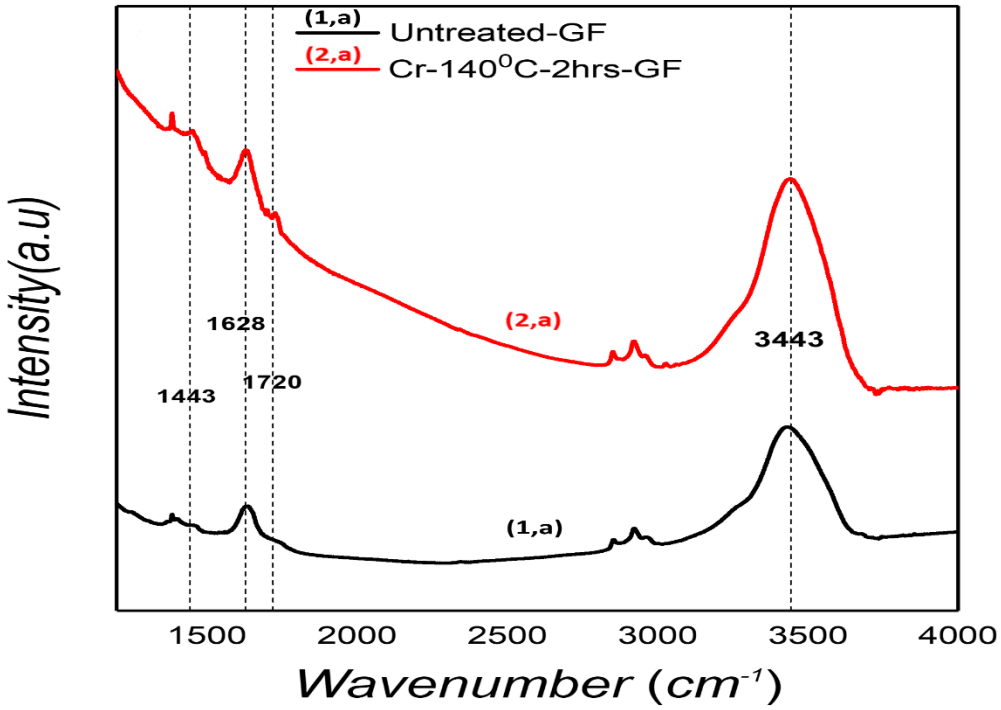


***Fig. B.8.*** *Characterization of the GF by Fourier-transform infrared spectroscopy (FTIR)*

seems to increase after treatment by the dichromate. Another important difference between the compared curves, is the new peak appearing at 1728 cm-1 and attributed to the stretching vibration of the carbonyl group (–C=O) [86,102]. To summarize, comparison of the FTIR spectra

demonstrates that the treatment by dichromate is responsible for the formation of oxygenated groups on the surface of the GF; however, this method does not enable to quantify the concentration of these groups.

2.3.3.3 *Surface analysis by linear sweep voltammetry (LSV)*

Linear sweep voltammetry is also used to confirm the existence of the oxygen groups on the felt**.** Fig. B.9 shows the voltammogram obtained at the steady state with the treated and untreated GF in the electrolyte of 3 M $H_2SO_4$ solution. The LSV curve of the untreated-GF only shows the oxygen and hydrogen evolution at 1.88 V and -0.88 V, respectively. Between this potential window, there is not any other oxidation nor reduction observed. Conversely, the voltammogram

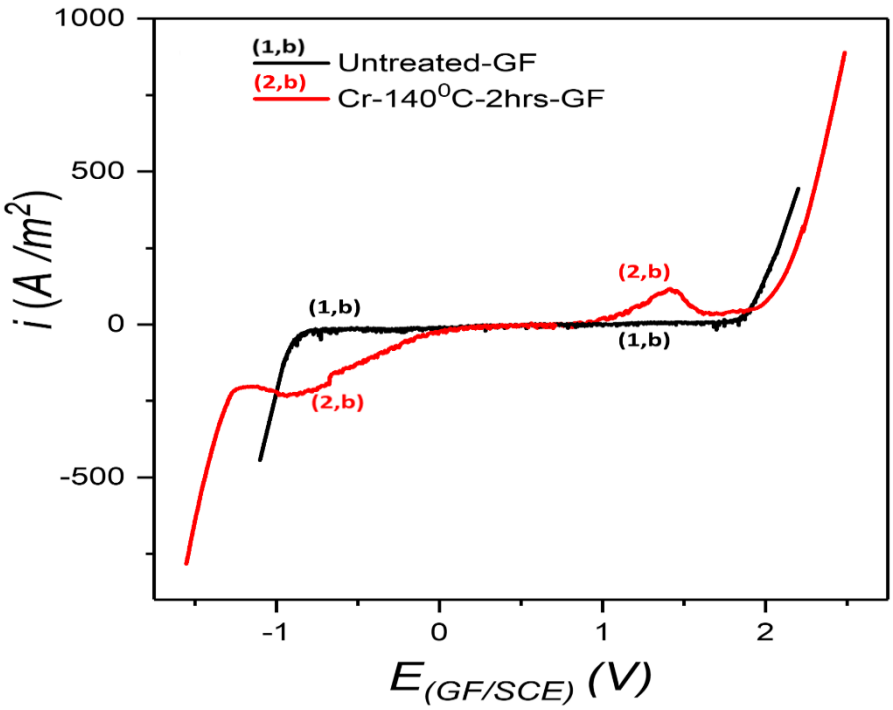


***Fig. B.9.*** *Characterization of the surface chemistry of GF by linear sweep voltammetry (LSV), $S_{GF}$=2.25 cm²; r= 1 mV/s; CE= Pt ~3 cm². Stirred solution of 3 M $H_2SO_4$ by magnetic bar at 350 RPM.*

obtained with the Cr-140 °C-2hrs-GF under the same set of conditions shows, in addition to the oxygen and hydrogen evolution, one anodic peak at 1.5 V and one cathodic peak at -0.6 V. These peaks are attributed to the oxidation and reduction of the carbon-oxygen groups present on the surface of treated felt, respectively. At 1.5 V, lower carbon oxidation state groups like hydroxyl group (C-OH) oxidize to higher oxides such as carboxylic and carbonyl groups (COOH, C=O) and vice versa for reduction side at -0.5 V [99].

### 2.3.4 Determination of Adsorption sites.

The activation overpotentials of the $VO^{2+}/VO_2^+$ redox couple reaction on the GF decrease as the adsorption tendency of vanadium species enhanced on GF [113]. To check the adsorption capacity of the GF towards vanadium compounds and to validate the efficiency of the treatment, the number of the surface sites available to the adsorption of the vanadium is quantified.

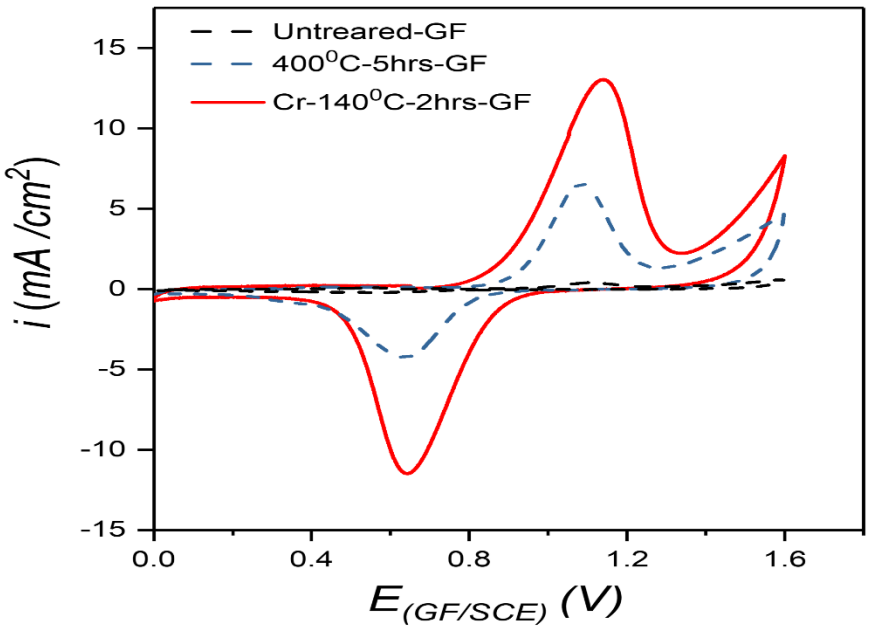


***Fig. B.10:*** *Cyclic Voltammetric curves obtained using untreated-GF, 400°C-5h-GF and Cr-140 °C-2h-GF, previously immersed in the solution of $VO^{2+}$ 0.5 M + 3 M $H_2SO_4$ for 5 minutes, and then rinsed with 3 M $H_2SO_4$. Electrolyte: 3 M $H_2SO_4$ unstirred solution; at 10 mV/s potential scan rate; $S_{GF}$=2.25 cm²; CE= Pt ~3 cm². First scan in the anodic direction.*

The precisely cut samples of each untreated-GF, 400 °C-5hrs-GF and Cr-140 °C-2hrs-GF are dipped in the 0.5 M $VOSO_4$ + 3 M $H_2SO_4$ solution for 5 minutes. After, the samples are taken out and thoroughly rinsed with 3 M $H_2SO_4$. Cyclic voltammetry curves are plotted in the unstirred solution of 3 M $H_2SO_4$ and the results are presented in fig. B.10. The untreated GF exhibits low magnitude signals of current i.e. $I_{(an.\ or\ cath.\ Peaks)} < 1$ mA/cm², showing the quasi-absence of any adsorption of the $VOSO_4$ at its surface.

The curve obtained by using 400 °C-5hrs-GF exhibits:

- an anodic peak of 6 mA/cm² between the potential range of 0.8 to 1.3 V, attributed to the oxidation of the adsorbed $V^{(IV)}$ and,

- a cathodic peak of 4.5 mA/cm² between the potential range of 0 to 0.6 V, attributed to the reduction of the electrogenerated $V^{(V)}$

The 140 °C-Cr-2hrs-GF shows the anodic peak of 14 mA/cm² and the cathodic peak of 12 mA/cm², almost doubled than thermally treated GF, implying a higher adsorption sites and consequently a better adsorption capability of the GF against the vanadium species.

The peaks of these voltammetry curves are used to determine the number of the adsorption sites on GF. This number is assumed to be equal to the number of molecules of vanadium converted and consequently the number of oxygen groups on surface, as these molecules are supposed to be adsorbed firstly on the oxygen groups of the electrode surface and then react. The following calculative sequence is applied i.e. integration of the peaks → amount of charge→ number of molecules→ number of sites→ number of surface carbon-oxygen groups.

The number "*a*" of the molecules of the vanadium ($VOSO_4$) adsorbed and converted, are estimated by the formula = Net charge of the anodic peak (Q) ×Avogadro number ($\mathcal{N}$) / ($1_{e^-} \times \mathcal{F}$) and the results are summarized in table B.2.

| | Untreated-GF | 400 °C-5hrs-GF | Cr-140 °C-2hrs-GF |
|---|---|---|---|
| Q (anodic peak) (C) | 0.01 | 0.14 | *0.32* |
| $a$ =number of molecules of $VO^{2+}$ converted =number of adsorption sites= number of oxygen groups/cm$^2$ geometrical area of GF | $5.3 \times 10^{16}$ | $87 \times 10^{16}$ | $200 \times 10^{16}$ |

***Table B.2.*** *Determination of the number of adsorption sites/oxygenated carbon atoms of the GF, on the untreated-GF, 400 °C-5 h-GF and Cr-140 °C-2 h-GF.*

The GF used for these measurements is a parallelepiped sized as 1.5 cm × 1.5 cm × 0.5 cm= 2.53 cm$^3$.

For the treated GF, the results lead to $200 \times 10^{16}$ molecules of vanadium adsorbed on the fibers of GF having a volume of 2.53 cm$^3$. As per assumption, the obtained number of molecules of vanadium corresponds to the number of C-O groups present on the GF fibers surface.

To get a rough estimation of the C-O groups on the GF fibers surface, we draw a parallel between the atoms of platinum presents on a smooth surface of a platinum plate, i.e. $10^{15}$ atoms/cm². Equivalent surface of the Cr-140°C-2hrs-GF = ($200\times10^{16}$ atoms/2.53 cm$^3$)/($10^{15}$ atoms/cm²)= 790 cm²/cm$^3$ in comparison with 21 cm²/cm$^3$ for the untreated GF. This equivalent surface appears to be high, especially for the GF fibers which appears to not have internal porosity into the fibers (Fig. B. 7). However, it shows that the GF exhibits high specific area, and this is very important for an optimized vanadium battery.

### 2.3.5 Wettability test.

The commercial graphite felt appears to exhibit hydrophobic behaviour, though its hydrophobicity seems to be strongly dependent on its age and storage location (corrosive atmosphere). Another objective of the chemical/thermal treatment of the GF by the dichromate is to improve its wettability towards the vanadium-sulfuric acid solution, expecting to enable all surface area of the electrode readily available for $VO^{2+} \rightleftharpoons VO_2^{+}$ reaction.

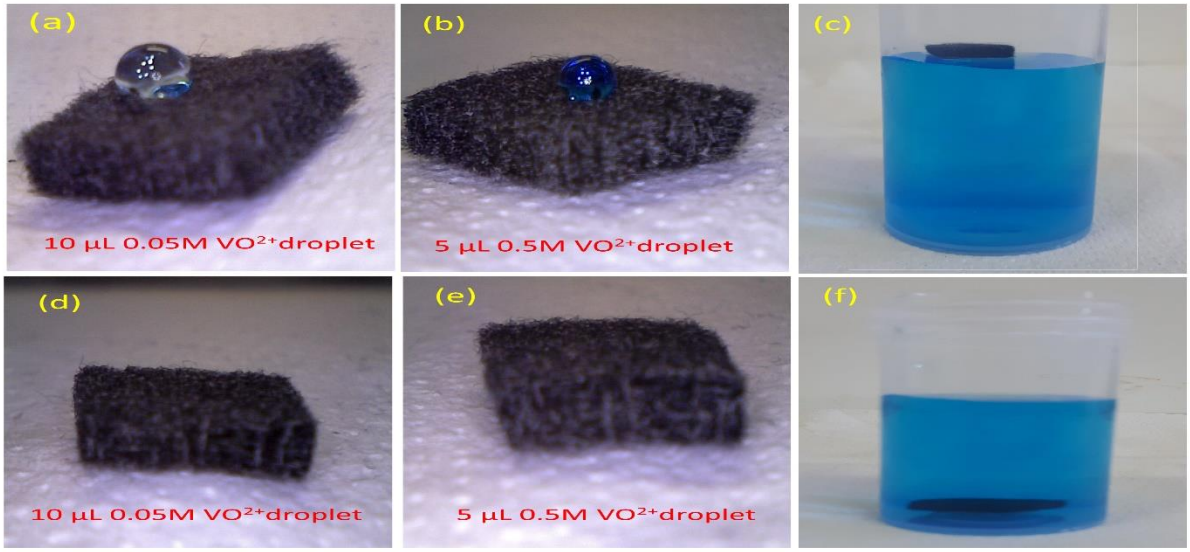


***Fig. B.11:*** *<u>Left side:</u> Images taken by Digital camera of electrolyte droplets deposited on GF; 10 µL droplet of 0.05 M $VO^{2+}$ +3 M $H_2SO_4$ on surface of Untreated-GF(a) and Cr-140 °C-2hrs-GF(d); 5 µL droplet of 0.5 M $VO^{2+}$+3 M $H_2SO_4$ on Untreated-GF (b) and Cr-140 °C-2hrs-GF (e). <u>Right side:</u> Tests of floating capacity of precisely cut Untreated-GF (c) and Cr-140 °C-2hrs-GF (f) in 0.05 M $VO^{2+}$ +2 M $H_2SO_4$ electrolyte.*

To evaluate the extent of wettability and hydrophilicity of the GF, two different experiments are performed. Two precisely cut (1 cm × 1 cm) GF samples are placed on the surface of a solution containing 0.05 M $VO^{2+}$ in 3 M $H_2SO_4$. The untreated-GF does not uptake the electrolyte and floats at the surface of the solution Fig. B.11, c. Contrary to that, the treated sample (140 °C-Cr-2 h-GF) immediately submerges into the vanadium solution Fig. B.11, f. This clearly demonstrates

that the chemical/thermal treatment of the GF by the dichromate decreases the repulsive interactions between the fibers and the electrolyte, thus enabling the hydrophilicity and wettability improvement.

A second wettability test is performed as: droplets of acidified solutions ($H_2SO_4$ 3 M) of the $VO^{2+}$ at two different concentrations (0.05 M and 0.5 M) are deposited on the surface of both untreated-GF (Fig. B.11, a, b), and treated one (140 °C-Cr-2 h-GF, Fig. B.11, d, e). For both solutions, the droplets are retained on the surface of untreated-GF (a, b), showing its poor affinity toward the aqueous acidic solution of the vanadium compounds. Conversely, both droplets penetrate immediately into the treated graphite felt Fig B.11(d, e). The modification of the GF-surface energy is quantified by using the Owens-Wendt "one liquid" method [116].

This technique enables the calculation of the surface energy of the electrode (Graphite felt), by measuring the liquid-contact angle of the two different liquid droplets of known polar and dispersive surface energy components on the solid surface (graphite felt) as per equation (B.7) and (B.8).

$$\gamma_{GF} = \gamma_{GF}^{P} + \gamma_{GF}^{D} \qquad \text{(B.7)}$$

$$\gamma_L(1 + \cos\theta)/(2(\gamma_L^D)^{0.5}) = (\gamma_{GF}^P\,\gamma_L^P/\gamma_L^D)^{0.5} + (\gamma_{GF}^D)^{0.5} \qquad \text{(B.8)}$$

Where: $\gamma_{GF}$= surface energy of GF; $\gamma_{GF}^P$= dispersive component of the surface energy of GF; $\gamma_{GF}^P$= polar component of the surface energy of GF; $\gamma_L$= total energy of the liquid; $\gamma_L^D$= Dispersive component of the surface energy of GF; $\gamma_L^P$= polar component of the surface energy of GF; θ= solid-liquid contact angle.

As shown in Fig. B.11 (d, e), the droplets of vanadium solutions diffused into the treated GF because of the fibrous structure of it, so it is not possible to perform contact angle measurement

in this case. To overcome this problem, untreated and treated Graphite felts are crushed and spread over a hydrophobic flat tape. Then, 5 µL droplet of water ($\gamma_L^D$=21.8 *m*N/m, $\gamma_L^P$=51.0 *m*N/m) and glycerol ($\gamma_L^D$=37.0 *m*N/m, $\gamma_L^P$=26.4 *m*N/m) were carefully placed on the two flat surfaces having graphite felt powder. As shown in the Fig. B.12 ( a, b), the contact angle of the water and glycerol on the untreated GF surface is 101° and 85°, respectively; these values reduce respectively to 75° and 69° on the treated GF surface (Fig. B.12, c, d). By plotting $(\gamma_L(1+\cos\theta))/(2(\gamma_L^D)^{0.5})$ vs $(\gamma_L^P/\gamma_L^D)^{0.5}$, the slope and intercept of the linear line give $(\gamma_{GF}^P)^{0.5}$ and $(\gamma_{GF}^D)^{0.5}$, respectively

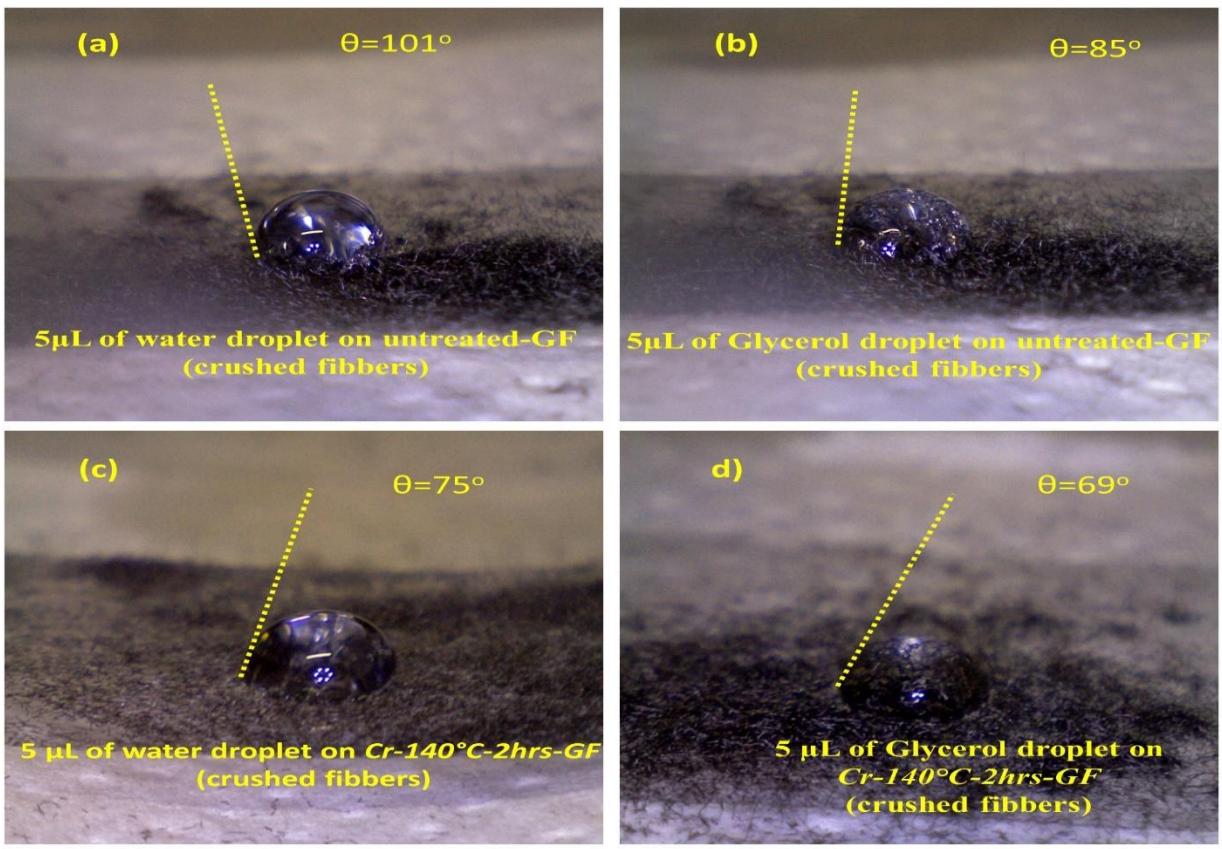


***Fig. B.12:*** *Contact angle measurements on the grinded GF (broken fibers); Images on the top: water (a) and glycerol (b) droplets of 5 µL size, deposited on untreated GF.-Pictures on the bottom: water (c) and glycerol (d) droplets of 5 µL size, deposited on treated GF (Cr-140°C-2hrs-GF).*

The surface energy calculations are summarized in the table B.3. The activation of the GF induces an increase of 20.3% of the total surface energy of graphite felt. The polar surface energy component of GF increases from 0.9 *m*N/m to 15.9 *mN/m*, while the dispersive surface energy component decreased from 23.7 *mN/m* to 13.7 *mN/m*. It indicates that the chemical treatment replaces the weak electrostatic forces of the surface represented by dispersive component by stronger chemical bonds i.e. the polar component. As the GF surface have weak electrostatic forces because of defective carbon edges and delocalized π bonds [77,100] and these defective edges and delocalized bonds get oxidized by the chemical treatment.

| | $\gamma_{GF}^{P}$ (mN/m) | $\gamma_{GF}^{D}$=(mN/m) | $\gamma_{GF}$ (mN/m) |
|---|---|---|---|
| Untreated GF | 0.9 | 23.7 | 24.6 |
| Treated GF | 15.9 | 13.7 | 29.6 |

***Table B.3.*** *Measured surface energies of untreated and treated GF (results extracted from Fig. 8);* $\gamma_{GF}$ *= Total surface energy;* $\gamma_{GF}^{D}$ *= Dispersive component of total surface energy;* $\gamma_{GF}^{P}$ *= Polar component of total surface energy*

### 2.3.6 Half-cell evaluation.

The performance of the treated graphite felt as the positive electrode is evaluated by the charge discharge cycles in a H-shaped classical cell, as shown in fig B.13, by employing 0.5M $VO^{2+}$ + 3M $H_2SO_4$ solution as positive half-cell electrolyte and 3M $H_2SO_4$ solution as negative half-cell electrolyte. The special GF-electrode assembly is prepared to avoid any kind of vibration because of strong stirring conditions as shown by inset of fig. B.14.

To prepare the assembly, a piece of the graphite felt (1.5 cm × 3 cm) is cut precisely; then a set of six copper wires that are acting as current collectors, are inserted in this graphite felt, with;

- 1 cm length of each copper wire inside the felt, and
- 0.5 cm above from the surface area devoted for electrolysis.

A layer of an inert epoxy glue is introduced into the GF, to define precisely the electrochemically useful surface i-e the bottom of the GF band. The glue also enables to avoid the contact of the copper wires i-e the top of the GF band, with the solution. The structure is sandwiched between two glass plates with only 1.5 cm × 1.5 cm exposed surface area of the GF, available for the electrolysis. Before evaluating the charge-discharge performance of the electrode, it is important to ensure that the surface of GF involved in the reaction is precisely defined and there is not any reaction occurring in the other parts of the GF, nor in the epoxy glue used to define the perimeter of the working area. Hence, blank curves are plotted in 3M $H_2SO_4$ electrolyte, as shown in fig. B.14 , with two different working electrodes as follows;

i) Set of six copper wires with 1 cm length immersed into the electrolyte (Electrode A)

ii) The specially designed GF electrode assembly (Electrode B)

As shown in Fig. B.14, the electrode (A) shows the huge anodic current starting from the 0 V, that represent the oxidation of the copper wires. There is not any such signal in the curve of the electrode (B), except the evolution of oxygen and hydrogen is observed at ~1.8 V and ~ -0.9 V, respectively. It indicates that the solution is not diffusing upward till copper wires and epoxy glue is inert in the chosen operating conditions

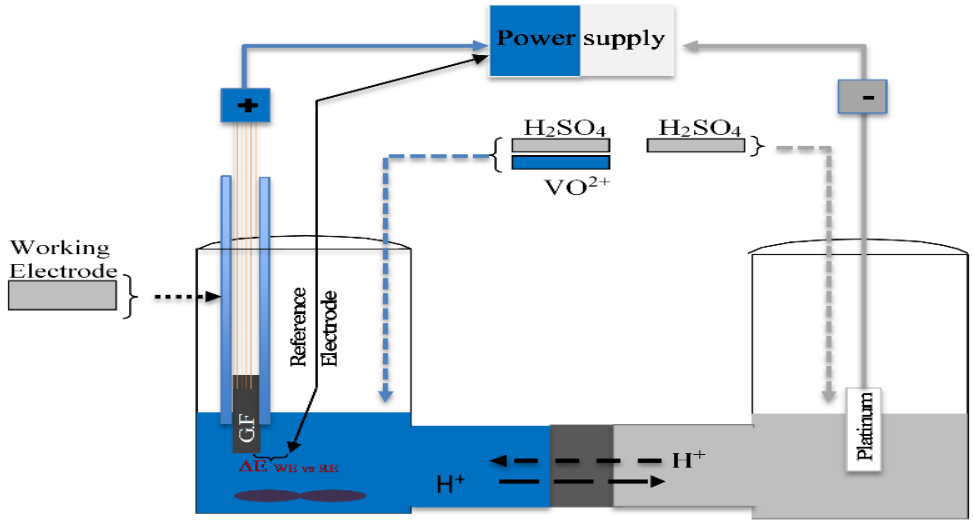


***Fig. B.13:*** *Half-cell used for charge-discharge cycles of vanadium positive half-cell.*

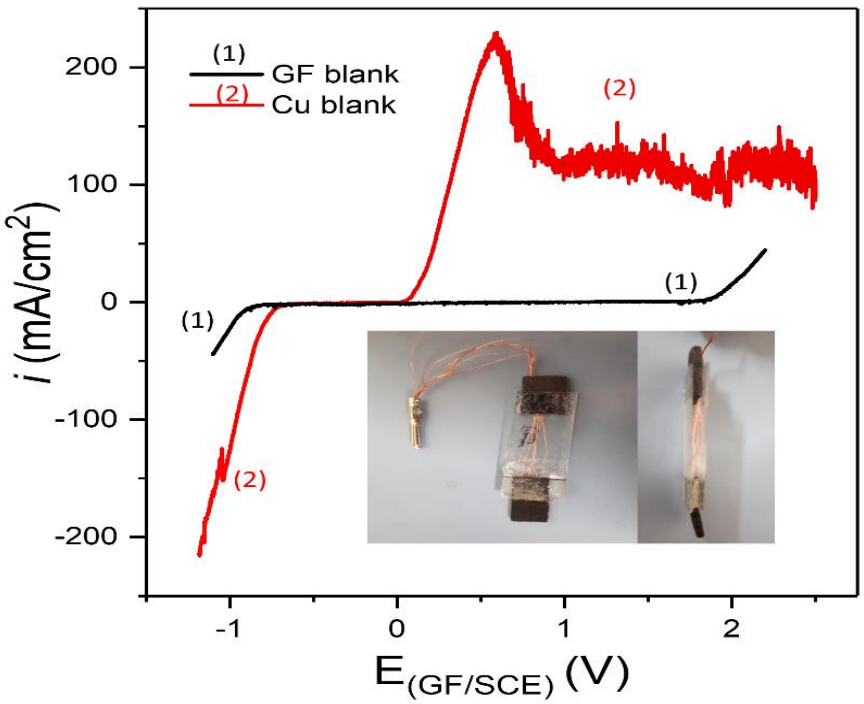


***Fig. B.14:*** *Comparison between linear sweep voltammograms (LSV) obtained with the Electrode (A) and Electrode (B), used as working electrodes, in stirred 3 M $H_2SO_4$ aqueous solution as electrolyte. Stirring rate with a magnetic bar (350 RPM); r = 1 mV/s; RE: SCE immersed into a Luggin capillary; CE: Pt mesh.* ***Inset****: Specially designed positive half-cell electrode sandwiched between two glass plates with copper wires as current collector*

After evaluating the electrode assembly, the charge-discharge cycles are performed to analyse the improvement occurred in the electrode due to treatment. The charging of positive half-cell, i.e. the oxidation of the $VO^{2+}$, is achieved under constant anodic current of 0.15 A / 2.25 cm². The electrolysis is stopped immediately as the electrode potential reach 1.65 V/SCE to avoid the oxidation of water. Fig. B.15 shows the comparative evolution of working electrode potential for both charge and discharge cycles. During the oxidation phase, the potential stays at ~1.19 V and ~1.07 V for untreated and treated graphite felt, respectively. The activation of the electrode resulted in the decrease of the overvoltage of ~0.12 V during the whole oxidation ($0<t_{(min)}<\sim237$) and confirms the beneficial effect of the chemical treatment by the chromium. The 94 % and 87 % conversion of $V^{(IV)}$ to $V^{(V)}$ is achieved for the treated and untreated GF, respectively. The 7 % increment is observed in the conversion of $V^{(IV)}$ to $V^{(V)}$ for the treated electrode. The improvement of concentration is because of the prolong time to reach 1.65V due to the lowering of treated electrode potential. In addition to that, the charging faradic yield improves from 95 % to 98 %.

For the reduction of the electrogenerated $V^{(V)}$ to $V^{(IV)}$, the same magnitude of the current is applied as while charging i.e. 0.15 A/cm$^2$. The current density is immediately reduced to 0.1 A/cm$^2$ as the potential of the treated GF reaches 0.75 V/SCE. The electrolysis is terminated when the electrode potential approaches 0.7 V/SCE to avoid any reduction of $V^{(IV)}$ to $V^{(III)}$. The treated graphite felt exhibits higher discharge potentials (~ 0.75 V) in comparison with untreated GF (0.4/ 0.3 V), showing the improvement of the reversibility of the graphite felt towards $V^{(V)}$ to $V^{(IV)}$ due to the activation. In addition to that , the treated electrode provides a certain stability of its potential during the reduction of $V^{(V)}$ to $V^{(IV)}$, comparatively to the untreated electrode in which no plateau is observed till 0.7 V. For the untreated GF, the discharge curve is observed

around 0.4 V, below the limiting fixed value of the potential; this confirms that the raw graphite felt exhibits poor electroactivity towards $V^{(V)} \rightarrow V^{(IV)}$ reaction.

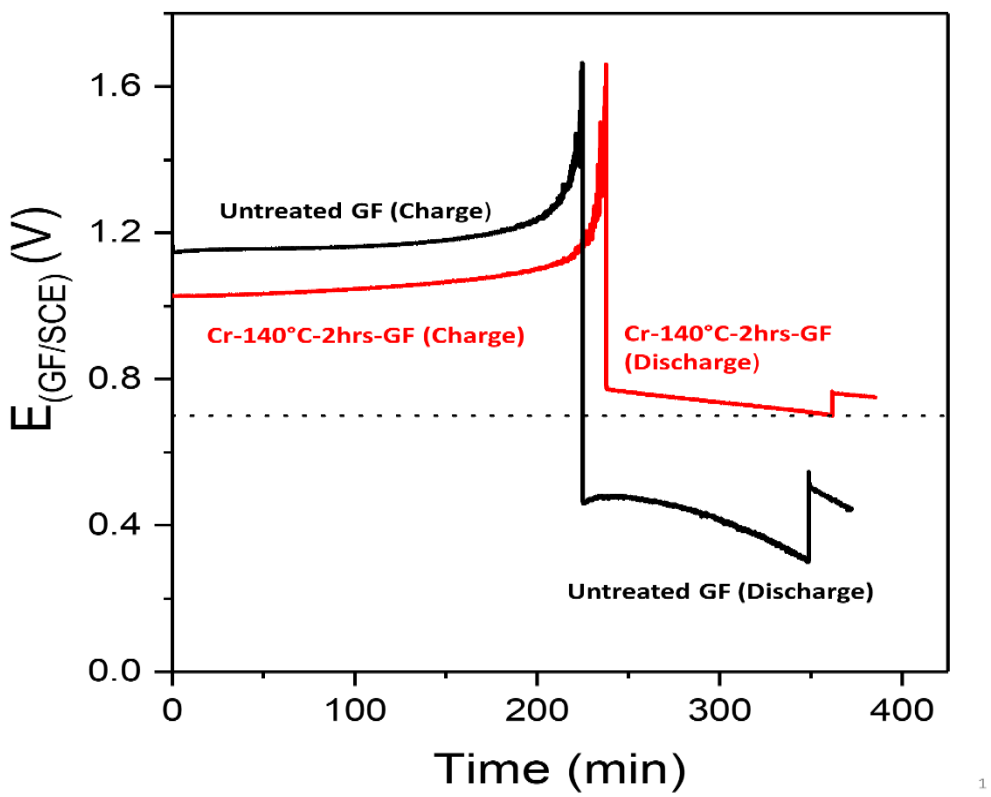


***Fig. B.15:*** *During the electrolysis, charge- discharge curves in half-cell assembly, with untreated-GF and Cr-140°C-2hrs-GF as positive half-cell electrodes;* $S_{GF}$*=2.25 cm²; CE= Pt ~3 cm²; 45 cm³ 0.5 M* $VO^{2+}$ *in 3 M* $H_2SO_4$ *as positive half-cell electrolyte with magnetic bar stirring at 350 RPM; 3 M* $H_2SO_4$ *electrolyte at the counter electrode compartment of the half-cell electrolyte.*

For untreated and treated graphite felt, the same amount of charge is supplied during discharge, but vanadium $V^{(V)}$ to $V^{(IV)}$ conversion is different for both electrodes i-e 48 % and 58 % for untreated and treated graphite felt, respectively. The possible reason of low discharge conversion in case of untreated electrode may be the overlapping of the secondary cathodic reaction of $V^{(IV)} \rightarrow V^{(III)}$ with the primary reaction i.e. $V^{(V)} \rightarrow V^{(IV)}$.

The three charge-discharge cycles are performed with Cr-140°C-2hrs-GF successively. The performance of treated electrode remains stable over the three consecutive cycles (16 h), thus demonstrating that the enhanced electroactivity of the treated GF against the vanadium is durable. The performance of the untreated-GF and Cr-140 °C-2hrs-GF is compared in table B.4

| Electrode used | Conversion (%) | | Faradic yield (%) | | Average voltage (V) | |
|---|---|---|---|---|---|---|
| | Recharge | Discharge | Recharge | Discharge | Recharge | Discharge |
| Untreated-GF | 87 | 48 | 95 | 73 | 1.19 | 0.42 |
| Cr-140 °C-2hrs-GF | 93 | 58 | 98 | 78 | 1.07 | 0.74 |

***Table B.4:*** *Results of half-cell electrolysis using untreated-GF and Cr-140 °C-2hrs-GF electrode.*

## 2.4. Conclusion

The electrochemical activity of a commercial graphite felt, expected to be used as positive half-cell electrode for vanadium redox flow batteries (VRFBs), is enhanced by thermal-chemical treatment with $K_2Cr_2O_7$ solution in sulfuric acid. The graphite felt is heated at different temperatures ($100<T_{(°C)}<160$) for different durations ($2<t_{(h)}<8$) in acidic dichromate solution, and afterward characterized by various physicochemical methods and techniques such as Fourier-transform infrared spectroscopy, scanning electron microscopy, voltammetry, and high magnification digital camera. The treatment successfully modifies the surface chemistry and morphology of the GF by creating carbon-oxygen functional groups (C=O, C-OH, -COOH) and inducing roughness.

The results indicate that the best electrochemical performance is achieved by chemical activations at 140 °C for 2h. The enhancement of the electrocatalytic properties of the graphite

felt against the $VO_2^+/VO^{2+}$system is evident by voltammograms and preparative electrolysis results. In cyclic voltammograms, $\Delta E_{a/c}$ decreased from 0.99 V to 0.61 V, while $I_a/I_c$ ratio decrease from 2.11 to 1.23.

The enhancement of the electroactivity is also evident by the increment of the intrinsic heterogeneous electronic transfer constant $k°$ by 2.2 folds for $VO^{2+}$oxidation and 5.5 folds for $VO_2^+$ reduction. Moreover, the carbon – oxygen sites formed on the surface of the fibers, increases from $5.3 \times 10^{16}$ to $200 \times 10^{16}$ after activation.

The treated graphite felt appears to be efficient and durable as demonstrated by the three successive electrolysis. The prescribed thermo-chemical treatment of the GF offer several advantages for the vanadium batteries i-e it is novel, operationally easy, effective as well as efficient and sustainable.

# Chapter: 3 *Activation of the electrode for vanadium redox flow battery (VRFB) by electrochemical treatment, chemical treatment and particle doping*

# **Chapter: 3** *Activation of the electrode for vanadium redox flow battery (VRFB) by electrochemical treatment, chemical treatment and particle doping*

## Context

In previous chapter, the chemical activation by the acidic $K_2Cr_2O_7$ solution was proposed, to activate the GF for the vanadium redox flow batteries. The electrode showed enhanced electro kinetic activity in classical half-cell electrolysis of the VRFBs. In this chapter, further activation approaches are tried to investigate. As discussed in the previous chapters, that the redox reactions in the flow batteries, are taking place on electrodes; and hence, the power density of the flow cell depends on the active surface area of the electrodes and their electro-kinetic activity. So, the electrode material, its surface area and kinetic activity is critical in the optimization of the vanadium redox flow battery stack. It is also important, because the stack is contributing approximately 30 % of the total cost of VRFBs [35].

The goal of this chapter is to explore further, different possibilities and methods for the activation of the GF electrode, that can show better electroactivity against the $VO^{2+} \rightleftharpoons VO_2^{+}$ redox reaction , than the results obtained in the chapter.2 (by acidic 5 M $K_2Cr_2O_7$). In addition to effectiveness of the activation method; the more points are also taken into consideration such as, the duration would be shorter, and the involved reagents should be less toxic. In the bibliography chapter 1, it is discussed that the GF electrode can be activated by the electrochemical oxidation, metal / metals oxide fabrication on the electrode surface, chemical and thermal treatment. In this chapter, all these different approaches would be used. The

electrodes that shows the improved electroactivity in cyclic voltammetry analysis, would be further characterized by the various tools. Also, the performance of the electrode is evaluated on the stack level, in the pilot scale electrochemical reactor. The brief discussion about the assembling of the pilot scale reactor and its individual components are also included in this chapter. Following methods and reagents are used in this chapter

1) Chemical activation by the $H_3PO_4$ acid;

2) Electrochemical activation in the solution of the $(NH_4)_2CO_3$.

3) Chemical activation within basic media (KOH).

4) Chemical activation with the acidic $KMnO_4$ solution

5) Fabrication of the $KMnO_4$ derived particles on surface of the electrode.

## 3.1 Methods.

*3.1.1 Cyclic voltammetry:* The electrode electrocatalytic activity is evaluated at transient state by cyclic voltammetry (CV) in classical three electrode cell. The 1 $cm^2$ piece of the GF is precisely cut and subject to CV at the following experimental parameters; scan rate: 10 mV. $s^{-1}$; in 0.05 M $VO^{2+}$ + 2 M $H_2SO_4$ electrolyte; between the potential ratio of 0 V to 1.6 V in unstirred conditions. The platinum foil of 3 $cm^2$ and saturated calomel electrode (SCE) are used as counter and reference electrode, respectively.

*3.1.2 Linear sweep voltammetry:* curves are plotted with the precisely cut graphite felt of 1.5 ×1.5 $cm^2$ at the following parameters; scan rate of 1 mv/sec, at stirring rate of 350 rpm. The experiments start in the anodic direction from the open circuit potential till 1.2 V, in the 0.5 M $VO^{2+}$ + 3 M $H_2SO_4$ electrolyte to study the kinetics of the of $V^{(IV)}$ to $V^{(V)}$. The reverse scan is performed towards cathodic direction in the electrolyte of $0.47<VO_2^+{}_{(M)}<0.49$ + 3M $H_2SO_4$, to evaluate the performance of GF for $V^{(V)}$ to $V^{(IV)}$ reaction. The $VO_2^+$ solution used for the reverse scan is obtained by the electrolysis of the 0.5 M $VO^{2+}$ + 3 M $H_2SO_4$ in half cell.

*3.1.3 Fourier transform infrared spectroscopy (FTIR):* The changes occurred in the surface chemistry of the GF are analyzed by the (FTIR) on thermo Nicolet 6700 (Thermo Fisher Scientific, USA). The untreated and treated GF are grinded for the sample preparation to perform the FTIR analysis. The 2.5mg of the grinded powder is mixed with 250 mg of the KBr and subject to the 10 ton of pressure to form a disk of 13 mm diameter.

*3.1.4 Scanning electron microscopy (SEM)*: The modification of surface morphology and roughness of the electrode is analysed at the acceleration voltage of the 10 KV by the scanning electron microscopy (SEM) on the Phenom XL (Thermo Fisher scientific, USA).

*3.1.5 Classical H-shaped half-cell:* The H-shaped divided lab scale reactor (shown in the inset of fig. C.15), is used to perform the charge discharge cycles. Initially positive half-cell constitutes by 0.5 M $VO^{2+}$ + 3 M $H_2SO_4$, while the negative half-cell contains the 3M $H_2SO_4$. The 1.5 cm x 1.5 cm GF electrode is used as the positive electrode, while 3 $cm^2$ strip of the platinum is used as negative electrode. The saturated calomel electrode (SCE), placed in a lugging capillary, is introduced to follow the potential of the positive electrode.

*3.1.6 Pilot scale electrochemical reactor:* The performance of the activated electrode is evaluated in the *electrochemical reactor* by charge-discharge cycles of vanadium redox flow batteries (VRFBs). The reactor consists of;

- Two electrolytic section (positive and negative)
- 100 $cm^2$ electrode of GF in each section.
- Membrane
- Gaskets
- Teflon and steel plates

The electrolytic compartment was fabricated by the two plastic plates with widow for the electrode (fig C 1, a, b). The electrode is placed in the window, and both plates are clamped with each other to fix the electrode (fig C. 1, b). In the similar way, the other electrolytic compartment was prepared. The corners of the electrolytic compartment are rounded to curve shape, to reduce the dead zones for the solution and to ensure uniform flow of the electrode over the electrode. The strip of the GF electrode was coming outside of these plates to act as the current collector. To reduce the ohmic resistance of the current collector (GF), the strip of platinized titanium is inserted into the part of the GF that is outside of the electrolytic compartment. To stop the

diffusion of electrolyte from the internal electrolytic section into current collector part of the electrode, the glue was inserted into the outer part of the electrolytic section, this polymerised and block the fibrous graphite electrode and stop the leakage.

Both electrolytic sections are separated by the nafion membrane to avoid the cross contamination and to have ionic connection. Then sequentially the Teflon and steel plates are placed on both sides of structure to assemble the filter press, with the help of screws and rods. The gaskets were placed between all the individual component of filter press to avoid the leakage. All the components of the filter press are shown in the fig C.1, c.

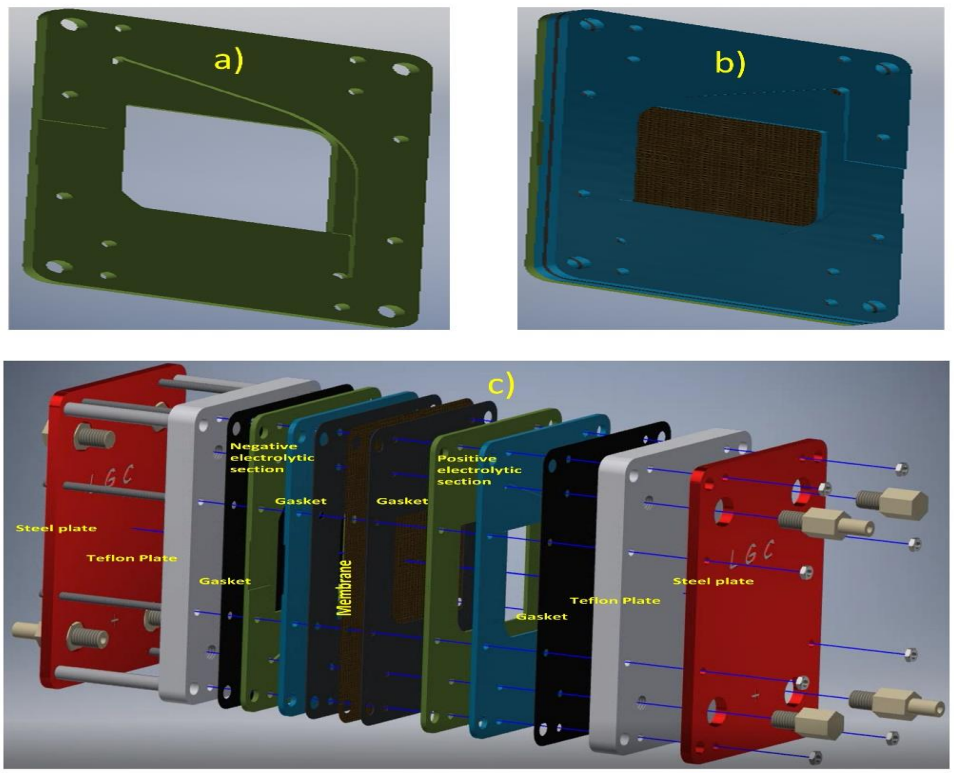


**Fig. C.1 *a*)** *The side view of the internal part of the plate of one electrolytic section; b) the clamping of the two electrolytic plates after inserting electrode inside; c) dismantle electrochemical reactor of VRFBs, comprising of steel plate, Teflon plate, gaskets, membrane, positive and negative half-cell electrolytic sections*

Two storage tanks containing the anolyte and catholyte, each having the capacity of 1 L, were coupled to the electrochemical plug flow reactor. The constant flow of electrolyte was maintained through the reactor during charge and discharge process. The electrolyte enters the reactor from downward and exit from upward, while doing the redox reaction on the interface of the electrode surface. The negative half-cell electrolyte is unstable in the presence of the oxygen and tend to re-oxidize to $V^{2+}$ . So, the constant supply of the supply of Argon was continuously provided in the negative storage tank to provide the inert environment. Whole assembly of the pilot scale electrochemical plug flow reactor is shown in fig. C.2.

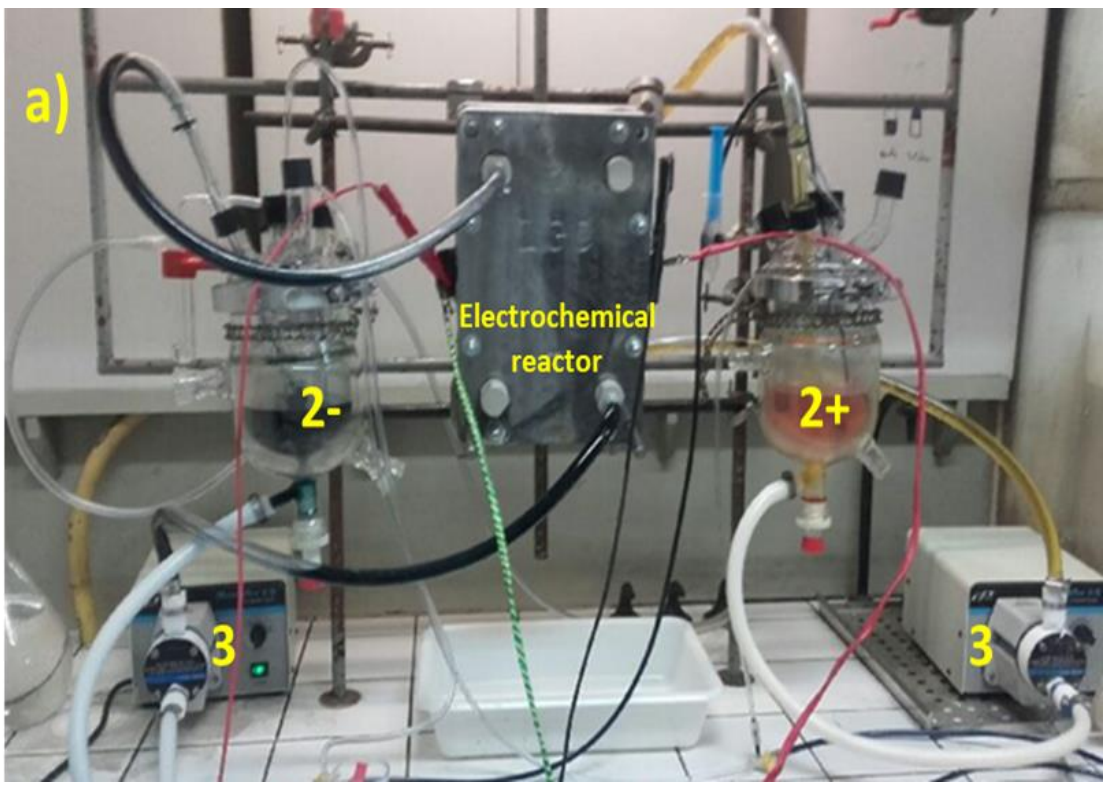


**Fig. C.2** **a)** *The vanadium redox flow battery having electrochemical reactor with 10 cm x 10 cm electrodes (1), accompanied by* posolyte *(2+) and* negolyte storage tanks *(2-) of 1 L capacity; with two pumps (3) for continuous flow of the electrolyte.*

## *3.2 Results and discussion*

### *3.2.1 Activation of the electrode by the $H_3PO_4$*

The phosphoric acid (85 %) is odorless and relatively mild solid, as in comparison with the nitric acid and sulphuric acid. In the literature, the concentrated sulphuric acid ( > 90 %) and nitric acid ( 67 %) was used to activate the graphite felt for the flow batteries at their boiling point [117]. It is very complicated to deal with boiling $H_2SO_4$ and $HNO_3$. In this section, $H_3PO_4$ is investigated to see its effeteness to treat graphite felt for VRFBs application.

The raw graphite felt, washed thoroughly with the distilled water for use as the reference. The phosphoric acid was taken in the round bottom flask. To heat the electrode in the phosphoric acid under reflux conditions, the round bottom flask was attached to the condenser. The contact flow of tab water was maintained through the condenser to condensed back all the vapor of acid. The temperature of the round flask was controlled by heating the oil bath.

After setting up the equipment, the graphite felt was heated in the phosphoric acid (85 %) for 5 h. at 80 $^{o}$C under the reflux conditions. Then the hot oil bath was replaced by the water bath to cool down the phosphoric acid to the 25 $^{o}$C. Then, the condenser was carefully detached from the round bottom flask and acid was carefully discarded from it. The electrode was carefully picked from the flask and washed with the distilled water several times. For the comparison, two different samples were also prepared by $H_2SO_4$ and $HNO_3$, respectively.

The same experimental setup was used for preparing GF samples by $H_2SO_4$ and $HNO_3$ . One sample was prepared by heating the GF in the 98 % sulphuric acid for 5 h, and other was prepared by heating in nitric acid (68 %), under reflux conditions. The sample were thoroughly washed with the distilled water. and dried in the oven for further use.

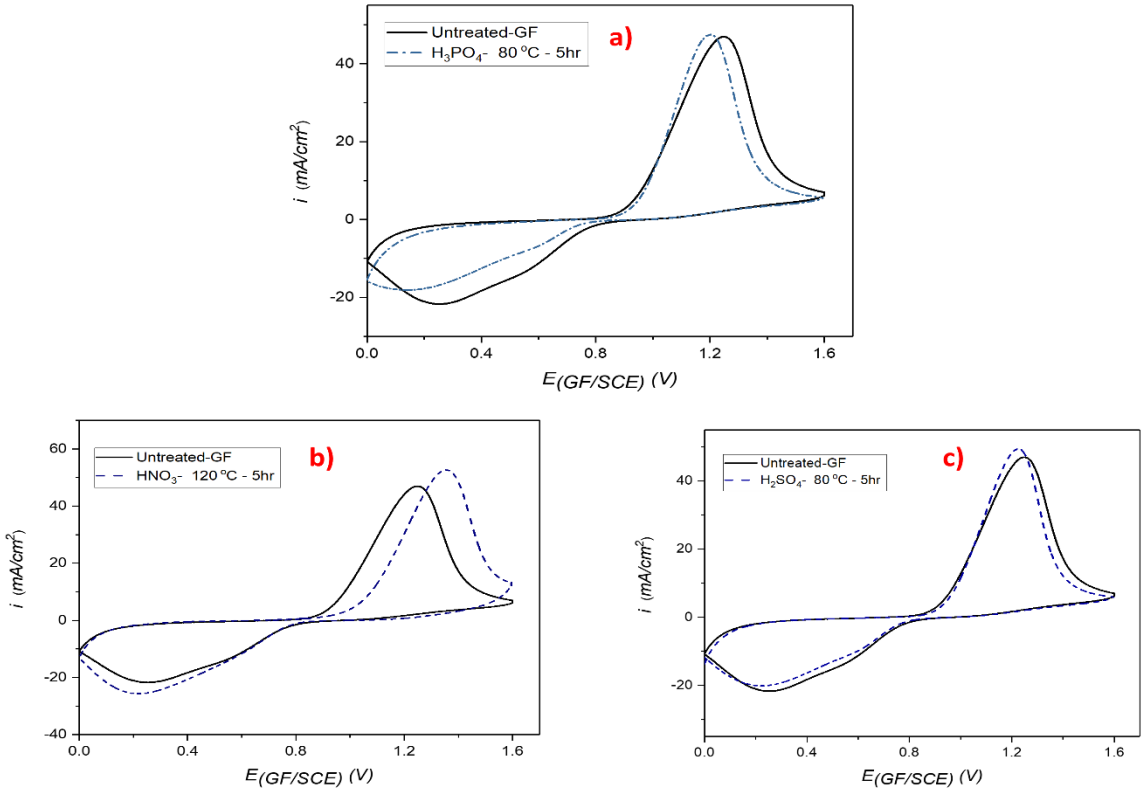


**Fig. C. 3** *The CV curves of GF electrode treated with the a) $H_3PO_4$ at 80 °C (5 h), b) with $HNO_3$ at 120 °C (5 h), and with $H_2SO_4$ at 80 °C (5 h); the GF is immersed in 0.05 M $VO^{2+}$ + 2 M $H_2SO_4$ ; at scan rate of 10 mV $s^{-1}$, 3 $cm^2$ platinum foil as counter electrode and saturated calomel electrode (SCE) as reference electrode*

Fig C. 3 shows the cyclic voltammograms of all the $H_2SO_4$ , $HNO_3$ and $H_3PO_4$ treated electrodes. The $H_3PO_4$ treated electrodes did not induce any improvement in the performance of the electrode. The electrodes activated by the $H_2SO_4$ and $HNO_3$, also showed more and less same behavior as the untreated electrode. In all the curves, there is not any well-defined cathodic signal in the reverse scan (just like the untreated electrode). This indicates that adsorption affinity and electrolyte interaction with the all acid treated electrode towards $VO^{2+}/VO_2^+$ is very poor and it does not induce any improvement in the catalytic activity of the electrode. The very negligible variation in the anodic current, in comparison with untreated electrode, is possibly due to some adsorbed acidic adsorbed species.

### *3.2.2 Activation of the electrode by KOH*

In pervious section, the effect of acids is analyzed for the activation of the GF, but electrode do not show any enhancement of his kinetics. In this section, the effect of base on the activation of the GF is investigated. The KOH can possibly have to react with the surface of the GF electrode. Different samples of the GF were prepared and treated in various conditions.

In first investigation, the GF was pretreated at 350 $^{o}$C in the muffle furnace 1) to remove the bubbles of air from the fibrous structure of the electrode 2) to anneal the surface 3) and to create the surface defects in the surface. The thermal pretreated electrode is expected to be more reactive with the KOH solution. The pretreated electrode was immersed in 1 M KOH and heated at 70 $^{o}$C for 90 min. During this process, some part of the KOH solution was lost due to water evaporation; because heating was done under non-reflux conditions. The sample is carefully extracted from the basic solution and washed thoroughly with the distilled water several times. This electrode is named as "Heat-KOH". The second sample is also prepared by following the same procedure as in first sample, but the sequence of the heat and KOH treatment is changed. The sample was heated in KOH solution first and then subject to the heat treatment (KOH-Heat).

The cyclic voltammograms of both samples are shown in fig C.4. The potential peak differences *($\Delta E_{a/c}$)* and anodic to cathodic peak current ratio *(Ia / Ic)* of the voltammograms shows that the KOH-HEAT sequence is more effective than the HEAT-KOH treatment (table C. 1). The *($\Delta E_{a/c}$) and (Ia / Ic) of* the KOH- Heat is 0.75 and 1.54 respectively; in comparison with the HEAT-KOH, which have *($\Delta E_{a/c}$) = 0.97 and (Ia / Ic) = 1.95*

The better performance of "KOH-HEAT" GF could be due to the fact; the KOH grooves the surface to some extent, and when the heat treatment was applied, it oxidizes a more important

surface and attach more surface compounds. In opposite sequence (HEAT-KOH), when GF was heated first, it impregnates some oxygenal groups on its surface; but the KOH treatment neutralize these surface oxygenal groups compounds, because most of them are acidic in nature.[118]

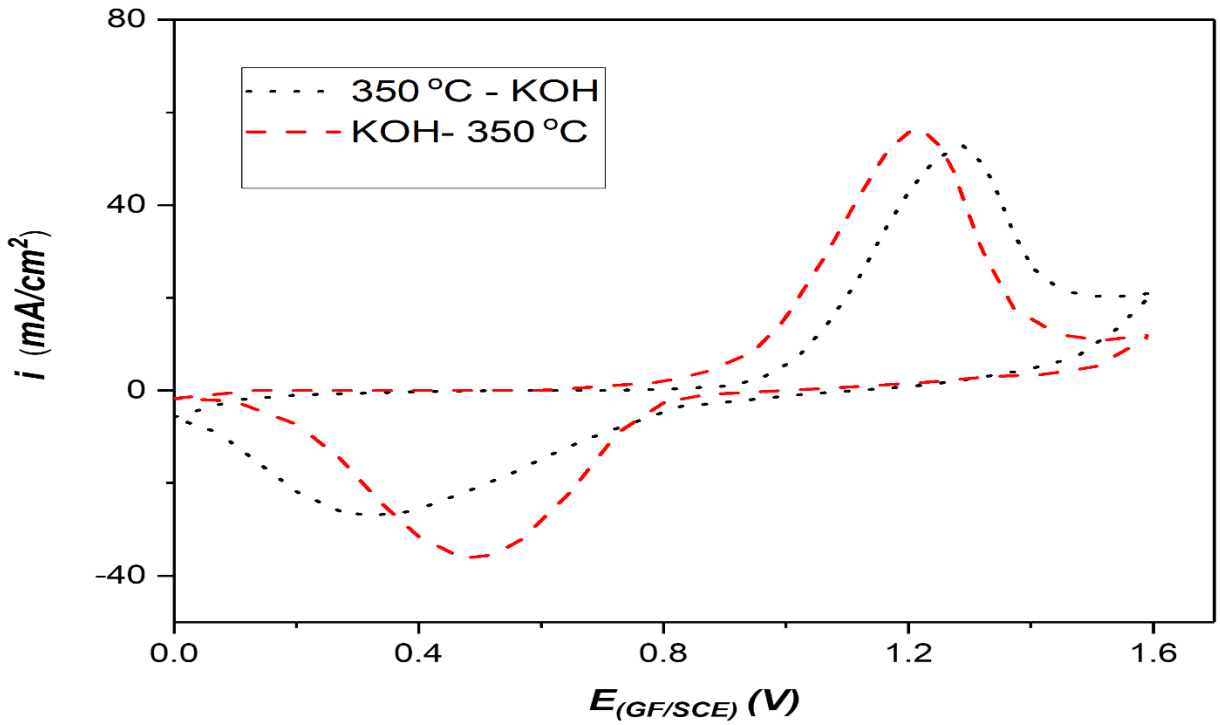


**Fig. C.4** *The CV of treated electrode of both sequences " KOH-Heat" and "Heat-KOH" ; the GF is immersed in 0.05 M $VO^{2+}$ + 2 M $H_2SO_4$ ; at scan rate of 10 mV $s^{-1}$, 3 $cm^2$ platinum foil as counter electrode and saturated calomel electrode (SCE) as reference electrode*

| Electrode | *Ia (mA)* | *Ic (mA)* | *Ia/Ic* | *Ea (V)* | *Ec (V)* | $\Delta E_{a/c} = E_a - E_c$ *(V)* |
|---|---|---|---|---|---|---|
| **KOH-Heat** | 55.95 | -36.28 | 1.54 | 1.21 | 0.46 | 0.75 |
| **Heat-KOH** | 52.82 | -27.06 | 1.95 | 1.289 | 0.31 | 0.97 |

***Table C.1:*** *Comparative results of the performance parameters of GF treated by following two ways "KOH-Heat" and "Heat-KOH". The results are extracted from fig. C.4*

As the sequence "KOH-HEAT" is more effective, the effect of different parameters is further examined in this sequence. The effect of the thermal temperature of the furnace is first explored in this section. The following two samples were treated;

- The first GF is heated in 1 molar KOH solution for 90 min at the 70 $^{o}$ C. After it, the sample is thoroughly washed with the deionized water. And subsequently heated in furnace at **350 $^{o}$C** for the 5 hrs. (same as in last experiment). It is named as ***KOH-350 $^{o}$C.***

- In the preparation of second sample, only the temperature of the furnace is changed to the 400 $^{o}$C. Other conditions are same. So, the GF is heated in 1 molar KOH solution for 90 min at the 70 $^{o}$ C. After it, the sample is thoroughly washed with the deionized water and subsequently heated in furnace at **400 $^{o}$C** for 5 h. (***KOH-400 $^{o}$C).***

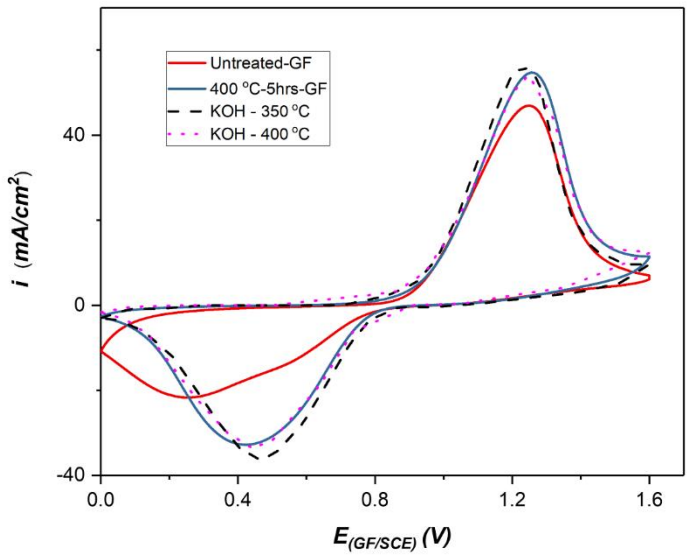


**Fig. C.5.** *The CV curves of "untreated electrode"-"heat treated electrode"-" KOH-350" -" KOH-400" ; the GF immersed in 0.05 M $VO^{2+}$ + 2 M $H_2SO_4$ ; at scan rate of 10 mV $s^{-1}$, 3 $cm^2$ platinum foil as counter electrode and saturated calomel electrode (SCE) as reference electrode*

- For the reference, heat-treated sample is also prepared, in which GF was heated at 400 $^{o}$C for 5 h in the muffle furnace. (400 $^{o}$C-5 h-GF)

The cyclic voltammetry curves of all samples are shown in the fig. C. 5 The voltammograms of the both samples "KOH-350 $^{o}$C" and "KOH-400 $^{o}$C" are almost overlapping with voltammograms of the 400 $^{o}$C-5 h-GF. It could be concluded that in the coupled heat-KOH treatment, the KOH is practically not contributing towards GF activation, at given parameters. Besides, when the temperature, is increased from 350 $^{o}$C to 400 $^{o}$C, the peak currents and potentials differences of the voltammograms does not change alot. So, in the coupled "KOH-Heat" treatment, the increment of the temperature from 350 $^{o}$C to 400 $^{o}$C is not really affecting the performance of the electrode.

In previous experiment, the duration of the heating in furnace was investigated in the coupled KOH-heat treatment. Also, it was observed that the KOH was not affecting the GF, at the duration of 90 min. In the next experiment, the duration of KOH is increased from 90 min to 180 min, to see the effect of the duration of KOH heating. For that, two different samples are prepared with two different durations of the KOH treatment.

- First sample was prepared by heating the GF in 1 molar KOH solution for **90 min** at the 70 $^{o}$ C. After it, the sample is thoroughly washed with the deionized water. And subsequently heated in furnace at 350 $^{o}$C for the 5 hrs. (same as in last experiment). It is named as ***KOH 90-350 $^{o}$C.***
- Second sample was prepared by heating the GF in 1 molar KOH solution for **180 min** at the 70 $^{o}$ C. After it, the sample is thoroughly washed with the deionized water. And subsequently heated in furnace at 350 $^{o}$C for 5 hrs. It is named as ***KOH 180-350 $^{o}$C.***

The voltammograms of both samples are shown in fig. C. 6. The voltammograms of both samples are almost overlapping with each other. It indicates, that increase in the duration of KOH treatment in the coupled "KOH-Heat" treatment, does not add any improvement in the performance of the electrodes.

***The conclusion*** remarks about the coupled KOH treatments: The minor improvement is observed in the case of coupled "KOH-heat" treatment ($I_a / I_c$ =1.54, $\Delta E_{a/c} = 0.75$ ), but it is far less effective than the acid $K_2Cr_7O_7$ treatment ( $I_a / I_c = 1.23$, $\Delta E_{a/c} = 0.61$ V) , that was proposed in chapter 2. So, it is not effective strategy to treat graphite felt. and, hence not be discussed further in this chapter

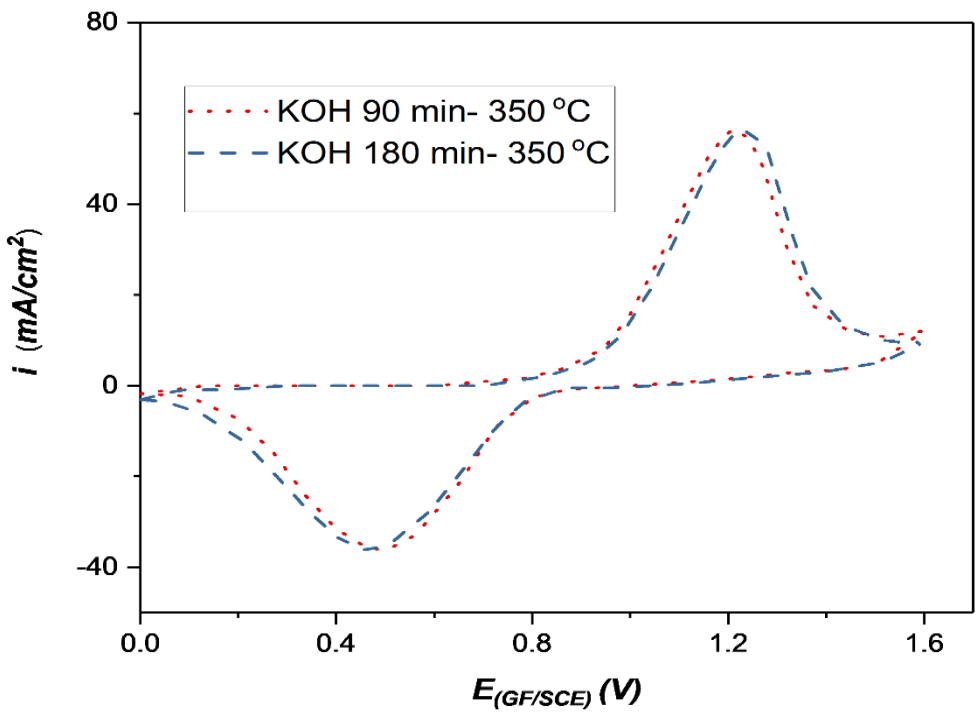


**Fig. C. 6** *The CV curves of treated electrode with both sequences " KOH 90-350 °C" and "KOH 180-350 °C" , the GF is immersed in 0.05 M $VO^{2+}$ + 2 M $H_2SO_4$ ; at scan rate of 10 mV $s^{-1}$, 3 $cm^2$ platinum foil as counter electrode and saturated calomel electrode (SCE) as reference electrode*

### *3.2.3 Activation of the electrode by an electrochemical treatment with $(NH_4)_2CO_3$*

Xin et. al [119] treated the carbon fibers in the ammonium salts, including $(NH_4)_2CO_3$, by electrochemical oxidation. The carbon fibers were successfully integrated by the surface oxygenal groups and the surface become rougher. In this section, the electrochemical treatment is applied on the GF for the VRFBs application, by using $(NH_4)_2CO_3$ aqueous electrolyte. First the untreated GF was thoroughly washed with the distilled water and then subject to the thermal pretreatment at 400 $^oC$ for 5 h (400 $^oC$-5hrs-GF). The strip of 3 x 10 $cm^2$ of the GF was precisely cut, and geometrical area of 3 x 3 $cm^2$ was precisely delimited by the glue.

The 3-electrode cell was used to apply the electrochemical activation method. The GF and platinum strip were used as the working and counter electrode respectively. A saturated calomel electrode was used as reference electrode.

- First set of samples were prepared by applying the anodic current of 30 mA for 1.5 min, 10 min and 20 min, respectively.
- Second set of samples were prepared by applying the voltage of 1 V and 2 V respectively, at the constant duration of 1.5 min.

During the electrochemical activation, the oxygen is producing at the Graphite felt-electrolyte interface, and it is important to have stirred condition to remove continuously the bubbles from the fibrous structure of the GF. After the end of the electrochemical activation, the working electrode was removed from the 3-electrode cell and washed thoroughly to remove any kind of the adsorbed species.

After drying all the samples, the cyclic voltammetry analysis was performed to analyze the electrochemical performance of these electrodes (Fig C. 7). The analysis of these curves shows

that the performance of the GF electrochemically treated, is lower than thermally treated electrode 400 °C-5hrs-GF, specifically in the cathodic region. In first set of samples, when the duration of the electrochemical treatment increases from 1.5 min towards 20 min at 30 mA, the

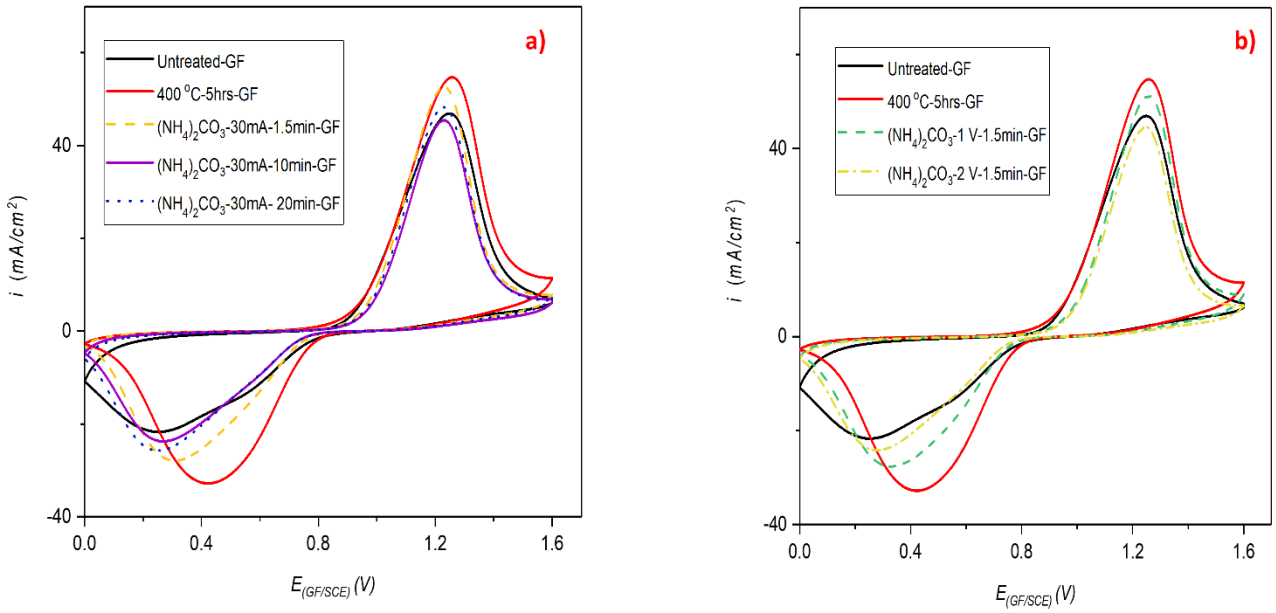


**Fig. C. 7** *The CV curves of electrochemically treated electrodes with $(NH_4)_2CO_3$ a) at 30 mA for the durations of the 1.5 min, 10 min and 20 min respectively. b) at 1 V and 2 V respectively for the constant duration of the 1.5 min;*
*The GF is immersed in 0.05 M $VO^{2+}$ + 2 M $H_2SO_4$ ; at scan rate of 10 mV $s^{-1}$, 3 $cm^2$ platinum foil as counter electrode and saturated calomel electrode (SCE) as reference electrode*

peak currents and peak potential difference decreased (Fig C. 7 a). There is almost no change in the anodic area nor cathodic area of the peaks, compared to the untreated electrode. The similar kind of behavior was observed in the second set of samples, in which when the applied anodic voltage was increased from the 1 V to 2 V at constant duration of the 1.5 min, the peak current of the voltammograms were decreased. The oxygen production at the electrode electrolyte interface during the electrochemical treatment, may strip the already existing oxygenal groups by

converting them into the $CO_2$ .[99] To conclude, the electrochemical oxidation of GF in the $(NH_4)_2CO_3$ ,does not improve the electro activity of the GF, against the $VO^{2+/}VO_2^+$

### *3.2.4 Activation of the electrode with potassium permanganate*

$KMnO_4$ is the strong oxidizer and can possibly be used to activate the carbon electrodes [120]. Also, Wang et al. [121] fabricated the $MnO_2$ nanosheets array-decorated carbon paper by $KMnO_4$ and it showed improved electroactivity as negative half-cell electrode in VRFBs. In this study, GF was activated by adopting two different approaches. First approach is concerned to change the surface chemistry and roughness of the GF, by heating it in the $KMnO_4$ acidic solution and named as class-1 for further reference. Second approach is concerned to fabricate residuals potassium permanganate particles on the surface of the GF, to analyse their effect against $VO^{2+}/VO_2^+$ reaction and described as Class -2 in further text. Both are discussed in detail, as following.

#### *3.2.4.1 Class -1 approach*

The purpose of this treatment is to functionalize the surface of the GF by harnessing the oxidizing power of acidic $KMnO_4$ solution. For this, the commercial GF was thoroughly rinsed with the distilled water and used as reference (untreated-GF). After, it was pre-treated at 400 $^oC$ for 2 h in muffle furnace to had better solution interaction while chemical activation (400 $^oC$ -2 h-GF). The annealed GF was heated at 140 $^oC$ for 2 h in 0.01 M $KMnO_4$ + 3 M $H_2SO_4$ solution, under non-reflux conditions ($KMnO_4$-140 $^oC$-2 h-GF). Then the GF was washed with hot and cold distilled water several times to remove any kind of the acidic and $KMnO_4$ residues.

*3.2.4.2 Class -2 approach*

During this operation, two different GF samples were prepared to investigate the following two possibilities:

1) To fabricate the thermally cracked $KMnO_4$ particles on the GF and check the enhancement of GF electroactivity against $VO^{2+}/VO_2^+$ redox system ($KMnO_4$-600 $^oC$-$N_2$-GF).

2) To deposit the $KMnO_4$ particles (without chemical decomposition) on the GF and investigate their catalytic effect against the $VO^{2+}/VO_2^+$ redox system ($KMnO_4$-400 $^oC$-air-GF).

First sample was prepared by dipping the GF in the beaker, containing 0.01 M $KMnO_4$ + 3 M $H_2SO_4$ solution, and then put this beaker in the oven at 80 $^oC$ until all the solution was evaporated. The obtained dry GF, covered with residual permanganate was heated at 600 $^oC$ in the nitrogenous environment for 90 minutes, to thermally decompose the $KMnO_4$ compounds and to have GF surface covered with cracked $KMnO_4$ particles ($KMnO_4$-600 $^oC$-$N_2$-GF).

Second sample was prepared by adopting the similar procedure as above, except 1) the operating temperature was fixed for oven at 400 $^oC$ and 2) the presence of the air in the oven. The purpose of heating at 400 $^oC$ was to attach the residual permanganate on the GF surface. As the objective here, was not to thermally crack the $KMnO_4$, so the temperature chosen was lower (400 $^oC$) than the previous one (600 $^oC$). Both samples were washed thoroughly with the distilled water containing few drops of $H_2SO_4$

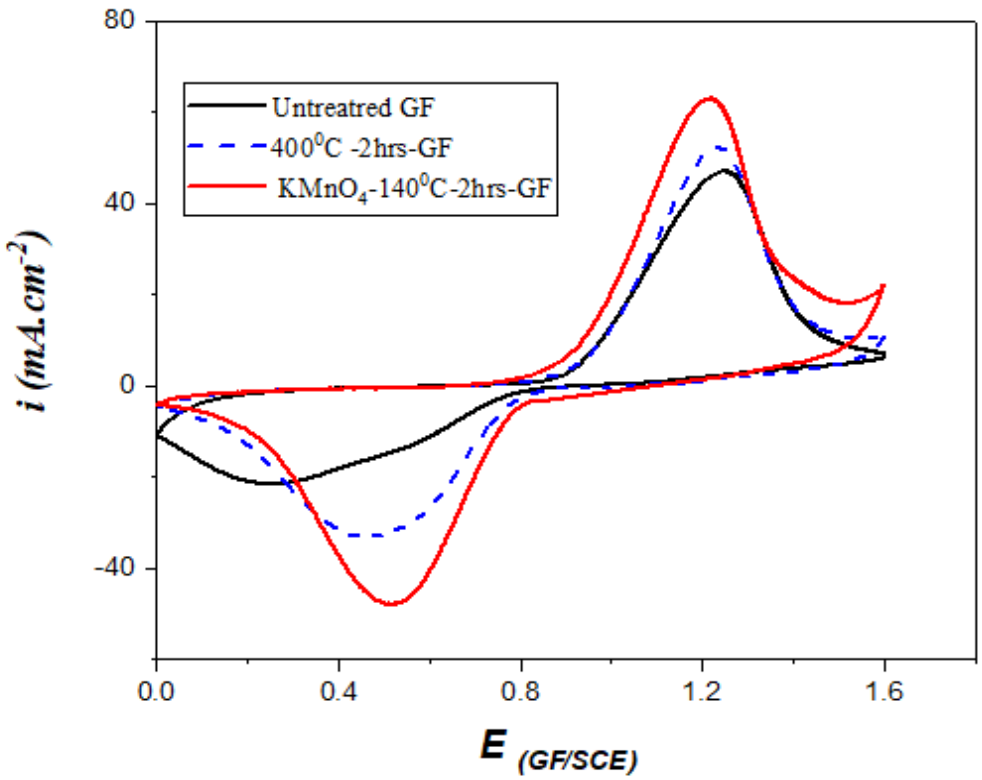


**Fig. C.8** *The CV curves of the class-1 electrodes; the GF is immersed in 0.05 M $VO^{2+}$ + 2 M $H_2SO_4$ ; at scan rate of 10 mV $s^{-1}$, 3 $cm^2$ platinum foil as counter electrode and saturated calomel electrode (SCE) as reference electrode*

Fig. C. 8 shows the voltammograms of the class-1 treaded electrodes. The peak observed around 1.1 V- 1.3 V shows the oxidation of the $VO^{2+}$ to $VO_2^+$, while peak in the reverse scan shows the reduction of the $VO_2^+$ to $VO^{2+}$. In the case of untreated electrode, the reverse scan does not have the well-defined peak, indicating the poor reversibility of the electrode. All the performance parameters (*Ia, Ic, Ia/Ic,* $\Delta E_{a/c}$) are improved due to the prescribed activation procedure, as summarized in the table C. 2. The increment of ~35 % is observed in the magnitude of peak currents and peak potential difference is minimized by 300 mV. The improvement of the electrochemical activity of the GF is due to the oxygenal functional groups and roughness, that is fabricated on surface because of the chemical treatment. The oxygenal groups act as the catalytic sites for the $VO^{2+}/VO_2^+$ redox reaction. The surface roughness increases the available surface

area for positive half-cell reaction and reflected in the increase of the anodic ($I_a$ ) and cathodic ($I_c$ ) currents.

| GF samples | $I_a$ (mA) | $I_c$ (mA) | $I_a$ / $I_c$ | $\Delta E_{a/c}$= $E_a$ -$E_c$ (V) |
|---|---|---|---|---|
| Untreated-GF | 46.9 | 21.7 | 2.16 | 0.99 |
| 400 ºC -2h-GF | 52.5 | 33.25 | 1.57 | 0.77 |
| $KMnO_4$-140 ºC-2h-GF | 63.1 | 48.03 | 1.31 | 0.70 |

***Table C. 2****: Comparative results of the performance parameters of class- 1 electrodes. The results are extracted from fig. C.8 voltammograms.*

Fig. C.9 shows the voltammograms of the class-2 treaded electrodes, in which the $KMnO_4$ particle are adsorbed on the electrode surface. Four peaks are observed in the CV, two in anodic directions and two in cathodic section. Peaks at 1.1 V/1.4 V and 0.4 V/0.6 V are the signals of the oxidations of $VO^{2+}$ and reduction of $VO_2^+$, respectively. The additional peaks at 0.8 V/1.3 V and 1.5 V/1.6 V is due to the reduction and oxidation of $KMnO_4$ derived species, respectively.

Following conclusions could be drawn from these CV observations of class-2 electrodes;

1) The residual $KMnO_4$ and all the compounds resulting from its reduction are strongly adsorbed on the surface, as the 10$^{th}$ cycle of the CV has the huge signal of their reduction and oxidation

(2) The residual $KMnO_4$ does not exhibit any catalytic behaviour against the $VO^{2+}/VO_2^+$ redox couple; and in addition to that, these particles are getting additional power to oxidize and reduce back on the surface. 3) There is still little increase in the peak current of $VO^{2+}/VO_2^+$ reaction in comparison with the untreated electrode, certainly because of the increase in the surface area of the GF .

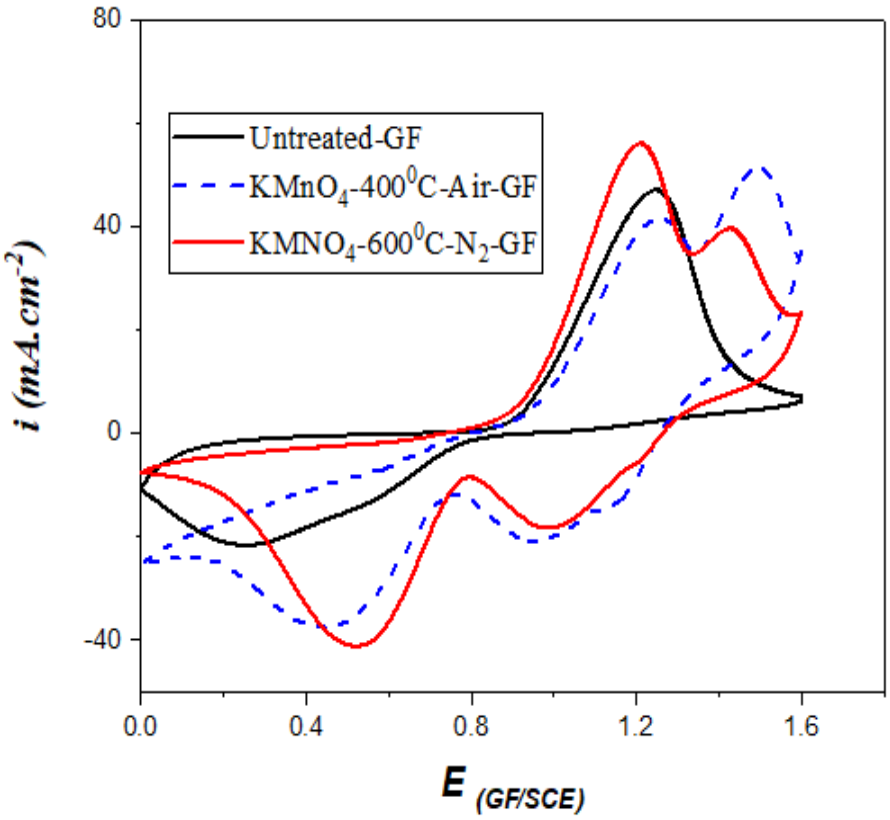


**Fig. C 9** *The curves CV of the class-2 electrodes; the GF is immersed in 0.05 M $VO^{2+}$ + 2 M $H_2SO_4$ ; at scan rate of 10 mV $s^{-1}$, 3 $cm^2$ platinum foil as counter electrode and saturated calomel electrode (SCE) as reference electrode*

So, the CV analysis concluded that the class-1 GF electrode, chemically activated by an acidic $KMnO_4$ solution ($KMnO_4$- 140 $^oC$-2 h-GF) exhibits enhanced electrocatalytic activity against $VO^{2+}/VO_2^+$ redox reaction. On the other end, the class-2 GF electrodes having residual $KMnO_4$ particles (and derived adducts) on their surfaces, do not show any improvement against positive half- cell reaction, and will not be discussed further in the text. All the further discussion in this chapter, will be based upon the class-1 electrode, in which the GF was heated at 140 $^oC$ for 2 h in 0.01 M $KMnO_4$ in 2 M acidic conditions.

### *3.2.5 Linear sweep voltammetry (LSV) for $k^o$ calculations*

Linear sweep voltammetry was used to investigate the electro-kinetic parameters of $VO^{2+} \rightleftharpoons VO_2^+$ reaction on 'untreated-GF' and '$KMnO_4$-140 °C-2 h-GF', as shown in fig .C 10. A fresh solution containing 0.5 M $VO^{2+}$ + 3 M $H_2SO_4$ was used to plot the anodic curves, while the solution obtained after electrooxidation of initial solution (preparative electrolyses), was used to register the cathodic curves. The curves clearly show that the kinetics of the $VO^{2+}/VO_2^+$ reaction is improved by the activation procedure. The electronic transfer limited region of LSV curve (0.7< $E_{\oplus\, in\, V/SCE}$<1.17) is considered for the calculations of the kinetic parameters ($k^0$, $\alpha$ and $\beta$), by using simple form of the Butler Volmer Law( $I = n\,F\,S\,k^{\circ}\,C_{bulk}\,exp\frac{(+\alpha\ or-\beta)n\prime F}{RT}\eta$ ) and the results are summarized in the table C.3. The $k^o$ value of the anodic reaction increases almost three folds (1.7 µm $s^{-1}$→ 4.14 µm $s^{-1}$), while for the cathodic reaction, this enhancement is 6 times (0.9→5.6 µm $s^{-1}$ ).

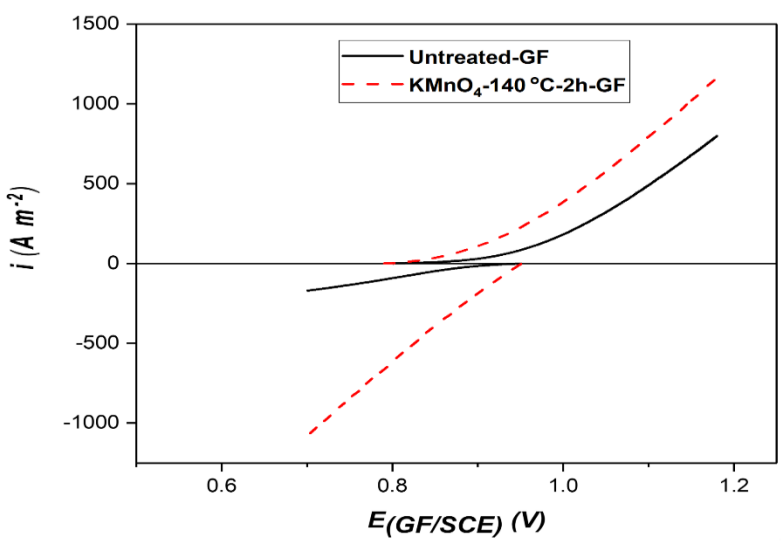


**Fig. C. 10** *LSV curves of the untreated-GF and $KMnO_4$-140 °C-2h-GF with 2.25 $cm^2$ geometrical area; at r= 1 mV $s^{-1}$, with stirring rate 350 rpm; counter electrode= Pt 3 $cm^2$; Reference electrode = SCE; anolyte initial solution: 0.5 M $VO^{2+}$+ 3 M $H_2SO_4$; catholyte initial solution=0.47<$VO_2^+{}_{(M)}$<0.49 + 3 M $H_2SO_4$*

| GF electrodes | Reaction involved | α | $\beta$ | $k°$ µm $s^{-1}$ |
|---|---|---|---|---|
| Untreated-GF | $VO^{2+} \rightarrow VO_2^+$ | 0.1 | - | 1.7 |
| $KMnO_4$-140 °C-2h-GF | | 0.17 | - | 4.14 |
| Untreated-GF | $VO_2^+ \rightarrow VO^{2+}$ | - | 0.1 | 0.92 |
| $KMnO_4$-140 °C-2h-GF | | - | 0.13 | 5.63 |

***Table C.3:*** *Comparative data of kinetic parameters concerning redox system $VO^{2+}/VO_2^+$ on untreated-GF and $KMnO_4$-140 °C-2h-GF, calculated by logarithmic analysis of the LSV curves in fig. C.10.*

### *3.2.6 FTIR and SEM analysis*

The surface of the electrode was characterized by FTIR analysis, before and after treatment. The obtained spectra are compared in fig. C. 11. The peak at the 3443 $cm^{-1}$ corresponds to the stretching vibration of -OH group [81], while the peak at the 1628 $cm^{-1}$ is assigned to the hydroxyl group in enol -C=C-OH [87]. The intensity of both peaks increased after activation of the GF, thus indicating the increase in the concentration of oxygenal groups on the surface of electrode. These groups are supposed to act as catalytic sites towards the positive half-cell reaction, as the $VO^{2+} \rightleftharpoons VO_2^+$ reaction involves the oxygen transfer; and presence of the oxygen groups on the GF could possibly assist this transfer.

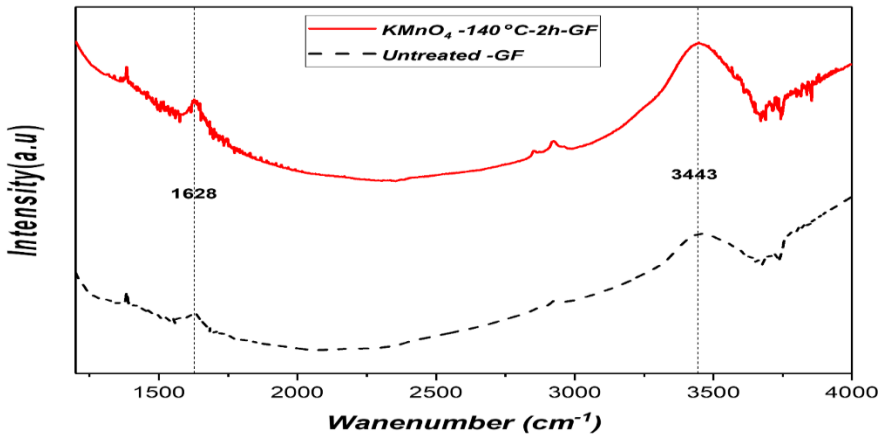


***Fig. C. 11:*** *FTIR spectra of the untreated-GF and the $KMnO_4$-140 °C-2 h-GF.*

The changes occurred in the surface morphology of the GF were also characterized by the SEM analysis. Fig. C. 12 show the comparative images of *Untreated-GF* (a,b,c) and *$KMnO_4$-140 $^oC$-2 h-GF* (d,e,f), at different magnifications. Activation method did not cause any physical damage in the overall fibrous structure, as no fragments of broken fibres are visible in fig. C.12, d. The

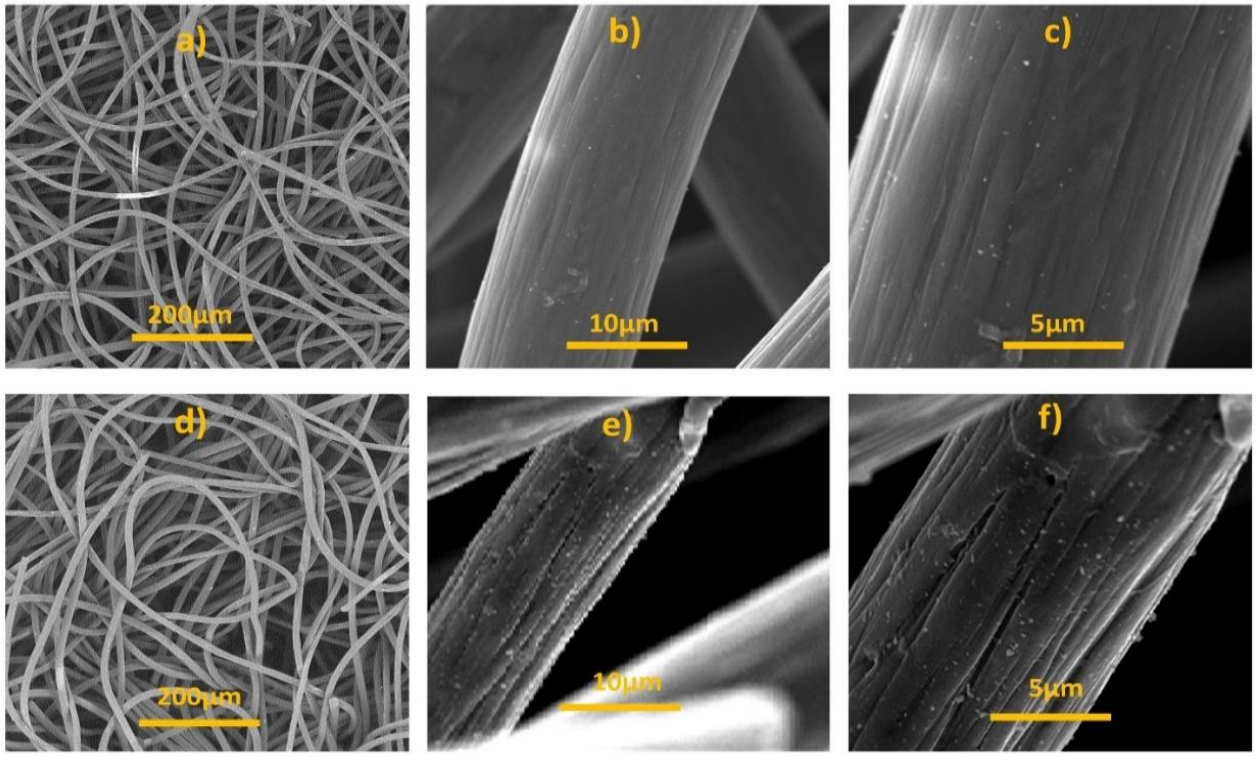


***Fig. C. 12:*** *The surface morphology characterization of the untreated GF (a,b,c) and $KMnO_4$-140 $^oC$-2 h-GF (d,e,f), at different magnifications*

surface of the untreated GF is relatively smooth with some scratches; these scratches becomes sharper after activation. The sharp scratches and higher roughness provide more available surface area for the positive half-cell reactions. This observation is also consistent with the CV results, in which peak current enhanced on the *$KMnO_4$-140 $^oC$-2h-GF* and it is directly linked with the increase of active surface area. The SEM images of the class-2 treated electrode is shown in fig. C.13 (a,b,c). It is evident that $KMnO_4$ particles are successfully adsorbed on the GF

surface. It was discussed with detail in the cyclic voltammetry section (3.2.4.2), that these particles are practically not contributing towards the vanadium reactions

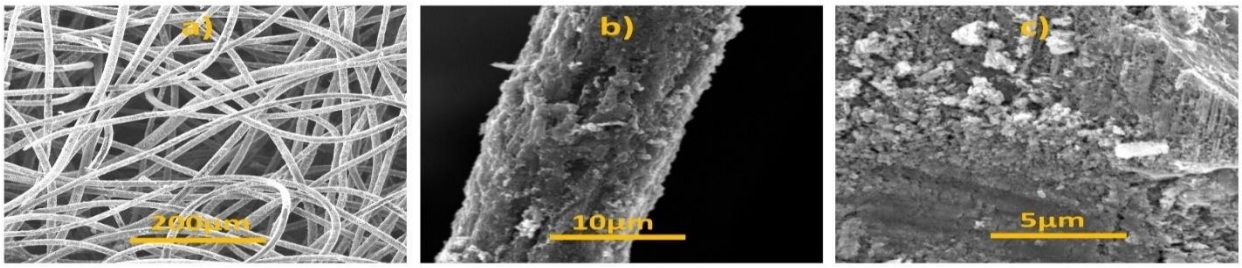


***Fig. C 13:*** *SEM images of the $KMnO_4$-600 $^oC$-$N_2$-GF at different magnifications (class 2 electrode)*

### *3.2.7 Surface free energy quantification of electrode*

The better electrode-electrolyte interaction is one of the important parameters towards the kinetics of the redox reactions. The surface of the graphite felt is intrinsically hydrophobic and requires activation for the improvement of its wettability. The proposed chemical activation successfully enhanced the wettability of the electrode. To observe this electrode-electrolyte interaction, 5 µl droplet of the 0.5 M $VO^{2+}$+ 3 M $H_2SO_4$ was placed on untreated-GF and $KMnO_4$-140 $^oC$-2 h-GF. The droplet retained on the surface of the untreated GF, while it penetrates immediately in the 3D fibrous structure of treated GF, as shown in fig. C. 14 a, d. This observation clearly indicates that the activation successfully increases the surface energy of the electrode that resulted into the improvement of its wettability.

Improvement in the wettability can be quantified by surface energy calculations. For this, the semi quantitative approach is used, mentioned somewhere else [122]. Eq. C.1 and C.2 are representative equations for these calculations. The electrode-electrolyte contact angles of two different liquids of known dispersive and polar components are required. The $\gamma_{GF}^{P}{}^{0.5}$ (slope) and $\gamma_{GF}^{D}{}^{0.5}$ (intercept) are obtained by the plot of $(\gamma_L(1+cos\,\theta))/(2(\gamma_L^D)^{0.5})$ vs $(\gamma_L^P/\gamma_L^D)^{0.5}$.

$$\gamma_{GF} = \gamma_{GF}^{P} + \gamma_{GF}^{D} \quad \text{(C.1)}$$

$$\gamma_L(1 + \cos\theta)/(2(\gamma_L^D)^{0.5}) = (\gamma_{GF}^P \gamma_L^P/\gamma_L^D)^{0.5} + (\gamma_{GF}^D)^{0.5} \quad \text{(C.2)}$$

where; $\gamma_{GF}$, $\gamma_{GF}^P$ $\gamma_{GF}^D$ represents the total, polar and dispersive surface free energy of electrode, respectively; And $\gamma_L$, $\gamma_L^P$ , $\gamma_L^D$, indicates the total, polar and dispersive surface free energy of liquid. $\theta$ represents the electrode-electrolyte contact angle.

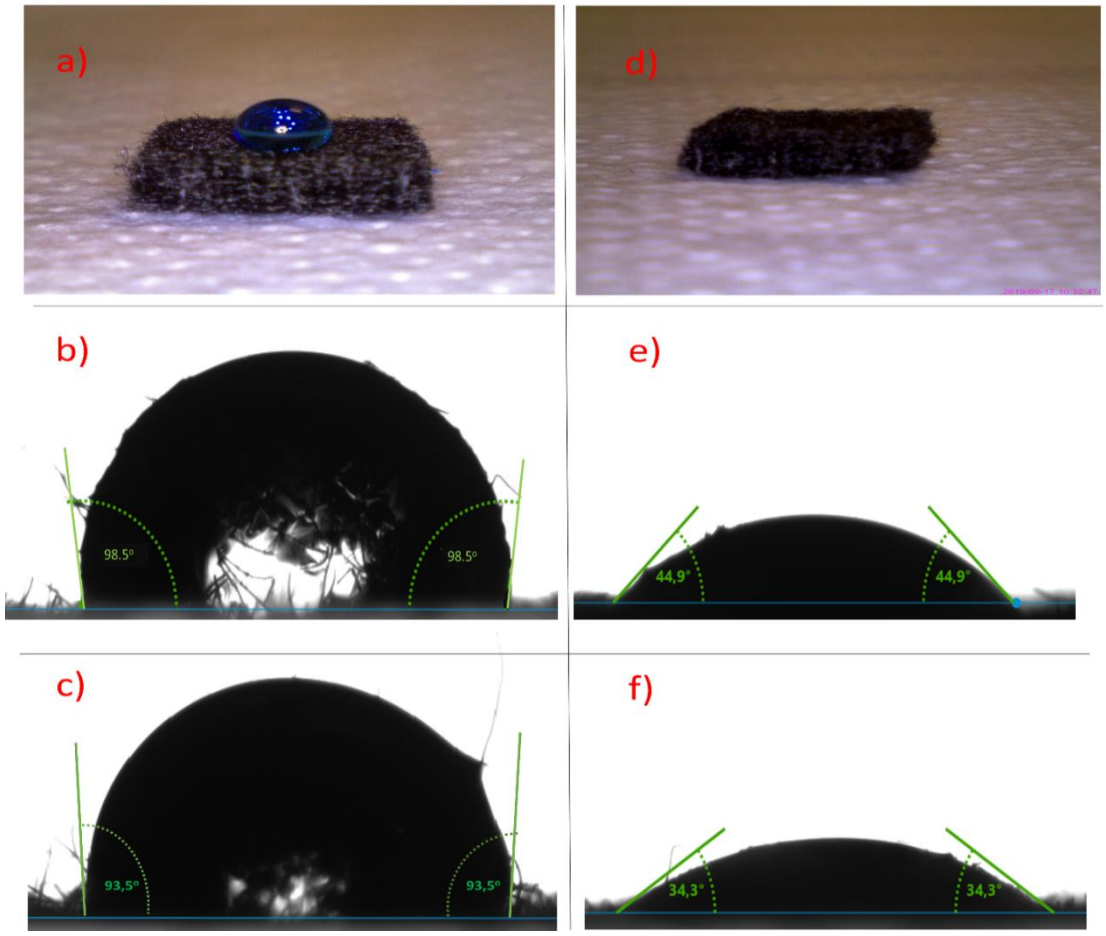


***Fig C. 14:*** *Wettability evaluation by placing 5 µL droplet of 0.5MVO$^{2+}$ + 3 M $H_2SO_4$ on untreated GF(a) and $KMnO_4$-140 °C-2h-GF(d); The 10 µL droplet of water on untreated GF (b) and $KMnO_4$-140 °C-2 h-GF (e); 10 µL droplet of glycerol on untreated GF (c) and $KMnO_4$-140 °C-2 h-GF (f)*

In this study, water and glycerol were used for the quantification of the surface energy of the GF. The untreated and treated GF was crushed and spread over the hydrophobic tape. After, the

contact angles of the glycerol and water droplets (10 µl each) were measured on this approximate flat surface. The contact angle of the water droplet decreased from 98.5° to 44.9° (fig. C.14 b,e), while the glycerol angle was changed from 93.5° to 34.3° (fig. C.14 c,f). The results of the surface free energy calculations are summarized in table C.4

| Electrode | $\gamma_{GF}^{P}$ (mN/m) | $\gamma_{GF}^{D}$=(mN/m) | $\gamma_{GF}$ (mN/m) |
|---|---|---|---|
| Untreated GF | 6.5 | 7.4 | 13.9 |
| $KMnO_4$-140 °C-2h-GF | 30.25 | 23.04 | 53.29 |

***Table: C. 4*** *The results of surface free energy calculations of untreated GF and $KMnO_4$-140 °C-2 h-GF*

Due to activation of electrode, the surface free energy is increased from 13.9 mN/m to 53.29 mN/m. This increment is responsible for the better wettability and electrode-electrolyte interaction.

### *3.2.8 Charge-Discharge cycles*

To evaluate the performance of activated GF against $VO^{2+} \rightleftarrows VO_2^{+}$ reaction, charge-discharge cycles were performed in following two different reactors, 1) *H shaped divided electrochemical cell and* 2) *electrochemical reactor*. The electrolysis was carried out under galvanostatic conditions at constant current density.

#### *3.2.8.1 H shaped divided electrochemical cell*

The electrolysis was initially performed in H type divided cell, as shown in the inset of fig. C.15. The posolyte was constituted by 0.5 M $VO^{2+}$ + 3 M $H_2SO_4$ , while the negolyte was an aqueous

solution of 3 M sulfuric acid. Operating in a half-cell enables to check the performance of the positive electrode without having any interference from the reactions involved at the negative electrode. The posolyte was mechanically stirred at 350 rpm, while the $H_2$ bubbles, produced during protons electro-reduction., ensured stirring of the negolyte.

The electrolysis was performed in anodic direction at constant current density of 667 A $m^{-2}$, enabling the oxidation of $V^{(IV)}$ to $V^{(V)}$. The electrolysis was carried out until the working electrode voltage approached 1.65 V. Then the cathodic current density of 667A $m^{-2}$ was applied to convert back $V^{(V)}$ to $V^{(IV)}$. The voltage evolution of charge-discharge electrolysis of *untreated-GF* and *$KMnO_4$-140 $^oC$-2 h-GF* is shown in fig. C.15. Due to the activation of GF, the average charging voltage decreased from 1.18 V to 1.04 V and average discharge voltage increased from 0.42 V to 0.75 V. These observations confirm the positive effect of the treatment on the

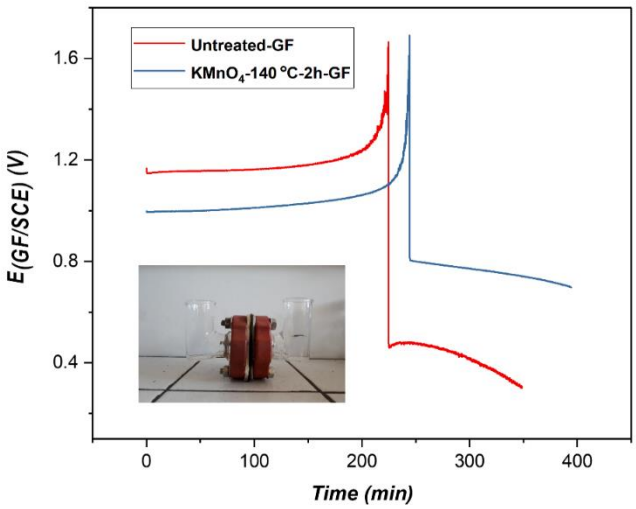


***Fig. C. 15:*** *Evolution of the working electrode potential of untreated-GF and $KMnO_4$-140 $^oC$-2 h-GF, during charge- discharge electrolysis, performed in a H shaped divided electrochemical cell (inset). Nafion membrane is used for separation of electrolytic compartments. posolyte: 0.5 M $VO^{2+}$ + 3 M $H_2SO_4$; negolyte: 3 M $H_2SO_4$; $S_{GF}$: 2.25 $cm^2$.*

electrode, as the decrease of the overvoltage translates to the increase in energy and voltage efficiency. Three consecutive charge-discharge cycles were performed to check the durability of electrode performance; and the electrode maintained the performance during these cycles.

### *3.2.8.2 Filter press divided electrochemical reactor*

The *electrochemical reactor* was used to perform the charge-discharge cycles under galvanostatic mode, to evaluate the performance of electrode on the full-scale redox flow battery. Both, posolyte and the negolyte were initially constituted by 0.5 M $VO^{2+}$ + 3 M $H_2SO_4$. The initial volume of the posolyte (500ml) was double than the negolyte to compensate the difference in the electrolysis duration, induced by the electron's ratio $(V^{IV}\rightarrow VO^{V})/(V^{IV}\rightarrow V^{II})$ =1/2. The electrolysis was carried out under a constant current of 0.5 A ($S_{GF}$=100 cm²), until the cell voltage reached 2 V; then the applied current decreased to 0.35 A, and the electrolysis pursued again until the cell voltage approached 2V. This sequence was repeated in two additional stages at 0.2 A and 0.1 A respectively, until the 80% state of charge (SOC) of battery was achieved. After it, half volume of the posolyte was removed, and subsequently charge-discharge cycle were performed under galvanostatic conditions by using *untreated-GF* and *$KMnO_4$-140 $^oC$-2h-GF* electrodes. The constant current density of 50 A $m^{-2}$ was applied during charge discharge cycles. 2 V was set as the upper voltage limit, because the solvent tends to oxidize at higher voltages and can be observable in the form of $O_2$ evolution. On the other end, the release of $H_2$ is also possible in the negative electrode compartment if the applied current is higher than the total limiting current of the successive reduction of $VO^{2+}$ to $V^{2+}$.

The cell voltage evolution during electrolysis for electrolyte preparation, is shown in the fig. C.16. Only the first and last voltage point is plotted at each current. The cell voltage is lower in

the case of treated electrode than the untreated electrode, during all the operation (this observation indicates the enhanced electrocatalytic behaviour of the activated electrode).

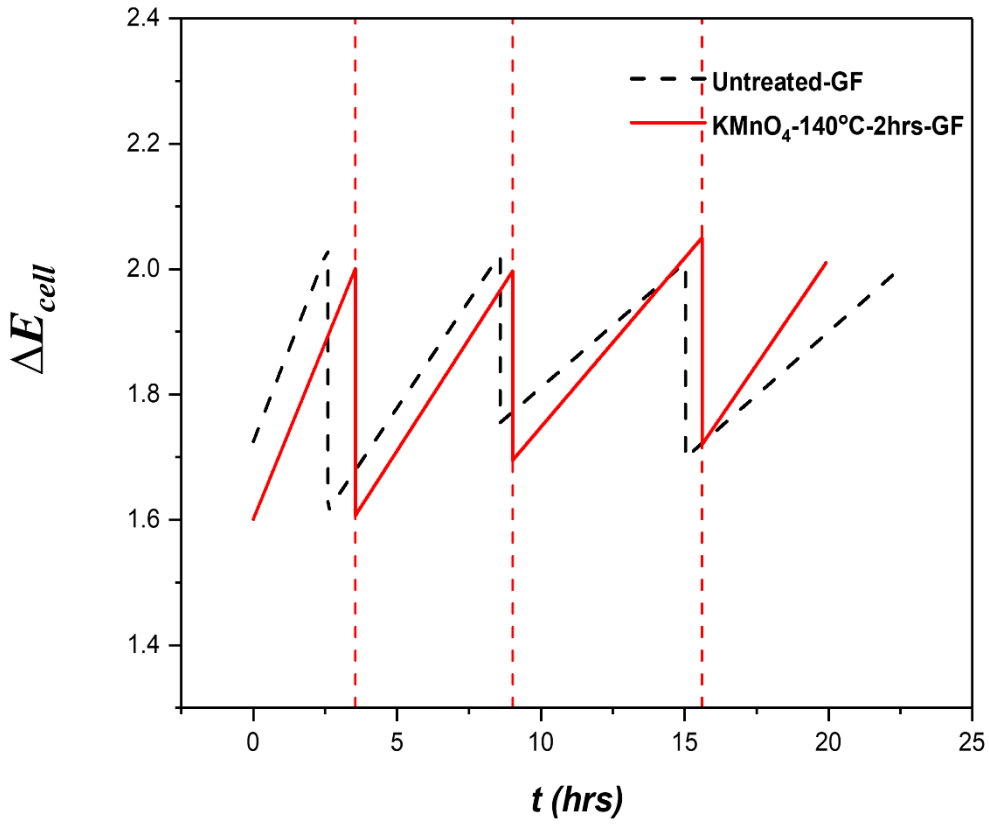


***Fig. C.16:*** *Initial and final values of voltages during the electrolyte preparation by using untreated GF and* $KMnO_4$-140 °C-2 h-GF

Cell voltage curves during charge-discharge cycle are shown in fig. C.17. Due to activation of electrode, the average charging voltage decreased from 1.86 V (untreated) to 1.76 V (treated) and average discharging voltage increased from 0.59 V (untreated) to 0.80 V(treated). At a current density of **50** A $m^{-2}$, there is an improvement of 20 % and 13 % in energy and voltage efficiency (VE), respectively. This observation reveals that, in comparison with untreated electrode, the activated electrode requires lower power for charging; and obtained power during

discharge is higher. Also, the duration of the charging and discharging is prolonged, resulted in the higher conversions.

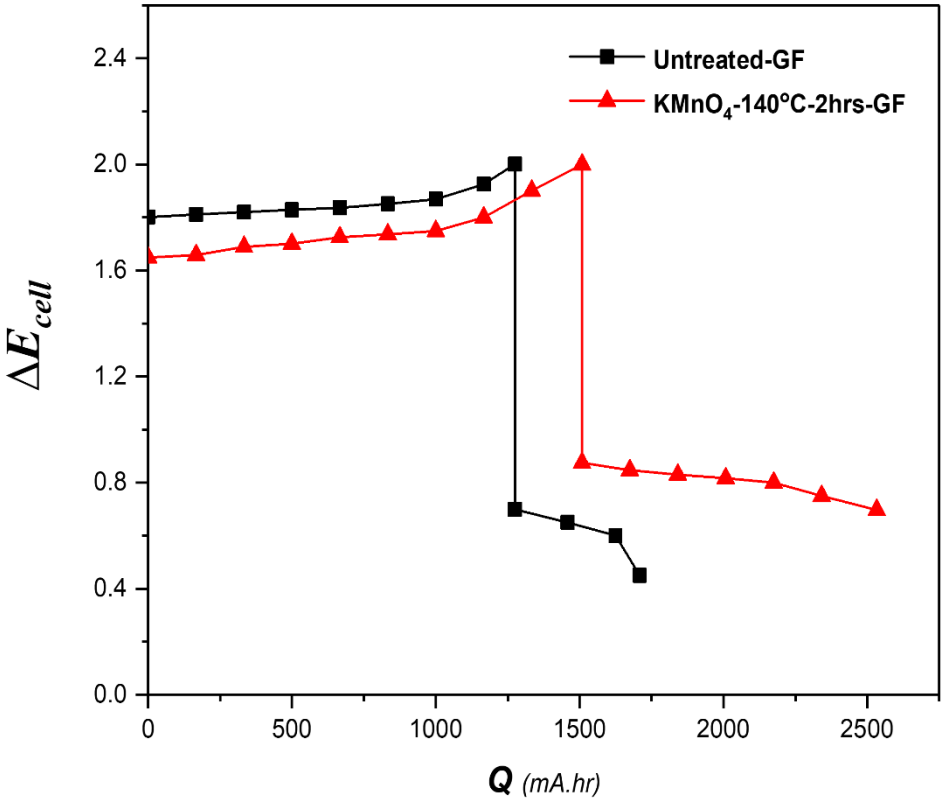


***Fig. 17:*** *charge discharge cycles of untreated GF and* $KMnO_4$-140 °C-2 h-GF *in the stack with positive and negative electrode of geometrical area of 100* $cm^2$

## 3.3 Conclusion

The proposed chemical method of acidic $KMnO_4$, successfully activated the GF, to be used as positive electrode in the VRFBs. In the CV analysis, ~35 % enhancement was observed in the peak current of $VO^{2+} \rightleftharpoons VO_2^+$ redox reaction. The electronic transfer kinetic constant *($k^o$)* of charge and discharge reactions in positive half-cell, were enhanced by 2.6 and 6.1 times, respectively. The surface free energy calculations by contact angle measurements reveals that the electrode-electrolyte affinity was improved after activation, that plays an important role in the surface catalysis. The surface oxygenal groups, integrated during activation process was expectedly catalysing the positive half-cell reactions. Moreover, the available surface area for the reactions was enhanced because the activation made the surface rough and grooved. The activated GF showed the promising results during charge-discharge cycles, conducted at the following two different reactors 1) *H-shaped divided electrochemical cell* and 2) *filter press divided electrochemical reactor*. The prescribed activation process is operationally very easy, as it does not require any complicated procedures. The activation procedure is relatively easy than the $K_2Cr_2O_7$ procedure, as it is occurring in non-reflux conditions. The voltage and energy efficiency of the VRFBs is improved by 13% and 20 %, that is greater than the results reported in the literature e-g < 10 % (see chapter #1)

# ***Chapter: 4 Comparative study of the role of $sp^3$ hybridization and different oxygenal groups on the graphite felt electrodes, towards positive half-cell redox couple in vanadium redox flow batteries***

## Chapter: 4 Comparative study of the role of $sp^3$ hybridization and different oxygenal groups on the graphite felt electrodes, towards positive half-cell redox couple in vanadium redox flow batteries

***Abstract*:** Graphite felt was activated and used as electrode material for the vanadium redox flow battery. Activation methods leads to fabricate epoxy, OH, C=O, COOH groups on graphite felts and change their surface morphology ($sp^2/sp^3$ hybridization); thus, improving their electroactivity. The proportion of various oxygenal groups depends upon the nature and duration of the activation process. Experimentally, it is difficult to investigate their individual roles, because most of these are present simultaneously in the electrode. That is why different hypotheses are made about their kinetic role. In this study, density functional theory (DFT) calculations are conducted to evaluate their individual role towards positive half-cell reaction of the vanadium redox flow battery. The DFT calculations show that oxygenal groups improve the electroactivity of the graphite felt towards ($VO_2^+ + 2H^+ + e^- \rightleftharpoons VO^{2+} + H_2O$), in the following order; C=O > COOH, > OH > basal plane. Projected density of states (PDOS) calculation showed, that these groups increase the $sp^3$ hybridization of the electrode exactly in the same order. It concludes that the increase in $sp^3$ hybridization of the electrode improves the electroactivity of the electrode. Oxygenal groups are just responsible of this $sp^3$ increment. These insights can help in the better selection of activation processes and their parameters.

## 4.1 Introduction

Chemical, thermal and electrochemical oxidative treatment is widely investigated to improve the electro activity of the graphite felts [84,113,123]. These oxidative approaches fabricate different oxygenal groups (epoxy, OH, COOH, C=O) on electrodes and increase the $sp^3$ hybridization of the carbon atoms in the material; the extent of their individual proportions depends upon the nature and extent of oxidative activation process [86]. Some activation procedures lead to the fabrication of higher OH concentrations, [84,124] while other inscribe more C=O and COOH groups [125]. The common aspect of all the activation procedures is that they induce structural changes in felt, resulting the increment of $sp^3$ hybridization of the electrode, that is believed to provide more reaction sites for the reaction of the vanadium flow battery.

Because of the presence of all these groups (epoxy, OH, COOH, C=O ) and "structural changes" in the electrode surface, it is difficult to distinguish experimentally the individual roles of each component, in the catalysis of vanadium redox reaction [126]. For that reason, there is a lot of different experimental hypotheses about the oxygenal groups. Dai et. al. suggested that COOH groups are acting as catalyst sites [113]. Li et. al. proposed that the COOH groups improves the reaction rate, while the C-OH and C=O impede the reactions [127]. Skyllas-Kazacos hypothesized that C-OH groups are the active sites for the reaction. On the contrary, some other reports suggest the impeding roles of oxygenal groups towards positive half-cell reaction, and indicate that the structure of electrode is predominant factor. [64,126]. Lie et al. proposed that the oxygenal groups are the sole reason of the catalysis, and surface area is not playing any significant role. The computer simulations methods like molecular dynamics or electronic structure calculations could provide theoretical insight into such experimentally complicated situations [128–131]

In this study, the density functional theory (DFT) calculations are performed to evaluate the individual roles of epoxy, OH, C=O, COOH and surface morphological changes for the $VO^{2+}/VO^{2+}$ redox reaction. The correlation between the surface morphology and oxygenal groups are also established by projected density of state calculations (PDOS).

## 4.2. Principle of plane wave density functional theory calculations (DFT)

The Schrodinger equation is the fundamental equation of quantum mechanics, that describe the properties of the matter at their atomic or molecular level by analyzing the quantum behavior [132], as shown in eq. D.1

$$i \frac{\partial (\emptyset)}{\partial t} = H . \emptyset \qquad \text{(D. 1)}$$

Where $\emptyset$ = electronic wave function; H = Hamiltonian operator; $i$= complex number

The electronic wave function ($\emptyset$) of a system, comprised of multiple nuclei and electrons, depends upon their positions in the space and their changing coordinates with time. The electronic structure calculations are based on the ground state energy and it does not vary with time [133]. So, for that reason, the factor of time can be excluded from the equation , and time independent Schrodinger equation is classically considered for ground state electronic calculations, as in eq. D.2

$$E . \emptyset = H . \emptyset \qquad \text{(D.2)}$$

Where; $\emptyset$ = electronic wave functions = $f$ ( $electrnic\ cordinates, nuclei\ coordinates$ )

$E = ground\ state\ energy\ of\ system$

$$\boldsymbol{H} = K.E_{nuclei} + Self\ interaction\ of\ nuclei + K.E_{electrons} + Self\ inteaction\ of\ electrons + interaction\ between\ electrons\ and\ nuclei$$

$$= \frac{1}{2}\sum\frac{h}{m_n}\nabla_x^2 + \frac{1}{2}\sum\frac{Z_x Z_y}{4\pi\epsilon(L_x - L_y)} + \frac{1}{2}\sum\frac{h}{m_e}\nabla_k^2 + \frac{1}{2}\sum\frac{e^2}{4\pi\epsilon(r_k - r_l)} + \frac{1}{2}\sum\frac{Z_x e^2}{4\pi\epsilon(r_k - L_x)} \qquad \text{(D.3)}$$

The Hamiltonian of Schrodinger equation (eq.3), dealing with the multiple nuclei-electron system, consist of the kinetic energy and the potential energy terms of both electron and nuclei [134]. The electrons are much lighter than the nuclei, so changes occurring in the electrons are much faster than nuclei; and both motions can be modelled as two separate problems. The mixed electron-nuclei mathematical expression (Schrodinger equation) can be split into these two different expressions by Born–Oppenheimer approximation [135]. In one expression, the equation is derived for the moving electrons for the fixed nuclei, and in the second equation, the mathematical model is associated as the function of the coordinates of the nuclei.

The electronic calculations are based on the expression relating the electrons motions in fixed nuclei environment; and solving this equation gives the ground state energy of the structure, from whom all the properties of the matter (kinetic and thermodynamics etc.) can be deduced. In this case, the Hamiltonian operator (H) and wave function (Ø) is based on the all the electron related terms, as in equation D.2, D.4.

$$E.\emptyset = H.\emptyset \qquad \text{(D.2)}$$

$$H = \left(\frac{1}{2}\sum\frac{h}{m_e}\nabla_k^2 + \frac{1}{2}\sum\frac{Z_x e^2}{4\pi\epsilon(r_k - L_x)} + \frac{1}{2}\sum\frac{e^2}{4\pi\epsilon(r_k - r_l)}\right.; \emptyset = \text{f (coordinates of electrons)} \qquad \text{(D.4)}$$

It is impossible to solve the Schrodinger equation analytically, as it is *"multidimensional"* and *"many-body"* problem. In the real cartesian coordinate system, each electron has three coordinates, and if there is x number of electrons in the system, then the Schrodinger equation

(eq. D.2) become 3.x-dimensional problem. For example, Schrodinger equation becomes 42-dimensional problem if it would be solved to calculate the ground state energy of just one molecule of the $N_2$ gas. One can imagen the complexity of mathematical problem to solve eq. D.2. Not only this, determination of the wave function of one electron, involves the wavefunctions of all the other electrons simultaneously, and due to this characteristic of Schrodinger equation, it is also known as *"many-body"* problem. [136,137]

With the help of density functional theory calculations, the Schrodinger equation can be solved; hence the properties of the matter (kinetic and thermodynamics etc.) can be determined [138]. DFT calculations are based on the fundamental principles of the quantum mechanics, that's why it is also called first principle calculations [139]. Prof. Walter Kohn got the noble prize in 1998, for proposing the idea of the DFT calculations, used for solving the Schrodinger equation. The DFT are based on the two theorems proposed by the Hohenberg-Kohn (HK), that explained that the ground state energy of electronic structure (solution of Schrodinger equation) can be related to electron density by unique functional E[n(r)], and the true electron density is that which gives the absolute minima of this functional. Conclusion of the both theorems is: if the true functional of energy density is known, the exact ground state energy can be measured. That is why it is called the density functional theory calculations [140]. The concept of the probability of the presence of the electrons at position (r) are more physically relevant than their individual movements . This probability can mathematically be related to wave functions by the equation D.5.

$$n(r) = \sum conjugate\,\{\emptyset_k\ (r)\} * \ \emptyset_k(r) \qquad \text{(D.5)}$$

DFT reduce and scale down the multidimensional mathematical problem, posed by the Schrodinger eq, just to 3 dimensions; as all the calculations are based on the electron density at positions r ($x$, $y$, $z$)[139]. The functional that are proposed by the HK, that is relating the n(r) and E, are not exactly known and hence to reach the exact solution is still not possible. This functional can be split into two functionals: e-g one consists of the known analytical terms and other consist of the unknown.

$$E_{total}\{n(r)\} = E_{known}\{n(r)\} + E_{unknown}\{n(r)\} \qquad \text{(D.6)}$$

$$E_{known}\{n(r)\} = \frac{1}{2}\int \frac{h}{m_e}\nabla_k^2 . n(r)\, d^3r + \frac{1}{2}\int \frac{Z_x . e^2 . n(r)}{4\pi\epsilon(r_k - L_x)}\, d^3r + \frac{e^2}{2}\iint \frac{n(r).n(r^{\blacksquare})}{4\pi\epsilon(r - r^{\blacksquare})} d^3r\, d^3r^{\blacksquare} \qquad \text{(D.7)}$$

The terms indicated in the equation (D.6) are functions representing the kinetic energy of the electrons, interaction between electron-nuclei and interaction between the electrons respectively. To determine this problem of $E_{unknown}$, the Prof. Sham and Prof. Kohn proposed equation (eq. D.8), for one electron particle.

$$\{(K.E + V(r) + V_{Hartee}(\mathrm{r}) + V_{xc}(\mathrm{r})\} * \emptyset_k(r) = E * \emptyset_k(r) \qquad \text{(D.8)}$$

$$\{(\frac{h}{2m_e}\nabla^2 + \frac{Z_x . e^2}{2(r - L_x)} + \frac{e^2}{2}\frac{n(r^{\blacksquare})}{(r - r^{\blacksquare})} d^3r^{\blacksquare} + V_{XC}) * \emptyset_k(r)\} = \in * \emptyset_k(r) \qquad \text{(D.9)}$$

This proposed equation could approximately fix the problem of the $E_{unknown}\{n(r)\}$ with approximate exchange-correlation ($V_{XC}$). The kohn-sham can be solved by the following iterative process: 1) Start with the initial guess of the electron density $n(r^{\blacksquare})$. Based on the initial trial density, the Hartree potential is calculated. Sequentially, the single particle equation (D.8) is solved to determine the individual electron wave function $\emptyset_k(r)$. Equation (D.5) enables calculations of the electron density by using $\emptyset_k(r)$. If the calculated electron density and the trail electron density is within tolerance, then it is the true electron density, otherwise repeat the

iterative procedure until the system converge. The ground state energy could be deduced from this electron density, and hence all the properties of the matter [141]. The accuracy of this result depends, how accurate ($V_{XC}$) is used in the problem. Developing these exchange correlations is also huge task in the field of theoretical physics and chemistry and lot of effort been carried out to develop these models for different systems. The simplest exchange correlation is the *local density approximation* (LDA). The gaseous system is supposed with constant and uniform electron density in the space to derive LDA. There are many exchange-correlations exist, such as generalized gradient approximation (GDA) and Perdew–Burke–Ernzerh functional (PBE) etc. Each exchange-correlation is limited to specific systems and of approximate nature with underlying assumptions. The selection of right exchange correlation is important for the accuracy of the calculations[142].

All the above discussion is how accurately can get the solution of Schrodinger equation, with the help of DFT calculations. Though the DFT calculations convert the 3.x dimensional problem into just 3-dimensional problem and make the expression solve able, but still requires a lot of computational resources to perform these calculations for real material, indeed it can exists up to $10^{23}$ electrons involved and the action to solve the Kohn-Sham equation for all of these individual electron is huge mathematical task. The crystalline structures are mostly having similar and repetitive structure, and this periodicity can help to reduce the computational cost for DFT calculations. Just few atoms are considered for DFT calculations and use this periodicity all over as per Baloch theorem [143]. This theorem proposed that such periodic systems have the general solutions as equation D.10.

$$\emptyset_k(r) = e^{i.k.r} . u_k(r) \qquad \text{(D.10)}$$

Where the $e^{i.k.r}$ represents the plane waves. It is the reason why these DFT calculation are called plan wave calculations; The term $u_k(r)$ is the periodic potential function. The term r and k represent the real and reciprocal k space. The calculations are more numerically converge able in the reciprocal k space, so in the DFT calculations the k space is considered. The real space means that the position of the atom is defined in the cartesian space by vectors, and the volume of that space is named as supercells. This real space can be converted into the reciprocal k space by equation D.11. The reciprocal k space in which the atoms are defined is called Brillouin zone[136].

$$(vectors\ of\ real\ space\ .\text{vectors of reciprocal k space}) = 2\pi \qquad \text{(D.11)}$$

In the real space, to evaluate the integrals numerically, the function curve is divided into number of number of parts and then evaluating integrals at each point and sum up. The more the number of these divided parts, the more accurate the solution is. Likewise, the concept of k-points in the reciprocal space to compute integral, is just like choosing discrete points in the real space. The general solution proposed by the Baloch (equation D.10) is the 3D Fourier basis set and can be written in the form of the kinetic energy. Like any expansion series, the first few terms contribute major portion in the solution. So, to have good numerical convergence, the some cutoff energy is provided in the calculations and all the above terms are neglected.[144,145]

## 4.3 Methods

We performed DFT calculation using GPAW software. All the calculations are based on the projector augmented wave (PAW) method [146,147]. The structures were built in the "Atomic Simulation Environment (ASE) software, that are used to describe atoms and their visualization [148]. The water splitting energy on the graphene layer was calculated at different cut off

energies from 400 eV to 800 eV to choose less computational costly cut-off energy, without compromising the accuracy of calculations. The system started converging from 400 eV, as shown in fig. D.1, a. So, the plane-wave cut off energy of 400 eV was used in all the calculations. The convergence test for the selection of optimized k- points was also conducted, by plotting energies of relaxed graphene sheet at different n x n x 1 (n = 2 to 12). The k point of 5 x 5 x 1 is chosen for all the calculations, as the system started converging from this point and it seem good trade-off between accuracy and computational cost, as shown in fig.D.1. Bayesian error estimation functional with van der Waals correlation (BEEF–vdW) is used as the exchange-correlation functional. The supercell having 40 Å z-axis is used and structures were place in the middle of it. The periodic boundary conditions were applied in the x and y direction.

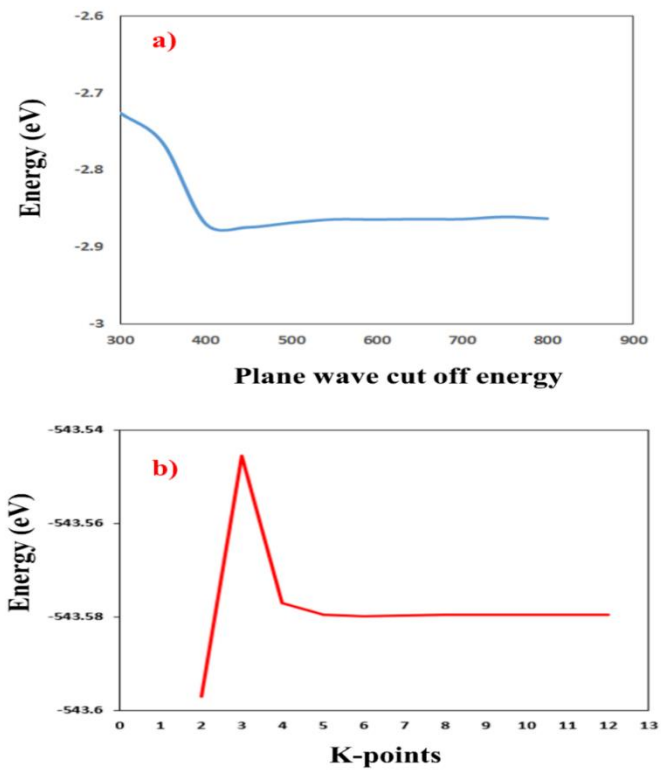


***Fig D.1.*** *a) convergence test of the plane wave cut off energy by calculating the water splitting reaction at electrode surface from 300 eV to 900 eV. b) Convergence test of the K- point by calculating the electrode surface free energy from 2 x 2 x 1 to 12 x 12 x1*

## 4.4 Results and discussion

One layer of graphite (pristine- 0 0 0 1) was modelled as reference initial structure. This is assumed computationally equivalent to the untreated graphite felt.

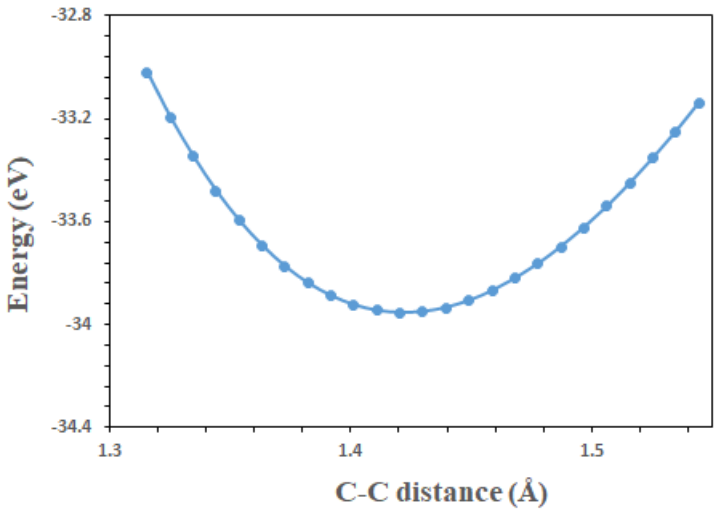


***Fig D.2:*** *The convergence test for measuring the optimized C-C bond length by measuring total energy of the C-C at different bond lengths, in range of 1.43 Å ± 0.1 Å*

Optimized C-C bond length was determined by measuring total energy of C-C bond, against different bond lengths in the range of ± 0.1 Å from the value of 1.43 Å. As shown in fig D.2, the optimized value is 1.4215 Å, which is almost same to experimental value(1.42 Å) [149]. All the modelled geometries are based on the C-C optimized bond length, before subjecting to the relaxation. Because of the optimized C-C bond length (1.4215 Å), the overall structure has minimized strains from the individual bonds.

As the purpose of this study is to investigate the interaction of the $VO^{2+}/VO_2^{+}$ with the groups: epoxy, OH, C=O, COOH groups and to establish possible correlations between "structural changes ($sp^2/sp^3$ hybridization) ⇌ oxygenal groups ⇌ $VO^{2+}/VO_2^{+}$ affinity with electrode". For that, following modelled geometries were considered.

a) Single layer of the basal surface of the graphite (BG) - Fig 3.D, a

b) Hydroxyl group on the basal surface (BG-OH)- Fig 3.D, b

c) Epoxy group on the basal surface (BG-O)- Fig 3.D, c

d) Basal surface with 6C defect in it; all defects covered with the H atoms to reduce dangling bonds [150]. This model is used to study the C-H kinetics against the positive half-cell reaction and named as (BG-D-H) fig 3.D,d. At high temperatures, in the presence of oxidizing environment, the defects are created in basal surface, and the most stable one is the defect of the 6 carbon ring [151]. All the oxidative activation processes available in bibliography are either with very high temperature (400 $^{o}$C- 1000 $^{o}$C) or with intense chemical conditions for the long time (~ 10-15 h). These process creates the defects in the basal plane and create edges [80,89,123] And then it is more likely covered with functional groups on further oxidation [100,102,127]

e) Then, hydrogen is removed from the one defect, to study intrinsically the basal defect interaction with the vanadium ions. (BG-D) fig 3.D, e

f) In a similar way, C=O, C-OH and -COOH are inserted one by one, on the defects by removing the hydrogen sequentially (BG-D-OH, BG-D-O, BG-D-COOH) - Fig 3.D (f, g, h)

The DFT calculations performed in this study are periodic in the x and y direction, so the presence of the defect could possibly interact with each other due to periodicity and can affect the calculations. Thus, the size of the surface should be big enough to avoid any such interaction. To find the optimum system size, the convergence calculations with the following number of atoms are investigated e-g 32, 50, 72, 98, 128, 162. All the structures have the defect of 6

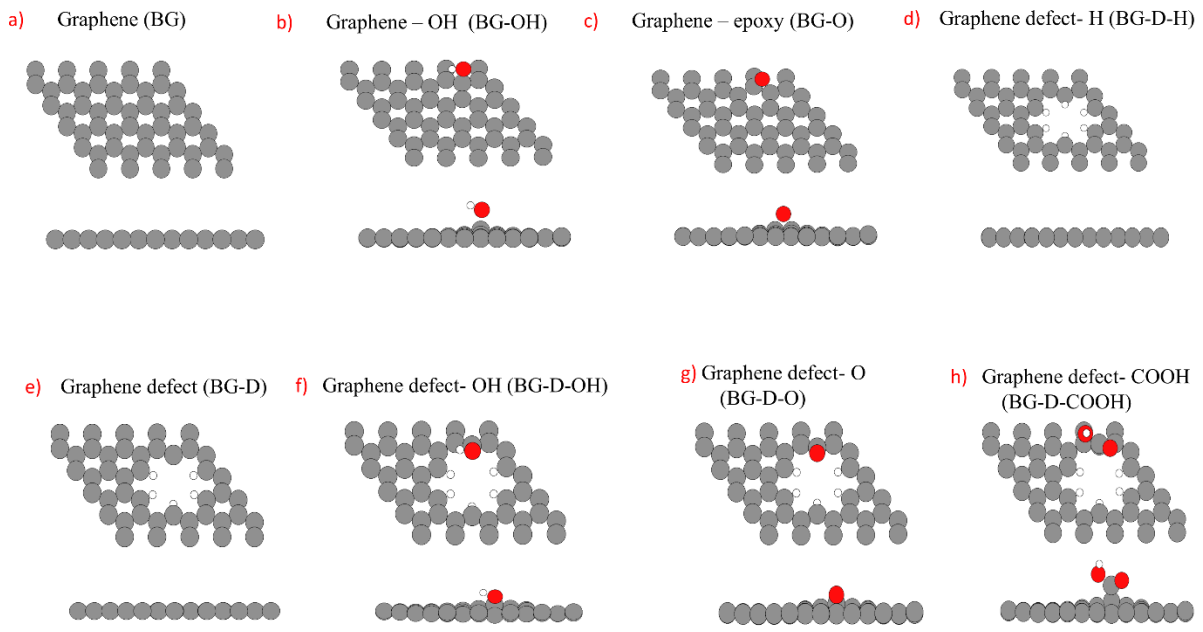


***Fig 3.D*** *Relaxed structures of a) Basel surface (BG) b) Basel surface with OH (BG-OH), c) Basel surface with O (BG-O), d) Basel defect covered with hydrogen (BG-D-H) e) Basel defect (BG-D), f) Basel defect covered with hydroxyl (BG-D-OH), g) Basel defect covered with carbonyl (BG-D-O) h) Basel defect covered with carboxylic (BG-D-COOH)*

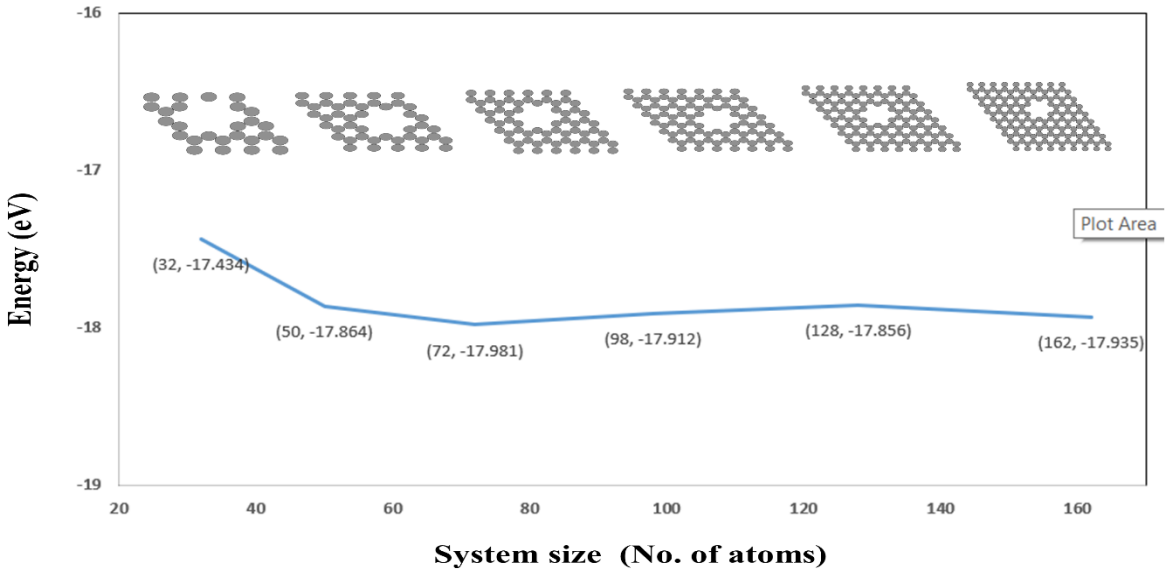


***Fig 4.D*** *The convergence test to select the optimum size of the system, without having any effect of interaction of defects, due to the periodicity of system in the x and y direction*

carbon atoms in the basal plane. The structures were subjected to the relaxation with minimum force of 0.05 eV. As shown in the fig 4.D, the relaxed energy of the structures started converging from the system of the 50 carbon atoms. So, in this study, the basal surface of 50 carbon atoms were used; as it is computationally economical without having any interaction problem in periodicity.

The affinity of $VO^{2+}/VO_2^{+}$ redox on electrode surface are studied without solvation, to avoid any interference from the solvent. As the solvent interaction is also important in the electrode-electrolyte interface, thus the study of the water-interaction with all the representative surfaces is done separately. The adsorption energies of $V^{(IV),}$ $V^{(V)}$ and $H_2O$ are determined on all the surfaces of GF surfaces by the following equation D.12.

$$E_{(adsorption)} = E_{(surface+adsorbate)} - E_{(surface)} - E_{(adsorbate)} \quad \text{(D.12)}$$

Where $E_{(adsoption)}$ is the adsorption energy; $E_{(surface+adsorbate)}$ and $E_{(surface)}$ is equal to the total energy of surface, with and without adsorbate respectively. $E_{(adsorbate)}$ represents the energy of adsorbate molecule.

The adsorption energies provide insights about interactions of the reactant species with the electrode surface and are related to the catalysis of the reaction [152,153]. Remember of the results from the chapter 2 (section 2.3.4), in which the classical adsorption test was conducted with untreated and treated electrodes to determine the adsorption sites for the $VO^{2+}$. The 'Untreated-GF', '400 °C-5hrs-GF' and 'Cr-140 °C-2hrs-GF' have '$5.3 \times 10^{16}$, '$87 \times 10^{16}$' and '$200 \times 10^{16}$' adsorption sites, respectively. The cyclic voltammetry results showed enhanced electro-kinetic activity of the electrode which exhibited highest adsorption sites. (chapter *2*-section *2.3.1.4 )* [154].

As discussed in the section of principles, that DFT calculations are mostly based on the numerical methods, and all numerical methods are classically based on finding the local minima of the respective functions. Because the aim of the study is to see the interaction of the $VO^{2+}/VO_2^{+}$ with the electrode surface; and initial orientation of the adsorbates, while setting up calculations in the DFT software, can affect the numerical convergence and results. For that reason, in each DFT calculation of this chapter, different orientation of $V^{(IV)}$, $V^{(V)}$ and $H_2O$ are tried to obtain the most thermodynamically stable state. The initial orientations of all adsorbates are shown in fig. 5.D

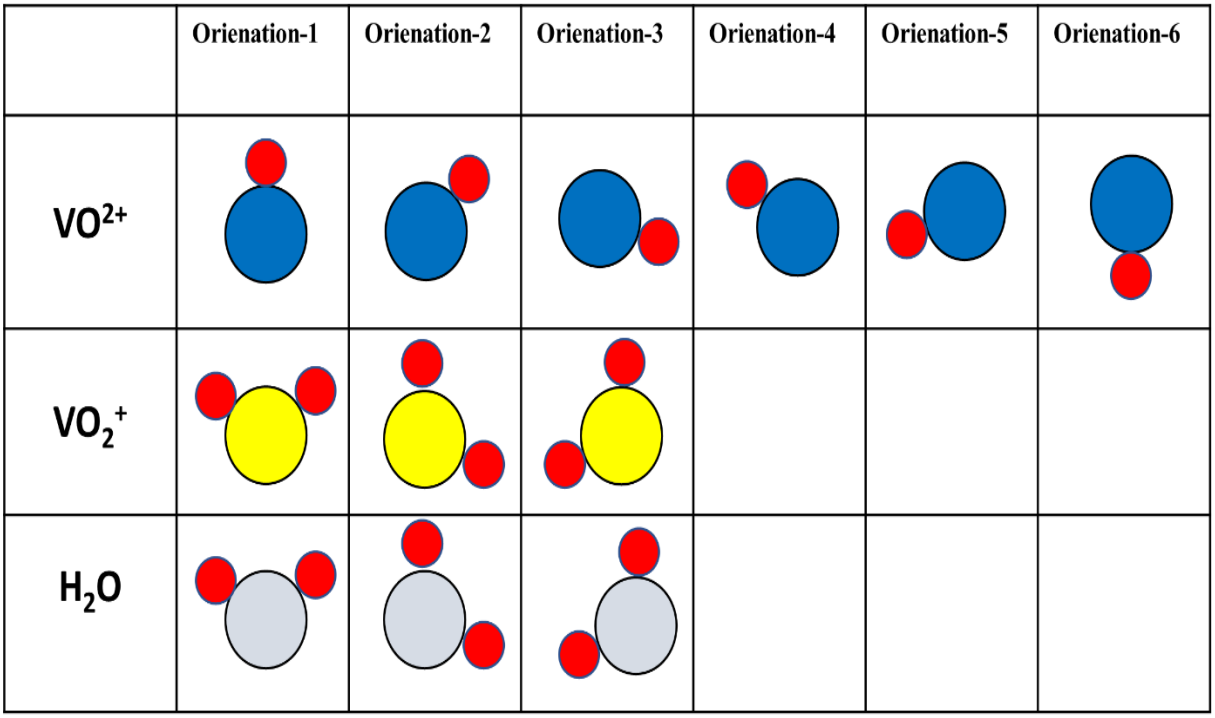


***Fig 5.D*** Different initial orientation of the $VO^{2+}$, $VO_2^{+}$ and $H_2O$ used as adsorbate, in the adsorption calculations

### *4.4.1 Interaction of the $V^{(IV)}$ with modified electrode surfaces*

The interaction of the $VO^{2+}$ with modified electrode surfaces of fig. 3.D (a,b,c,d,e,f) is studied in this section, in order to quantify their adsorption energies. For that, the molecule of the $VO^{2+}$ is built in ASE software and then the relaxation of this structure is done in the GPAW to optimize bond lengths and angles. Then, the optimized molecule of the $VO^{2+}$ is carefully placed 2.5 Å

| **Orientation #** | **BG (eV)** | **BG -OH (eV)** | **BG-epoxy (eV)** | **BG-D-H (eV)** | **BG-D(eV)** | **BG-D-OH (eV)** | **BG-D-O (eV)** | **BG-D-COOH (eV)** |
|---|---|---|---|---|---|---|---|---|
| 1 | -0.599 | Unstable OH | Unstable OH | -1.758 | -2.174 | -1.35 | -2.154 | -1.633 |
| 2 | -0.155 | | | -1.716 | -3.273 | -0.235 | 0.02 | - |
| 3 | -1.31 | | | -1.723 | -3.164 | -0.945 | -2.171 | - |
| 4 | -1.312 | | | -1.724 | -3.165 | -1.293 | -2.688 | -2.538 |
| 5 | -1.311 | | | -1.724 | -3.199 | -1.328 | -2.171 | - |
| 6 | -1.317 | | | -1.724 | -3.226 | -0.309 | -2.696 | -1.715 |
| Most stable | -1.317 | | | -1.758 | -3.273 | -1.35 | -2.696 | -2.538 |

***Table D.1*** *Adsorption energies (eV) of the $VO^{2+}$ at different representative geometries*

above on the modified surfaces separately. The optimization means to find the total ground state energy of the total structure by the software, under the parameters mentioned in the "methods" section 4.3. The software has built-in codes to perform DFT calculations. The software started with initial guess of electron density and then sequentially calculate the effective potential, the wave functions and the electron density. This iterative process was maintained until the solution converged. Then, the corresponding energy can be calculated from electron density. The principle and theory in solving these calculations are already explained in section 4.2.

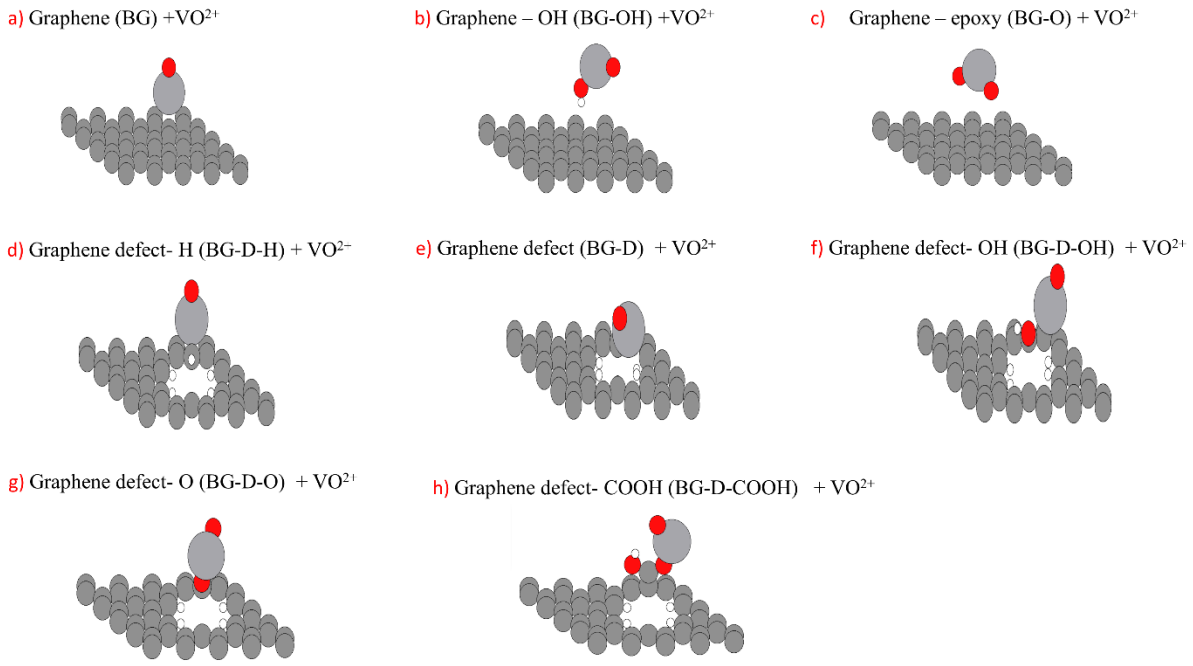


***Fig. 6.D*** *Relaxed structures of composite geometry containing adsorbate* $VO^{2+}$ on *a) Basal surface (BG) b) Basal surface with OH (BG-OH), c) Basal surface with O (BG-O), d) Basal defect covered with hydrogen (BG-D-H) e) Basal defect (BG-D), f) Basal defect covered with hydroxyl (BG-D-OH), g) Basal defect covered with carbonyl (BG-D-O) h) Basal defect covered with carboxylic (BG-D-COOH)*

For the adsorption calculations, first the total energy of the geometry containing "graphite surface and adsorbate both" are calculated from the software, and then the total energies of "graphite surface" and "adsorbate" are calculated separately. Then adsorption energies are calculated by the equation D.12. Six different results of adsorption energy are obtained for each reference geometry, because for each geometry six calculation are performed with 6 different initial orientations of adsorbate. The results with maximum adsorption energy in absolute value, correspond to the most thermodynamically stable structure and highlighted for each geometry in the table D.1, at the end of every column. For example, the first column of the table D.1 is related to the adsorption energy of $VO^{2+}$ on the basal surface (BG). The maximum value of adsorption is obtained from the calculation started with the orientation 6 (-1.317 eV). The least stable structure for this geometry (BG), is obtained for the orientation-1 of $VO^{2+}$ (-0.599 eV).

There is almost a difference of 50 % between these two values. So, one can see, it is important for the DFT calculation to examine the different initial structures for good numerical convergence and to find the most stable structure. All the most stable final structures of every geometry with adsorbate $VO^{2+}$, are shown in the fig. D.6

Other important observation can be noted from the geometry of BG-O and BG-OH, that the epoxy and OH group on the basal surface, strip away when the $VO^{2+}$ approaches the surface (fig D. 6 b, c). It indicates that the epoxy group and OH group on the basal surface is unstable; and it is more likely due to the 2D $sp^2$ planner and stable structure of the basal plane, and it is not reactive enough. While the O, OH and COOH formed on the defects in the basal plane are stable and shows enhances interaction with the $VO^{2+}$ molecule. This observation is consistent with experimental observation and will be more discussed in next sections [155]. The COOH and C=O groups in the basal defects showed maximum interaction with the graphite. The adsorption energies of $VO^{2+}$ on different oxygenal groups are in the following order:

*BG-D (-3.273 eV) > C=O (-2.696 eV) > -COOH (-2.538 eV) > C-H (-1.758) > -OH (-1.35 eV) > BG ( -1.317 eV)*

It is evident from the DFT calculations, that the graphite modified surfaces with oxygenal groups have better affinity for the $VO^{2+}$, than the untreated graphite. The experimental results in the chapter 2 and 3, also validate these results, in which it was observed that the oxygenal groups were improving the reaction kinetics of $VO^{2+}$. DFT helped to evaluate their individual roles.

### *4.4.2 Interaction of the $V^{(V)}$ with modified electrode surfaces*

The adsorption of the $V^{(V)}$ is investigated with all the modified geometries, in the similar way as in the case of $VO^{2+}$. For every reference geometry, three calculation are performed; starting with

three different orientations of $VO_2^+$ (fig 5.D). The results of adsorption energies are summarised in the table D.2 and the most stable structures for every geometry is shown in the fig. 7.D

| Orientation # | BG(eV) | BG -OH (eV) | BG-epoxy (eV) | BG-D-H (eV) | BG-D (eV) | BG-D-OH (eV) | BG-D-O (eV) | BG-D-COOH (eV) |
|---|---|---|---|---|---|---|---|---|
| 1 | -1.043 | unstable | unstable | -1.396 | -2.713 | -0.894 | -2.286 | -2.12 |
| 2 | -1.066 | | | -1.408 | -2.689 | -1.012 | -2.321 | -1.961 |
| 3 | -1.112 | | | -1.339 | -3.29 | -1.144 | -2.29 | -2.13 |
| Most stable | -1.112 | | | -1.408 | -3.29 | -1.144 | -2.321 | -2.13 |

**Table D.2** *Adsorption energies (eV) of the $VO_2^+$ at different representative geometries*

The adsorption energies in the table 2 show that, $VO_2^+$ has greater adsorption energy on surfaces, containing functional groups on their basal defects. Among those, the COOH and C=O groups on the basal defects, shown the maximum affinity towards the $VO_2^+$ and their respective adsorption energies are 2.13 eV and 2.3 eV. The descending order of adsorption energies of the $VO_2^+$, on all the surfaces, is indicated below

*BG-D (-3.29 eV) > C=O (-2.321 eV) > COOH (-2.13 eV) > C-H (-1.408) > OH (-1.144 eV) > BG (- 1.112 eV)*

The order of adsorption energies of the $VO_2^+$ against different functional groups are quite similar with trend of $VO^{2+}$. It can be concluded that all the basal defects covered with different functional groups enhanced the affinity in of the electrode against the vanadium (V), comparative to the bare surface.

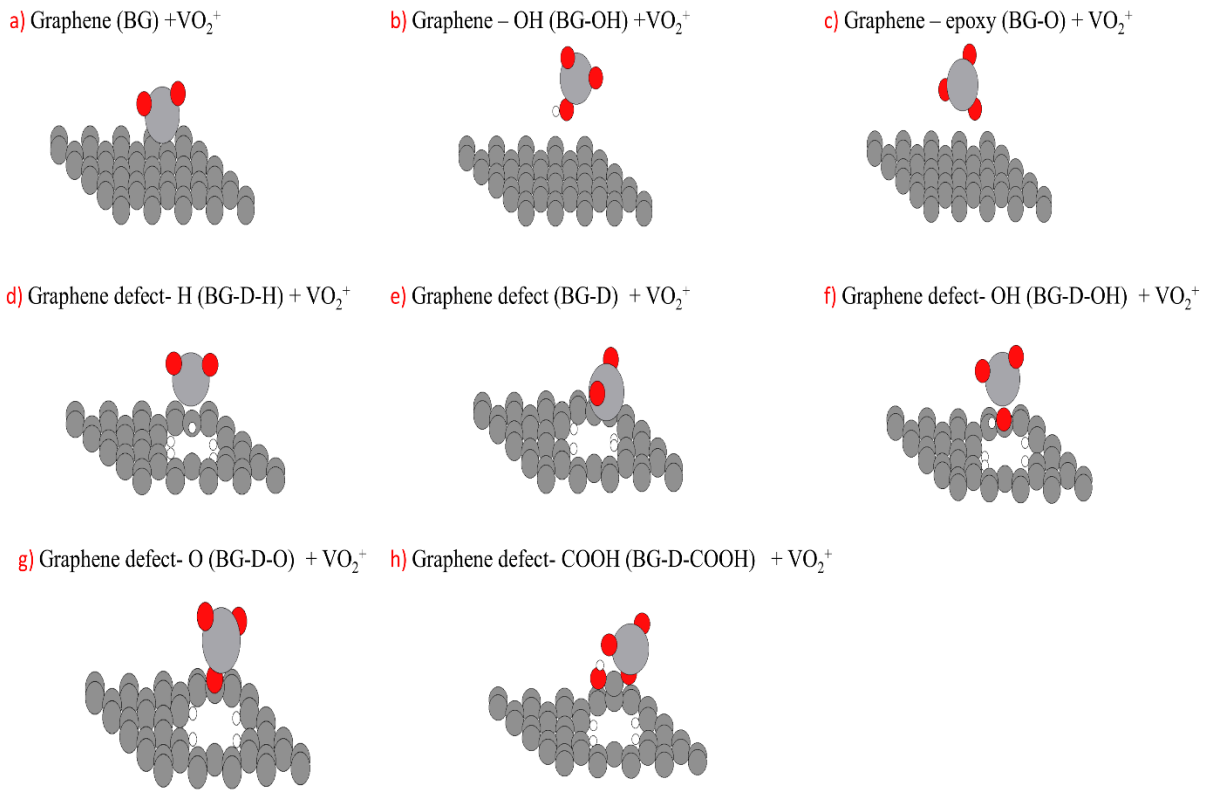


***Fig. 7.D*** *Relaxed structures of composite geometry containing adsorbate* $VO_2^+$ on *a) Basal surface (BG) b) Basal surface with OH (BG-OH), c) Basal surface with O (BG-O), d) Basal defect covered with hydrogen (BG-D-H) e) Basal defect (BG-D), f) Basal defect covered with hydroxyl (BG-D-OH), g) Basal defect covered with carbonyl (BG-D-O) h) Basal defect covered with carboxyl (BG-D-COOH)*

### *4.4.3 Interaction of the $H_2O$ with modified electrode surfaces*

The GF is intrinsically hydrophobic and for the better electrode-electrolyte interaction, the surface of the GF should have good affinity towards the water. It is important to investigate the behaviour of the oxygenal functional groups, that are showing better affinity for $VO^{2+}$ and $VO_2^+$, towards the water. The adsorption calculations are performed in the similar way as previously mentioned. The adsorption energies of water on modified surfaces are improved due to the functional groups. Among all, -COOH groups is showing maximum adsorption energy i-e -0.375

eV. In chapter 2 (section 2.3.5) and 3 (3.2.7), it was discussed in the detail that activation successfully made the electrode hydrophilic. All the adsorption energies are enlisted in table D.3 and respective most stable structures are shown in fig 8.D

| Orientation # | **BG (eV)** | **BG -OH (eV)** | **BG-epoxy (eV)** | **BG-D-H (eV)** | **BG-D (eV)** | **BG-D-OH (eV)** | **BG-D-O (eV)** | **BG-D-COOH (eV)** |
|---|---|---|---|---|---|---|---|---|
| 1 | -0.1 | -0.169 | -0.082 | -0.25 | -0.287 | -0.194 | 0.069 | -0.265 |
| 2 | -0.172 | -0.148 | -0.099 | -0.196 | -0.244 | -0.169 | -0.199 | -0.357 |
| 3 | -0.175 | -0.155 | -0.148 | -0.159 | -0.278 | -0.159 | -0.186 | -0.305 |
| Most stable | -0.175 | -0.169 | -0.148 | -0.25 | -0.287 | -0.194 | -0.199 | -0.357 |

**Table D.3** Adsorption energies (eV) of the $H_2O$ at different representative geometries

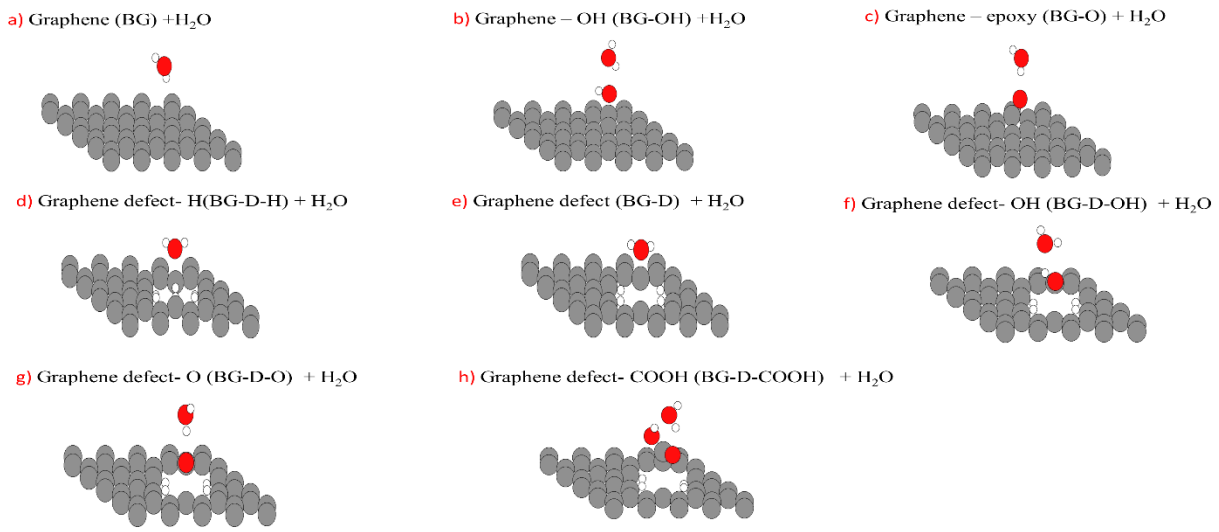


***Fig. 8.D*** *Relaxed structures of composite geometry containing adsorbate* $H_2O$ on *a) Basal surface (BG) b) Basal surface with OH (BG-OH), c) Basal surface with O (BG-O), d) Basal defect covered with hydrogen (BG-D-H) e) Basal defect (BG-D), f) Basal defect covered with hydroxyl (BG-D-OH), g) Basal defect covered with carbonyl (BG-D-O) h) Basal defect covered with carboxyl (BG-D-COOH)*

*4.4.4 Correlation between "$sp^3$ hybridization ⇌ oxygenal groups ⇌ $VO^{2+}/VO_2^+$ affinity with electrode"*

As discussed above, all the oxidative activation procedures of the carbon-based electrodes increase the $sp^3$ hybridization of carbon and oxygenal groups simultaneously and it is experimentally difficult to establish their individual contribution in the kinetics of the positive half-cell reaction. The projected density of state (PDOS) calculations are performed and their spectra are compared in the fig. 9.D, to establish the inter-relation of the different oxygenal groups, surface morphology, and their affinity with the electrode.

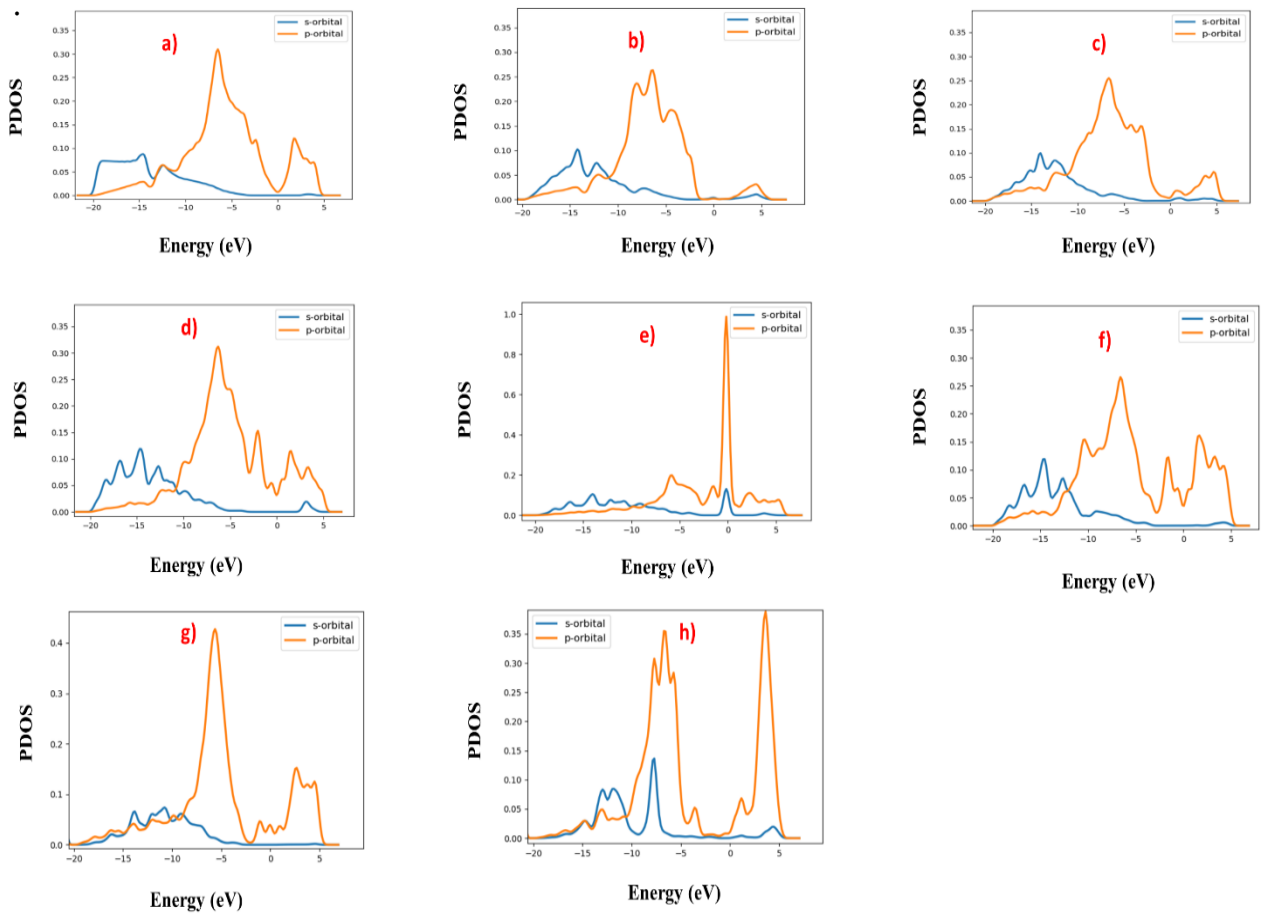


***Fig. 9.D*** *Projected density of state (PDOS) graphs a) Basal surface (BG) b) Basal surface with OH (BG-OH), c) Basal surface with O (BG-O), d) Basal defect covered with hydrogen (BG-D-H) e) Basal defect (BG-D), f) Basal defect covered with hydroxyl (BG-D-OH), g) Basal defect covered with carbonyl (BG-D-O) h) Basal defect covered with carboxylic (BG-D-COOH)*

In the calculations, density of states of s and p orbital are calculated, against different energy levels. The density of states is the probability of free electron to be present in the different orbitals. It means, the extent of the overlapping of s-orbital and p-orbital spectra in PDOS graph, show the hybridization of s and p orbitals; so the increase in the overlapping can directly link with the increase in $sp^3$ hybridization. [156].

In previous sections, it is discussed that the adsorption energies of $VO^{2+}/VO_2^+$ is greater on electrodes having oxygenal groups than the unmodified electrode surface. The PDOS spectra of the electrode can give insights for this improved adsorption energies. By qualitatively analysing the PDOS spectra of the BG-D-COOH (fig 9.D, h) and BG-D-O (fig 9.D, g) indicates that s and p spectra is overlapping with each other between the energy range of -20 eV to -10 eV, but there is not any overlapping observed in the case of unmodified electrode BG (fig 9.D, a).

The overlapping is quantified by integrating the s and p spectra curves separately, over the energy range of -20 eV to -10 eV; and sequentially dividing the area of p-spectra by the area of s-spectra. The evolution of the change in the s-p hybridization and corresponding interaction with the $VO^{2+}/VO_2^+$ is summarized in the table D.4. It is evident from the table, that the adsorption energies of $VO^{2+}$ and $VO_2^+$ increased with the increase of the s-p hybridization. For instance, the $VO^{2+}/VO_2^+$ showed almost double adsorption energy on electrode with carboxylic group (BG-D-COOH), in comparison with the BG-D-OH. The following difference is present in s-p hybridization of both electrodes : BG-D-COOH s = 57 % p = 43 % ⇌ BG-D-OH s = 70.6 % p = 29.4 %. In the same way, the s-p hybridization of the BG-D-O (s = 55.4 %, p= 44.6 %) is more than the BG-D-COOH; and consequently, the increase in the adsorption energy on the BG-D-O is more pronounced.

| | BG | BG-D-OH | BG-D-COOH | BG-D-O |
|---|---|---|---|---|
| s-p spectra proportions | s = 74.5 %<br>p = 25.5 % | s = 70.6 %<br>p = 29.4 % | s = 57 %<br>p = 43 % | s = 55.4 %<br>p = 44.6 % |
| $VO^{2+}$ adsorption energy (eV) | -1.31 | 1.35 | -2.53 | -2.69 |
| $VO_2^+$ adsorption energy(eV) | -1.11 | -1.14 | -2.13 | -2.32 |

***Table D.4.****The percentage s-p hybridization of BG, BG-D-OH, BG-D-COOH and BG-D-O; and respective adsorption energies of $VO^{2+}/VO_2^+$ on it.*

It is important to note, that the adsorption energies of $VO^{2+}$ and $VO_2^+$ are maximum on the BG-D (discussed in adsorption sections). Its PDOS spectra (fig 9.D, e) shows the huge rise around 0 eV, revealing the dangling and unstable bond nature. This bond is very reactive, and hence showing the max adsorption energies towards vanadium species. In real, these dangling bonds are most likely covered with other oxygenal groups, when it is introduced into the acidic electrolyte. [129]. Even then, to intrinsically study the interaction between the defect and vanadium ions is of theoretically point of interest; as in the operating conditions of the VRFBs, especially at higher state of charge electrolyte, the excessive oxidation could happen, that can lead to the formation of CO and $CO_2$ production (removal of oxygenal groups that can leave the defects behind) [85,99].

To summarize the discussion: it is evident that the extent of the overlapping caused by the basal defects covered by the oxygenal groups are in the following sequence i-e C=O > -COOH> -C-OH > basal surface. The adsorption energies of vanadium redox couples on the oxygenal groups are exactly in the same order. So, the conclusion could be drawn that the $sp^2/sp^3$ hybridization is directly linked with the affinity of the positive half-cell redox couple ($VO^{2+}/VO_2^+$) with the graphite electrode; resulted into the higher currents and lower overpotential.[154] The fabrication

of the oxygenal groups (-OH, C=O, -COOH) are just responsible for the $sp^3$ hybridization of the carbon atoms in graphite felts. Based on these observations, it is evident that the electrode structure is the predominant factor in the kinetics of positive half-cell reaction, instead of oxygenal groups. This observation is also in line with the experimental study[64] This insight could be very useful to the material modelling and engineering of the electrodes for the positive half-cell electrode

## 4.5 Conclusion

In this study, the individual roles of the different oxygenal groups and $sp^3$ hybridization in the positive half-cell reaction of vanadium redox flow couple ($VO^{2+}/VO_2^+$) are investigated, via DFT calculations. The oxygenal groups showing the catalytic effect, against the $VO^{2+}/VO_2^+$ redox couple in the following order i-e C=O > COOH, > OH > C-H. Projected density of states calculations (PDOS) shows that these groups are responsible for the increase in the $sp^3$ hybridization, and the order of their contribution to increase the $sp^3$ hybridization is also the same (C=O > COOH, > OH > C-H). From this, the conclusion could be drawn that the increase in the $sp^3$ hybridization of the structures is mainly contributing in the $VO^{2+}$ / $VO_2^+$ reaction. Oxygenal groups are just responsible of this increase.

# 5. General conclusion of thesis and future perspective.

## ***5. General conclusion of thesis and future perspective***.

In this thesis, various activation methods of graphite felts are extensively studied, in order to be used as the positive electrode of a vanadium redox flow battery. These studies are done on molecular, micro and pilot scale levels. The activation methods discussed are based on the electrochemical oxidation, as well as chemical and thermal treatments. Multiple tools are used to investigate and characterized the activation of electrode, such as cyclic voltammetry, linear sweep voltammetry, scanning electron microscopy, FTIR, contact angle measurements and DFT calculations. The electrodes that showed promising performance in initial trials are then evaluated in the classical half-cell electrolysis and electrochemical plug flow reactor.

In chapter 2, the GF electrode was activated by heating in 5 M acidic $K_2Cr_2O_7$ solution. The various operational conditions of temperature and duration were investigated, to get an enhanced activation of the electrode. For that reason, the following three different series of experiment were performed: 1) First, the effect of the temperature on the activation was investigated at 100 $^oC$, 140 $^oC$ and 160 $^oC$, at a constant duration of 2 hrs. 2) The other series of experiments were performed at constant temperature of 100 $^oC$, at the duration of the 2, 5 and 8 h. 3) The heating of electrode at 140 $^oC$ are further explored at the 2 h, 5 h and 8 h ; because in initial series of experiments 1 and 2 ; among all, the electrode treated at 140 $^oC$, showed best performance and it is decided to further explore this temperature for different range of durations.

The anodic to cathodic peak current ratio $(I_a/I_c)$ and peak potential difference $(\Delta E_{a/c}= E_a - E_c)$, extracted from voltammograms, show that heating the GF at 140 $^oC$ for 2h corresponds to the best operating condition for activation of the GF. Indeed, $(\Delta E_{a/c}= E_a - E_c)$ decreases from the 0.99 V → 0.61V, while $I_a/I_c$ decrease from the 2.1 → 1.23 . Fourier-transform infrared spectroscopy

(FTIR) analysis of the electrode surface shows that the different oxygenal groups such as hydroxyl (OH), carbonyl (C=O) and carboxylic (COOH), are inscribed on the surface of the fibbers. Most likely these groups catalyse the reaction on the surface and decrease the overpotential of both oxidation and reduction reactions. In addition to that, the presence of these oxides is also confirmed by linear sweep voltammetry (LSV), at the steady state, of the activated electrode in the blank 3 M $H_2SO_4$ acidic solution: the anodic and cathodic peak showed oxidation and reduction of the oxygenal groups present on the surface of the treated electrode. To quantify the improvement, the reaction sites (oxygenal groups) are determined by adsorption test. The number of sites of the GF increase from to "$5.3 \times 10^{16}$" to the "$200 \times 10^{16}$" due to the activation. The oxygenal groups not only catalyze the reactions, but also increase the hydrophilicity of the electrodes, by promoting the electrode-electrolyte interaction. Simple tests were conducted to evidence the enhancement, by dipping the electrode in the $VO^{2+}$ acidic solution. The untreated GF keeps on floating on the surface, while the treated electrode goes immediately into the electrolyte. Analysis of the surface morphology by scanning electron microscopy (SEM) showed the increase of the surface roughness of the treated electrode. The roughness of surface provides more surface area available for the reaction, and the increase in the peak CV current of treated electrode, quantitatively support this argument.

Based on cyclic voltammetry results mentioned above, it can be concluded that the enhancement of the electro kinetic activity of the electrode directly results from activation; and subsequent characterization shows that it is due to the surface chemistry and its morphological changes. The electroactivity performance is further explored at the stirred and steady conditions by linear sweep voltammetry. The modified surface of the treated electrode enables the improvement of the intrinsic heterogeneous electronic transfer constant ($k°$) from (1.7 μm/s → 3.8 μm/s) for the

battery recharge, and from (0.92 μm/s → 5.06 μm/s) for the battery discharge reaction of the positive half-cell. Due to the increase of the rate constants of charge discharge reactions, 3 % and 5 % improvement was observed in their faradic yield respectively, measured in the classical half-cell electrolysis.

All the above results demonstrate that treatment by acidic $K_2Cr_2O_7$ improve the performance of the electrode, to use it as the positive electrode in vanadium redox flow battery. Further work is carried out to explore more activation methods, that could be more suitable, either in terms of their environmental hazardousness, and in the terms of easiness of operation or resulted performance. The $H_3PO_4$ is relatively mild acid and oxidizer and in this work, the possibility of its use was investigated to activate the GF for VRFBs, but the cyclic voltammetry analysis of $H_3PO_4$ treated electrodes does not show any improvement. The effect of the basic media on the GF activation is also investigated by heating the electrode in 1 M KOH solution and submit it to the heat treatment. Minor improvement was observed in the CV, and treatment was more investigated. Electrochemical treatment in the aqueous electrolyte $(NH_4)_2CO_3$, is also examined under constant current of 30 mA, for various durations ($1 < t_{min} < 20$); and in another series of experiments, at the constant voltage. Instead of increasing the electrode activity, it decreased the performance of the electrode, possibly because of the adsorption of some salts on the electrode.

In quest of finding another possibility, $KMnO_4$ was used to treat electrode in following two different ways. 1) The $KMnO_4$ derived particles are introduced on the GF, expecting to use them as catalysts for the reactions. After fabrication of these particles, the GF was heated at 400 $^oC$ (in presence of air) and 600 $^oC$ (in presence of the $N_2$) to try to bind these particles strongly with GF, with and without cracking respectively. These particles are not electrochemically stable on the surface, neither they are catalysing the reactions. 2) In second way, GF is heated in the 0.01 M

$KMnO_4$ + 3 M $H_2SO_4$ solution. The activated GF by heating in the acidic $KMnO_4$, show better electroactivity against the $VO^{2+}/VO_2^+$. The heating is done in the simple beaker under non reflux conditions, in contrary to $K_2Cr_2O_7$ treatment, that is done in the reflux conditions. The $KMnO_4$ acidic treatment is easier than the $K_2Cr_2O_7$ and 35 % increase was observed in the peak currents of the CV. The average charge voltage decreases and obtained voltage increase, during the half cell electrolysis. The pilot scale stack charge-discharge cycle of VRFBs shows, that there is an improvement of 20 % and 13 % in energy and voltage efficiency (VE), respectively. The surface characterizations indicate the presence of the oxygenal groups and surface roughness, that is most likely the reason of this improvement. The proposed activation methods in this work are effective and operationally easy, improving the overall performance of the vanadium redox flow battery

With the help of the density functional theory calculations, the phenomena are studied on the molecular level to find out the fundamental reason of the increase in electrode kinetic activity. Experimentally, we came to know that the presence of oxygenal groups (OH, C=O, COOH) and structural changes (increase in $sp^3$ hybridization) are the cause of the kinetics improvement. DFT calculations shows that the $sp^3$ hybridization is the actual reason of the kinetics improvement. The oxygenal groups are just the cause of this increment in hybridization; and their contribution in creating hybridization is in the following order "C=O > COOH > OH > basal plane."

***Future perspectives***

The vanadium redox flow batteries, as previously described in detail, comprised of multicomponent such as current collector, membrane, electrodes and electrolyte. To effectively deploy VRFBs on commercial, all its individual components should be optimized, and should

have low ohmic drops and overpotential losses. Additionally, selections of the most optimized parameters of flow rates, designing of the stack, flow geometry and the possible heat-mass transfer problems; all are very important for the performance of the stack. Precisely speaking, the engineering aspect of the problem is important, and optimize these process parameters, can contribute significantly in the efficiency of the stack

In this thesis, we talked about the surface activation of the 3D fibrous GF electrode, expecting to improve the kinetic electroactivity and reversibility of the electrode. The other important related issues are the connection of this electrode with the current collector plates. Proper contact of the current collector and the electrode is necessary to avoid the ohmic losses. Usually, pressure exerted by the exterior plates of stack or/and some binder help to make this properly. But increasing the compression may damage the electrode or convert 3D fibrous electrode into planer electrode. The state of art current collector system should be design and investigate.

The flow of the electrolyte through stack, can make some channeling and dead areas inside electrode, so all the surface is not available for the reaction. So, the properly designing the core of the electrolytic compartments, with some insertion of flow patterns/channels can reduce any such dead area and uniformize the residence time of flow inside the stack. The further related problem is the formation of the heat spots in the electrode-electrolyte surface; it is important to avoid thermal rise, especially in the positive half-cell. Because the solubility of the vanadium (+5) decrease with increasing temperature and it starts precipitating. This phenomenon can passivate the electrode surface and clog the fibrous structure. It is important to investigate, how to avoid this temperature rise. A possible way to avoid this problem could be of the addition of some complexes, that increase the solubility of vanadium (+5) at high temperatures, so it may not affect with temperature rise.

There are also issues of the stability of the redox couple $V^{2+}/V^{3+}$ in the negolyte; the inert environment is required to avoid the oxidation of $V^{2+}$ by dissolved $O_2$. The electrolyte flows through all the loop of the flow battery and there is always the possibility of the penetration of oxygen in stack. This effect, not significant for short times, affect the electrolyte stability over the longer durations. It is interesting to investigate materials, reducing the diffusion flux of $O_2$ to avoid this problem.

If all the ohmic losses, overpotential and related losses are minimized, the vanadium redox flow battery can be suitable for the stationary energy storage applications and can play vital role in the energy management of the renewable resources.

## *6. List of publications from thesis*

1. Facile chemical activation of graphite felt by $KMnO_4$ acidic solution for vanadium redox flow batteries (doi.org/10.1016/j.apsusc.2020.146808)
   (**Published:** Applied surface science , ELSEVIER**)**

2. Enhancement of the electrochemical activity of a commercial graphite felt for vanadium redox flow battery (VRFB), by chemical treatment with acidic solution of $K_2Cr_2O_7$

   doi.org/10.1016/j.est.2019.100967

   (**Published:** Journal of energy storage, ELSEVIER**)**

3. Comparative study of the role of $sp^3$ hybridization and different oxygenal groups on the graphite felt electrodes, towards positive half-cell redox couple in vanadium redox flow batteries
   (**In process)**

# 5. References

***References***


[1] Statistical Review of World Energy | Energy economics | Home, (n.d.). https://www.bp.com/en/global/corporate/energy-economics/statistical-review-of-world-energy.html (accessed August 31, 2020).

[2] Causes | Facts – Climate Change: Vital Signs of the Planet, (n.d.). https://climate.nasa.gov/causes/ (accessed August 31, 2020).

[3] Renewable energy directive | Energy, (n.d.). https://ec.europa.eu/energy/topics/renewable-energy/renewable-energy-directive/overview_en (accessed August 31, 2020).

[4] Solar power | Energy, (n.d.). https://ec.europa.eu/energy/topics/renewable-energy/solar-power_en (accessed August 31, 2020).

[5] Year in review | Energy economics | Home, (n.d.). https://www.bp.com/en/global/corporate/energy-economics/statistical-review-of-world-energy/year-in-review.html#electricity (accessed September 4, 2020).

[6] H. Ibrahim, A. Ilinca, J. Perron, Energy storage systems-Characteristics and comparisons, Renew. Sustain. Energy Rev. 12 (2008) 1221–1250. doi:10.1016/j.rser.2007.01.023.

[7] M.C. Argyrou, P. Christodoulides, S.A. Kalogirou, Energy storage for electricity generation and related processes: Technologies appraisal and grid scale applications, Renew. Sustain. Energy Rev. 94 (2018) 804–821. doi:10.1016/j.rser.2018.06.044.

[8] X. Luo, J. Wang, M. Dooner, J. Clarke, Overview of current development in electrical energy storage technologies and the application potential in power system operation, Appl. Energy. 137 (2015) 511–536. doi:10.1016/j.apenergy.2014.09.081.

[9] M. Beaudin, H. Zareipour, A. Schellenberglabe, W. Rosehart, Energy storage for mitigating the variability of renewable electricity sources: An updated review, Energy Sustain. Dev. 14 (2010) 302–314. doi:10.1016/j.esd.2010.09.007.

[10] M. Aneke, M. Wang, Energy storage technologies and real life applications – A state of the art review, Appl. Energy. 179 (2016) 350–377. doi:10.1016/j.apenergy.2016.06.097.

[11] H. Chen, T.N. Cong, W. Yang, C. Tan, Y. Li, Y. Ding, Progress in electrical energy storage system: A critical review, Prog. Nat. Sci. 19 (2009) 291–312. doi:10.1016/j.pnsc.2008.07.014.

[12] S. Ould Amrouche, D. Rekioua, T. Rekioua, S. Bacha, Overview of energy storage in renewable energy systems, Int. J. Hydrogen Energy. 41 (2016) 20914–20927. doi:10.1016/j.ijhydene.2016.06.243.

[13] F. Díaz-González, A. Sumper, O. Gomis-Bellmunt, R. Villafáfila-Robles, A review of energy storage technologies for wind power applications, Renew. Sustain. Energy Rev. 16 (2012) 2154–2171. doi:10.1016/j.rser.2012.01.029.

[14] S.G. Chalk, J.F. Miller, Key challenges and recent progress in batteries, fuel cells, and hydrogen storage for clean energy systems, J. Power Sources. 159 (2006) 73–80. doi:10.1016/j.jpowsour.2006.04.058.

[15] Z. Qi, G.M. Koenig, Review Article: Flow battery systems with solid electroactive materials, J. Vac. Sci. Technol. B, Nanotechnol. Microelectron. Mater. Process. Meas. Phenom. 35 (2017) 040801. doi:10.1116/1.4983210.

[16] Y.K. Zeng, T.S. Zhao, L. An, X.L. Zhou, L. Wei, A comparative study of all-vanadium

and iron-chromium redox flow batteries for large-scale energy storage, J. Power Sources. 300 (2015) 438–443. doi:10.1016/j.jpowsour.2015.09.100.

[17] Y.K. Zeng, X.L. Zhou, L. An, L. Wei, T.S. Zhao, A high-performance flow-field structured iron-chromium redox flow battery, J. Power Sources. 324 (2016) 738–744. doi:https://doi.org/10.1016/j.jpowsour.2016.05.138.

[18] S.E. Waters, B.H. Robb, M.P. Marshak, Effect of Chelation on Iron–Chromium Redox Flow Batteries, ACS Energy Lett. 5 (2020) 1758–1762. doi:10.1021/acsenergylett.0c00761.

[19] V. Viswanathan, A. Crawford, D. Stephenson, S. Kim, W. Wang, B. Li, G. Coffey, E. Thomsen, G. Graff, P. Balducci, M. Kintner-Meyer, V. Sprenkle, Cost and performance model for redox flow batteries, J. Power Sources. 247 (2014) 1040–1051. doi:10.1016/j.jpowsour.2012.12.023.

[20] A. Crawford, V. Viswanathan, D. Stephenson, W. Wang, E. Thomsen, D. Reed, B. Li, P. Balducci, M. Kintner-Meyer, V. Sprenkle, Comparative analysis for various redox flow batteries chemistries using a cost performance model, J. Power Sources. 293 (2015) 388–399. doi:10.1016/j.jpowsour.2015.05.066.

[21] P. Alotto, M. Guarnieri, F. Moro, Redox flow batteries for the storage of renewable energy: A review, Renew. Sustain. Energy Rev. 29 (2014) 325–335. doi:10.1016/j.rser.2013.08.001.

[22] M. Skyllas-kazacos, G. Kazacos, G. Poon, H. Verseema, Recent advances with UNSW vanadium-based redox flow batteries, (2010) 182–189. doi:10.1002/er.

[23] S. Zhong, M. Skyllas-Kazacos, Electrochemical behaviour of vanadium(V)/vanadium(IV) redox couple at graphite electrodes, J. Power Sources. 39 (1992) 1–9. doi:10.1016/0378-7753(92)85001-Q.

[24] Q. Lai, H. Zhang, X. Li, L. Zhang, Y. Cheng, A novel single flow zinc-bromine battery with improved energy density, J. Power Sources. 235 (2013) 1–4. doi:10.1016/j.jpowsour.2013.01.193.

[25] H.R. Jiang, M.C. Wu, Y.X. Ren, W. Shyy, T.S. Zhao, Towards a uniform distribution of zinc in the negative electrode for zinc bromine flow batteries, Appl. Energy. 213 (2018) 366–374. doi:10.1016/j.apenergy.2018.01.061.

[26] Z. Xie, Q. Liu, Z. Chang, X. Zhang, The developments and challenges of cerium half-cell in zinc–cerium redox flow battery for energy storage, Electrochim. Acta. 90 (2013) 695–704. doi:https://doi.org/10.1016/j.electacta.2012.12.066.

[27] P.K. Leung, C. Ponce-de-León, C.T.J. Low, A.A. Shah, F.C. Walsh, Characterization of a zinc–cerium flow battery, J. Power Sources. 196 (2011) 5174–5185. doi:https://doi.org/10.1016/j.jpowsour.2011.01.095.

[28] Y. Liu, X. Xia, H. Liu, Studies on cerium (Ce4+/Ce3+)-vanadium(V 2+/V3+) redox flow cell - Cyclic voltammogram response of Ce4+/Ce3+ redox couple in H2SO4 solution, J. Power Sources. 130 (2004) 299–305. doi:10.1016/j.jpowsour.2003.12.017.

[29] P.K. Leung, C. Ponce De Leon, F.C. Walsh, The influence of operational parameters on the performance of an undivided zinc-cerium flow battery, Electrochim. Acta. 80 (2012) 7–14. doi:10.1016/j.electacta.2012.06.074.

[30] M. Skyllas-Kazacos, All-Wanadium Redox Battery, United States Pat. (1988). https://patentimages.storage.googleapis.com/8c/60/c7/fc476258aa5394/US4786567.pdf.

[31] L. Joerissen, J. Garche, C. Fabjan, G. Tomazic, Possible use of vanadium redox-flow batteries for energy storage in small grids and stand-alone photovoltaic systems, J. Power Sources. 127 (2004) 98–104. doi:https://doi.org/10.1016/j.jpowsour.2003.09.066.

[32] Vanadium-Flow Batteries: The Energy Storage Breakthrough We've Needed, (n.d.). https://www.forbes.com/sites/jamesconca/2016/12/13/vanadium-flow-batteries-the-energy-storage-breakthrough-weve-needed/#3c6e2d395bde (accessed September 14, 2020).

[33] P.K. Leung, M.R. Mohamed, A.A. Shah, Q. Xu, M.B. Conde-Duran, A mixed acid based vanadium-cerium redox flow battery with a zero-gap serpentine architecture, J. Power Sources. 274 (2015) 651–658. doi:10.1016/j.jpowsour.2014.10.034.

[34] X.L. Zhou, T.S. Zhao, L. An, Y.K. Zeng, L. Wei, Critical transport issues for improving the performance of aqueous redox flow batteries, J. Power Sources. 339 (2017) 1–12. doi:10.1016/j.jpowsour.2016.11.040.

[35] M. Zhang, M. Moore, J.S. Watson, T.A. Zawodzinski, R.M. Counce, Capital Cost Sensitivity Analysis of an All-Vanadium Redox-Flow Battery, J. Electrochem. Soc. 159 (2012) A1183–A1188. doi:10.1149/2.041208jes.

[36] X. Wu, J. Hu, J. Liu, Q. Zhou, W. Zhou, H. Li, Ion exchange membranes for vanadium redox flow batteries, Pure Appl. Chem. 86 (2014) 633–649. doi:10.1515/pac-2014-0101.

[37] X. Li, H. Zhang, Z. Mai, H. Zhang, I. Vankelecom, Ion exchange membranes for

vanadium redox flow battery (VRB) applications, Energy Environ. Sci. 4 (2011) 1147–1160. doi:10.1039/c0ee00770f.

[38] B. Schwenzer, J. Zhang, S. Kim, L. Li, J. Liu, Z. Yang, Membrane Development for Vanadium Redox Flow Batteries, ChemSusChem. 4 (2011) 1388–1406. doi:10.1002/cssc.201100068.

[39] J. Xi, Z. Wu, X. Teng, Y. Zhao, L. Chen, X. Qiu, Self-assembled polyelectrolyte multilayer modified Nafion membrane with suppressed vanadium ion crossover for vanadium redox flow batteries, J. Mater. Chem. 18 (2008) 1232–1238. doi:10.1039/B718526J.

[40] B. Jiang, L. Wu, L. Yu, X. Qiu, J. Xi, A comparative study of Nafion series membranes for vanadium redox flow batteries, J. Memb. Sci. 510 (2016) 18–26. doi:10.1016/j.memsci.2016.03.007.

[41] D. Chen, S. Wang, M. Xiao, Y. Meng, Preparation and properties of sulfonated poly(fluorenyl ether ketone) membrane for vanadium redox flow battery application, J. Power Sources. 195 (2010) 2089–2095. doi:10.1016/j.jpowsour.2009.11.010.

[42] L. Cao, A. Kronander, A. Tang, D.W. Wang, M. Skyllas-Kazacos, Membrane permeability rates of vanadium ions and their effects on temperature variation in vanadium redox batteries, Energies. 9 (2016). doi:10.3390/en9121058.

[43] Q. Chen, Y.Y. Du, K.M. Li, H.F. Xiao, W. Wang, W.M. Zhang, Graphene enhances the proton selectivity of porous membrane in vanadium flow batteries, Mater. Des. 113 (2017) 149–156. doi:10.1016/j.matdes.2016.10.019.

[44] X. Luo, Z. Lu, J. Xi, Z. Wu, W. Zhu, L. Chen, X. Qiu, Influences of permeation of vanadium ions through PVDF-g-PSSA membranes on performances of vanadium redox flow batteries, J. Phys. Chem. B. 109 (2005) 20310–20314. doi:10.1021/jp054092w.

[45] C. Sun, J. Chen, H. Zhang, X. Han, Q. Luo, Investigations on transfer of water and vanadium ions across Nafion membrane in an operating vanadium redox flow battery, J. Power Sources. 195 (2010) 890–897. doi:10.1016/j.jpowsour.2009.08.041.

[46] P.K. Leung, Q. Xu, T.S. Zhao, L. Zeng, C. Zhang, Preparation of silica nanocomposite anion-exchange membranes with low vanadium-ion crossover for vanadium redox flow batteries, Electrochim. Acta. 105 (2013) 584–592. doi:10.1016/j.electacta.2013.04.155.

[47] A. Parasuraman, T.M. Lim, C. Menictas, M. Skyllas-Kazacos, Review of material research and development for vanadium redox flow battery applications, Electrochim. Acta. 101 (2013) 27–40. doi:10.1016/j.electacta.2012.09.067.

[48] X. Teng, J. Dai, F. Bi, X. Jiang, Y. Song, G. Yin, Ultra-thin polytetrafluoroethene/Nafion/silica membranes prepared with nano SiO2 and its comparison with sol–gel derived one for vanadium redox flow battery, Solid State Ionics. 280 (2015) 30–36. doi:https://doi.org/10.1016/j.ssi.2015.08.005.

[49] J. Xi, Z. Wu, X. Teng, Y. Zhao, L. Chen, X. Qiu, Self-assembled polyelectrolyte multilayer modified Nafion membrane with suppressed vanadium ion crossover for vanadium redox flow batteries, J. Mater. Chem. 18 (2008) 1232. doi:10.1039/b718526j.

[50] J. Xi, Z. Wu, X. Qiu, L. Chen, Nafion/SiO2 hybrid membrane for vanadium redox flow battery, J. Power Sources. 166 (2007) 531–536. doi:10.1016/j.jpowsour.2007.01.069.

[51] X. Teng, Y. Zhao, J. Xi, Z. Wu, X. Qiu, L. Chen, Nafion/organic silica modified TiO2 composite membrane for vanadium redox flow battery via in situ sol-gel reactions, J. Memb. Sci. 341 (2009) 149–154. doi:10.1016/j.memsci.2009.05.051.

[52] D. Chen, M.A. Hickner, V5+ degradation of sulfonated Radel membranes for vanadium redox flow batteries, Phys. Chem. Chem. Phys. 15 (2013) 11299–11305. doi:10.1039/C3CP52035H.

[53] Z. Yuan, X. Li, Y. Zhao, H. Zhang, Mechanism of Polysulfone-Based Anion Exchange Membranes Degradation in Vanadium Flow Battery, ACS Appl. Mater. Interfaces. 7 (2015) 19446–19454. doi:10.1021/acsami.5b05840.

[54] C. Choi, S. Kim, R. Kim, Y. Choi, S. Kim, H. young Jung, J.H. Yang, H.T. Kim, A review of vanadium electrolytes for vanadium redox flow batteries, Renew. Sustain. Energy Rev. 69 (2017) 263–274. doi:10.1016/j.rser.2016.11.188.

[55] S. Peng, N. Wang, C. Gao, Y. Lei, X. Liang, S. Liu, Y. Liu, Influence of trishydroxymethyl aminomethane as a positive electrolyte additive on performance of vanadium redox flow battery, Int. J. Electrochem. Sci. 7 (2012) 4314–4321.

[56] J. Zhang, L. Li, Z. Nie, B. Chen, M. Vijayakumar, S. Kim, W. Wang, B. Schwenzer, J. Liu, Z. Yang, Effects of additives on the stability of electrolytes for all-vanadium redox flow batteries, J. Appl. Electrochem. 41 (2011) 1215–1221. doi:10.1007/s10800-011-0312-1.

[57] L. Li, S. Kim, W. Wang, M. Vijayakumar, Z. Nie, B. Chen, J. Zhang, G. Xia, J. Hu, G. Graff, J. Liu, Z. Yang, A Stable Vanadium Redox-Flow Battery with High Energy Density

for Large-Scale Energy Storage, Adv. Energy Mater. 1 (2011) 394–400. doi:10.1002/aenm.201100008.

[58] S. Kim, M. Vijayakumar, W. Wang, J. Zhang, B. Chen, Z. Nie, F. Chen, J. Hu, L. Li, Z. Yang, Chloride supporting electrolytes for all-vanadium redox flow batteries, Phys. Chem. Chem. Phys. 13 (2011) 18186–18193. doi:10.1039/C1CP22638J.

[59] N. Kausar, A. Mousa, M. Skyllas-Kazacos, The Effect of Additives on the High-Temperature Stability of the Vanadium Redox Flow Battery Positive Electrolytes, ChemElectroChem. 3 (2016) 276–282. doi:10.1002/celc.201500453.

[60] M. Rychcik, M. Skyllas-Kazacos, Evaluation of electrode materials for vanadium redox cell, J. Power Sources. 19 (1987) 45–54. doi:10.1016/0378-7753(87)80006-X.

[61] B. Sun, M. Skyllas-Kazakos, Chemical modification and electrochemical behaviour of graphite fibre in acidic vanadium solution, Electrochim. Acta. 36 (1991) 513–517. doi:10.1016/0013-4686(91)85135-T.

[62] A. Hassan, T. Tzedakis, Facile chemical activation of graphite felt by KMnO4 acidic solution for vanadium redox flow batteries, Appl. Surf. Sci. 528 (2020) 146808. doi:10.1016/j.apsusc.2020.146808.

[63] A. Bourke, M.A. Miller, R.P. Lynch, X. Gao, J. Landon, J.S. Wainright, R.F. Savinell, D.N. Buckley, Electrode Kinetics of Vanadium Flow Batteries: Contrasting Responses of $V^{II}$-$V^{III}$ and $V^{IV}$-$V^{V}$ to Electrochemical Pretreatment of Carbon, J. Electrochem. Soc. 163 (2016) A5097–A5105. doi:10.1149/2.0131601jes.

[64] A. Di Blasi, O. Di Blasi, N. Briguglio, A.S. Aricò, D. Sebastián, M.J. Lázaro, G.

Monforte, V. Antonucci, Investigation of several graphite-based electrodes for vanadium redox flow cell, J. Power Sources. 227 (2013) 15–23. doi:10.1016/j.jpowsour.2012.10.098.

[65] C. Flox, J. Rubio-Garcia, R. Nafria, R. Zamani, M. Skoumal, T. Andreu, J. Arbiol, A. Cabot, J.R. Morante, Active nano-CuPt3 electrocatalyst supported on graphene for enhancing reactions at the cathode in all-vanadium redox flow batteries, Carbon N. Y. 50 (2012) 2372–2374. doi:10.1016/j.carbon.2012.01.060.

[66] X.W. Wu, T. Yamamura, S. Ohta, Q.X. Zhang, F.C. Lv, C.M. Liu, K. Shirasaki, I. Satoh, T. Shikama, D. Lu, S.Q. Liu, Acceleration of the redox kinetics of VO2+/VO2+ and V3+/V2+ couples on carbon paper, J. Appl. Electrochem. 41 (2011) 1183–1190. doi:10.1007/s10800-011-0343-7.

[67] T. Liu, X. Li, C. Xu, H. Zhang, Activated Carbon Fiber Paper Based Electrodes with High Electrocatalytic Activity for Vanadium Flow Batteries with Improved Power Density, ACS Appl. Mater. Interfaces. 9 (2017) 4626–4633. doi:10.1021/acsami.6b14478.

[68] W.H. Wang, X.D. Wang, Investigation of Ir-modified carbon felt as the positive electrode of an all-vanadium redox flow battery, Electrochim. Acta. 52 (2007) 6755–6762. doi:10.1016/j.electacta.2007.04.121.

[69] Y. Men, T. Sun, Carbon felts electrode treated in different weak acid solutions through electrochemical oxidation method for all vanadium redox flow battery, Int. J. Electrochem. Sci. 7 (2012) 3482–3488. http://www.scopus.com/inward/record.url?eid=2-s2.0-84862649576&partnerID=40&md5=e1a9c1884672745548bc2159c9f04c5d.

[70] W. Li, J. Liu, C. Yan, Multi-walled carbon nanotubes used as an electrode reaction catalyst for VO2+/VO2+for a vanadium redox flow battery, Carbon N. Y. 49 (2011) 3463–3470. doi:10.1016/j.carbon.2011.04.045.

[71] J. González-García, P. Bonete, E. Expósito, V. Montiel, A. Aldaz, R. Torregrosa-Maciá, Characterization of a carbon felt electrode: structural and physical properties, J. Mater. Chem. 9 (1999) 419–426. doi:10.1039/A805823G.

[72] D.S. Aaron, Q. Liu, Z. Tang, G.M. Grim, A.B. Papandrew, A. Turhan, T.A. Zawodzinski, M.M. Mench, Dramatic performance gains in vanadium redox flow batteries through modified cell architecture, J. Power Sources. 206 (2012) 450–453. doi:10.1016/j.jpowsour.2011.12.026.

[73] D. Reed, E. Thomsen, B. Li, W. Wang, Z. Nie, B. Koeppel, V. Sprenkle, Performance of a low cost interdigitated flow design on a 1 kW class all vanadium mixed acid redox flow battery, J. Power Sources. 306 (2016) 24–31. doi:10.1016/j.jpowsour.2015.11.089.

[74] S. Kumar, S. Jayanti, Effect of flow field on the performance of an all-vanadium redox flow battery, J. Power Sources. 307 (2016) 782–787. doi:10.1016/j.jpowsour.2016.01.048.

[75] M. Gattrell, J. Park, B. MacDougall, J. Apte, S. McCarthy, C.W. Wu, Study of the Mechanism of the Vanadium 4+/5+ Redox Reaction in Acidic Solutions, J. Electrochem. Soc. 151 (2004) A123. doi:10.1149/1.1630594.

[76] M. INAGAKI, CHAPTER 4 - Carbon Fibers, in: M.B.T.-N.C.-C. of S. and F. INAGAKI (Ed.), Elsevier Science, Oxford, 2000: pp. 82–123. doi:https://doi.org/10.1016/B978-008043713-2/50004-2.

[77] L.F. Castañeda, F.C. Walsh, J.L. Nava, C. Ponce de León, Graphite felt as a versatile electrode material: Properties, reaction environment, performance and applications, Electrochim. Acta. 258 (2017) 1115–1139. doi:10.1016/j.electacta.2017.11.165.

[78] G. Oriji, Y. Katayama, T. Miura, Investigation on V(IV)/V(V) species in a vanadium redox flow battery, Electrochim. Acta. 49 (2004) 3091–3095. doi:10.1016/j.electacta.2004.02.020.

[79] K.J. Kim, M.-S. Park, Y.-J. Kim, J.H. Kim, S.X. Dou, M. Skyllas-Kazacos, A technology review of electrodes and reaction mechanisms in vanadium redox flow batteries, J. Mater. Chem. A. 3 (2015) 16913–16933. doi:10.1039/C5TA02613J.

[80] B. Sun, M. Skyllas-Kazacos, Modification of graphite electrode materials for vanadium redox flow battery application—I. Thermal treatment, Electrochim. Acta. 37 (1992) 1253–1260. doi:10.1016/0013-4686(92)85064-R.

[81] X. Wu, H. Xu, P. Xu, Y. Shen, L. Lu, J. Shi, J. Fu, H. Zhao, Microwave-treated graphite felt as the positive electrode for all-vanadium redox flow battery, J. Power Sources. 263 (2014) 104–109. doi:10.1016/j.jpowsour.2014.04.035.

[82] D.M. Kabtamu, J.Y. Chen, Y.C. Chang, C.H. Wang, Water-activated graphite felt as a high-performance electrode for vanadium redox flow batteries, J. Power Sources. 341 (2017) 270–279. doi:10.1016/j.jpowsour.2016.12.004.

[83] K.J. Kim, Y.J. Kim, J.H. Kim, M.S. Park, The effects of surface modification on carbon felt electrodes for use in vanadium redox flow batteries, Mater. Chem. Phys. 131 (2011) 547–553. doi:10.1016/j.matchemphys.2011.10.022.

[84] Y.C. Chang, J.Y. Chen, D.M. Kabtamu, G.Y. Lin, N.Y. Hsu, Y.S. Chou, H.J. Wei, C.H. Wang, High efficiency of CO2-activated graphite felt as electrode for vanadium redox flow battery application, J. Power Sources. 364 (2017) 1–8. doi:10.1016/j.jpowsour.2017.07.103.

[85] B. Sun, M. Skyllas-Kazacos, Chemical modification of graphite electrode materials for vanadium redox flow battery application-part II. Acid treatments, Electrochim. Acta. 37 (1992) 2459–2465. doi:10.1016/0013-4686(92)87084-D.

[86] L. Yue, W. Li, F. Sun, L. Zhao, L. Xing, Highly hydroxylated carbon fibres as electrode materials of all-vanadium redox flow battery, Carbon N. Y. 48 (2010) 3079–3090. doi:10.1016/j.carbon.2010.04.044.

[87] C. Gao, N. Wang, S. Peng, S. Liu, Y. Lei, X. Liang, S. Zeng, H. Zi, Influence of Fenton's reagent treatment on electrochemical properties of graphite felt for all vanadium redox flow battery, Electrochim. Acta. 88 (2013) 193–202. doi:10.1016/j.electacta.2012.10.021.

[88] X. Wu, H. Xu, Y. Shen, P. Xu, L. Lu, J. Fu, H. Zhao, Treatment of graphite felt by modified Hummers method for the positive electrode of vanadium redox flow battery, Electrochim. Acta. 138 (2014) 264–269. doi:10.1016/j.electacta.2014.06.124.

[89] Z. Zhang, J. Xi, H. Zhou, X. Qiu, KOH etched graphite felt with improved wettability and activity for vanadium flow batteries, Electrochim. Acta. 218 (2016) 15–23. doi:10.1016/j.electacta.2016.09.099.

[90] J. Wang, S. Kaskel, KOH activation of carbon-based materials for energy storage, J. Mater. Chem. 22 (2012) 23710. doi:10.1039/c2jm34066f.

[91] Y. Shao, X. Wang, M. Engelhard, C. Wang, S. Dai, J. Liu, Z. Yang, Y. Lin, Nitrogen-doped mesoporous carbon for energy storage in vanadium redox flow batteries, J. Power Sources. 195 (2010) 4375–4379. doi:10.1016/j.jpowsour.2010.01.015.

[92] T. Wu, K. Huang, S. Liu, S. Zhuang, D. Fang, S. Li, D. Lu, A. Su, Hydrothermal ammoniated treatment of PAN-graphite felt for vanadium redox flow battery, J. Solid State Electrochem. 16 (2012) 579–585. doi:10.1007/s10008-011-1383-y.

[93] K.J. Kim, M.-S. Park, J.-H. Kim, U. Hwang, N.J. Lee, G. Jeong, Y.-J. Kim, Novel catalytic effects of Mn3O4 for all vanadium redox flow batteries, Chem. Commun. 48 (2012) 5455. doi:10.1039/c2cc31433a.

[94] L. Wei, T.S. Zhao, L. Zeng, X.L. Zhou, Y.K. Zeng, Copper nanoparticle-deposited graphite felt electrodes for all vanadium redox flow batteries, Appl. Energy. 180 (2016) 386–391. doi:10.1016/j.apenergy.2016.07.134.

[95] B. Li, M. Gu, Z. Nie, Y. Shao, Q. Luo, X. Wei, X. Li, J. Xiao, C. Wang, V. Sprenkle, W. Wang, Bismuth nanoparticle decorating graphite felt as a high-performance electrode for an all-vanadium redox flow battery, Nano Lett. 13 (2013) 1330–1335. doi:10.1021/nl400223v.

[96] B. Li, M. Gu, Z. Nie, X. Wei, C. Wang, V. Sprenkle, W. Wang, Nanorod niobium oxide as powerful catalysts for an all vanadium redox flow battery, Nano Lett. 14 (2014) 158–165. doi:10.1021/nl403674a.

[97] H. Zhou, Y. Shen, J. Xi, X. Qiu, L. Chen, ZrO2-Nanoparticle-Modified Graphite Felt: Bifunctional Effects on Vanadium Flow Batteries, ACS Appl. Mater. Interfaces. 8 (2016)

15369–15378. doi:10.1021/acsami.6b03761.

[98] Z. González, C. Flox, C. Blanco, M. Granda, J.R. Morante, R. Menéndez, R. Santamaría, Outstanding electrochemical performance of a graphene-modified graphite felt for vanadium redox flow battery application, J. Power Sources. 338 (2017) 155–162. doi:10.1016/j.jpowsour.2016.10.069.

[99] F. Mohammadi, P. Timbrell, S. Zhong, C. Padeste, M. Skyllas-Kazacos, Overcharge in the vanadium redox battery and changes in electrical resistivity and surface functionality of graphite-felt electrodes, J. Power Sources. 52 (1994) 61–68. doi:10.1016/0378-7753(94)01938-X.

[100] W. Zhang, J. Xi, Z. Li, H. Zhou, L. Liu, Z. Wu, X. Qiu, Electrochemical activation of graphite felt electrode for VO2+/VO2+ redox couple application, Electrochim. Acta. 89 (2013) 429–435. doi:10.1016/j.electacta.2012.11.072.

[101] X. gang LI, K. long HUANG, S. qin LIU, N. TAN, L. quan CHEN, Characteristics of graphite felt electrode electrochemically oxidized for vanadium redox battery application, Trans. Nonferrous Met. Soc. China (English Ed. 17 (2007) 195–199. doi:10.1016/S1003-6326(07)60071-5.

[102] K.J. Kim, S.W. Lee, T. Yim, J.G. Kim, J.W. Choi, J.H. Kim, M.S. Park, Y.J. Kim, A new strategy for integrating abundant oxygen functional groups into carbon felt electrode for vanadium redox flow batteries, Sci. Rep. 4 (2014) 1–6. doi:10.1038/srep06906.

[103] N.R. Council, The National Academies Summit on America's Energy Future: Summary of a Meeting, The National Academies Press, Washington, DC, 2008.

doi:10.17226/12450.

[104] G. Kear, A.A. Shah, F.C. Walsh, Development of the all-vanadium redox flow battery for energy storage: a review of technological, financial and policy aspects, Int. J. Energy Res. 36 (2011) 1105–1120. doi:10.1002/er.1863.

[105] A.Z. Weber, M.M. Mench, J.P. Meyers, P.N. Ross, J.T. Gostick, Q. Liu, Redox flow batteries: A review, J. Appl. Electrochem. 41 (2011) 1137–1164. doi:10.1007/s10800-011-0348-2.

[106] H. Zhou, H. Zhang, P. Zhao, B. Yi, A comparative study of carbon felt and activated carbon based electrodes for sodium polysulfide/bromine redox flow battery, Electrochim. Acta. 51 (2006) 6304–6312. doi:10.1016/j.electacta.2006.03.106.

[107] H. Vafiadis, M. Skyllas-Kazacos, Evaluation of membranes for the novel vanadium bromine redox flow cell, J. Memb. Sci. 279 (2006) 394–402. doi:10.1016/j.memsci.2005.12.028.

[108] D.J. Park, K.S. Jeon, C.H. Ryu, G.J. Hwang, Performance of the all-vanadium redox flow battery stack, J. Ind. Eng. Chem. 45 (2017) 387–390. doi:10.1016/j.jiec.2016.10.007.

[109] M. Skyllas-Kazacos, L. Cao, M. Kazacos, N. Kausar, A. Mousa, Vanadium Electrolyte Studies for the Vanadium Redox Battery—A Review, ChemSusChem. 9 (2016) 1521–1543. doi:10.1002/cssc.201600102.

[110] W.W. Li, Y.Q. Chu, C.A. Ma, Highly Hydroxylated Graphite Felts Used as Electrodes for a Vanadium Redox Flow Battery, Adv. Mater. Res. 936 (2014) 471–475. doi:10.4028/www.scientific.net/AMR.936.471.

[111] D.S. Kim, D.J. Chung, H.-I. Park, M.Z. Ansari, T. Song, H. Kim, Direct Nitradated Graphite Felt as an Electrode Material for the Vanadium Redox Flow Battery, Bull. Korean Chem. Soc. 39 (2018) 281–286. doi:10.1002/bkcs.11380.

[112] P. Mazúr, J. Mrlík, J. Beneš, J. Pocedič, J. Vrána, J. Dundálek, J. Kosek, Performance evaluation of thermally treated graphite felt electrodes for vanadium redox flow battery and their four-point single cell characterization, J. Power Sources. 380 (2018) 105–114. doi:10.1016/j.jpowsour.2018.01.079.

[113] Z. He, Y. Jiang, H. Zhou, G. Cheng, W. Meng, L. Wang, L. Dai, Graphite felt electrode modified by square wave potential pulse for vanadium redox flow battery, Int. J. Energy Res. 41 (2017) 439–447. doi:10.1002/er.3626.

[114] K. Parvez, Z.-S. Wu, R. Li, X. Liu, R. Graf, X. Feng, K. Müllen, Exfoliation of Graphite into Graphene in Aqueous Solutions of Inorganic Salts, J. Am. Chem. Soc. 136 (2014) 6083–6091. doi:10.1021/ja5017156.

[115] E. Agar, C.R. Dennison, K.W. Knehr, E.C. Kumbur, Identification of performance limiting electrode using asymmetric cell configuration in vanadium redox flow batteries, J. Power Sources. 225 (2013) 89–94. doi:10.1016/j.jpowsour.2012.10.016.

[116] D.K. Owens, R.C. Wendt, Estimation of the surface free energy of polymers, J. Appl. Polym. Sci. 13 (1969) 1741–1747. doi:10.1002/app.1969.070130815.

[117] B. Sun, M. Skyllas-Kazacos, Chemical modification of graphite electrode materials for vanadium redox flow battery application-part II. Acid treatments, Electrochim. Acta. 37 (1992) 2459–2465. doi:10.1016/0013-4686(92)87084-D.

[118] H.P. Boehm, Surface oxides on carbon and their analysis: A critical assessment, Carbon N. Y. 40 (2002) 145–149. doi:10.1016/S0008-6223(01)00165-8.

[119] X. Qian, X. Wang, Q. Ouyang, Y. Chen, Q. Yan, Effect of ammonium-salt solutions on the surface properties of carbon fibers in electrochemical anodic oxidation, Appl. Surf. Sci. 259 (2012) 238–244. doi:10.1016/j.apsusc.2012.07.025.

[120] I. Bureau, Wo 2016/164017, (2016).

[121] Y. Jiang, X. Feng, G. Cheng, Y. Li, C. Li, Z. He, J. Zhu, W. Meng, H. Zhou, L. Dai, L. Wang, Electrocatalytic activity of MnO2 nanosheet array-decorated carbon paper as superior negative electrode for vanadium redox flow batteries, Electrochim. Acta. 322 (2019) 134754. doi:https://doi.org/10.1016/j.electacta.2019.134754.

[122] V.G. Papadakis, Estimation of Estimation of, J. Appl. Polym. Sci. 13 (1969) 1741–1747.

[123] Z. He, Y. Jiang, W. Meng, F. Jiang, H. Zhou, Y. Li, J. Zhu, L. Wang, L. Dai, HF/H2O2treated graphite felt as the positive electrode for vanadium redox flow battery, Appl. Surf. Sci. 423 (2017) 111–118. doi:10.1016/j.apsusc.2017.06.154.

[124] K. V. Greco, A. Forner-Cuenca, A. Mularczyk, J. Eller, F.R. Brushett, Elucidating the Nuanced Effects of Thermal Pretreatment on Carbon Paper Electrodes for Vanadium Redox Flow Batteries, ACS Appl. Mater. Interfaces. 10 (2018) 44430–44442. doi:10.1021/acsami.8b15793.

[125] S.M. Taylor, A. Patru, D. Perego, E. Fabbri, T.J. Schmidt, Influence of Carbon Material Properties on Activity and Stability of the Negative Electrode in Vanadium Redox Flow Batteries: A Model Electrode Study, ACS Appl. Energy Mater. 1 (2018) 1166–1174.

doi:10.1021/acsaem.7b00273.

[126] H. Fink, J. Friedl, U. Stimming, Composition of the Electrode Determines Which Half-Cell's Rate Constant is Higher in a Vanadium Flow Battery, J. Phys. Chem. C. 120 (2016) 15893–15901. doi:10.1021/acs.jpcc.5b12098.

[127] L. Estevez, D. Reed, Z. Nie, A.M. Schwarz, M.I. Nandasiri, J.P. Kizewski, W. Wang, E. Thomsen, J. Liu, J.G. Zhang, V. Sprenkle, B. Li, Tunable Oxygen Functional Groups as Electrocatalysts on Graphite Felt Surfaces for All-Vanadium Flow Batteries, ChemSusChem. 9 (2016) 1455–1461. doi:10.1002/cssc.201600198.

[128] Z. Jiang, K. Klyukin, V. Alexandrov, First-principles study of adsorption-desorption kinetics of aqueous V2+/V3+ redox species on graphite in a vanadium redox flow battery, Phys. Chem. Chem. Phys. 19 (2017) 14897–14901. doi:10.1039/c7cp02350b.

[129] Z. Jiang, K. Klyukin, V. Alexandrov, Ab Initio Metadynamics Study of the VO2+/VO2+ Redox Reaction Mechanism at the Graphite Edge/Water Interface, ACS Appl. Mater. Interfaces. 10 (2018) 20621–20626. doi:10.1021/acsami.8b05864.

[130] M. Meskinfam Langroudi, C.S. Pomelli, R. Giglioli, C. Chiappe, M. Aysla Costa de Oliveira, B. Mecheri, S. Licoccia, A. D'Epifanio, Interaction of vanadium species with a functionalized graphite electrode: A combined theoretical and experimental study for flow battery applications, J. Power Sources. 420 (2019) 134–142. doi:10.1016/j.jpowsour.2019.02.083.

[131] A. Xu, L. Shi, L. Zeng, T.S. Zhao, First-principle investigations of nitrogen-, boron-, phosphorus-doped graphite electrodes for vanadium redox flow batteries, Electrochim.

Acta. 300 (2019) 389–395. doi:10.1016/j.electacta.2019.01.109.

[132] H. Grosse, A. Martin, Particle Physics and the Schrödinger Equation, Cambridge University Press, Cambridge, 1997. doi:DOI: 10.1017/CBO9780511524394.

[133] H.J.W. Müller-Kirsten, Introduction to Quantum Mechanics: Schrödinger Equation and Path Integral, World Scientific, 2012. https://books.google.fr/books?id=iLC9MgEACAAJ.

[134] D.A. Fleisch, A Student's Guide to the Schrödinger Equation, Cambridge University Press, 2020. https://books.google.fr/books?id=VljPDwAAQBAJ.

[135] J.M. Combes, P. Duclos, R. Seiler, The Born-Oppenheimer Approximation BT - Rigorous Atomic and Molecular Physics, in: G. Velo, A.S. Wightman (Eds.), Springer US, Boston, MA, 1981: pp. 185–213. doi:10.1007/978-1-4613-3350-0_5.

[136] D. Sholl, J.A. Steckel, Density Functional Theory: A Practical Introduction, Wiley, 2009. https://books.google.fr/books?id=Q8iNmtswLWYC.

[137] J.F. Cornwell, Chapter 1 - The Basic Framework, in: J.F.B.T.-G.T. in P. Cornwell (Ed.), Tech. Phys., Academic Press, San Diego, 1997: pp. 1–18. doi:https://doi.org/10.1016/B978-012189800-7/50001-7.

[138] K. Capelle, A bird's-eye view of density-functional theory, Brazilian J. Phys. 36 (2006) 1318–1341. doi:10.1590/s0103-97332006000700035.

[139] R.M. Martin, Electronic Structure: Basic Theory and Practical Methods, Cambridge University Press, Cambridge, 2004. doi:DOI: 10.1017/CBO9780511805769.

[140] A. Görling, Density-functional theory beyond the Hohenberg-Kohn theorem, Phys. Rev.

A. 59 (1999) 3359–3374. doi:10.1103/PhysRevA.59.3359.

[141] R.G. Parr, Density Functional Theory of Atoms and Molecules BT - Horizons of Quantum Chemistry, in: K. Fukui, B. Pullman (Eds.), Springer Netherlands, Dordrecht, 1980: pp. 5–15.

[142] P.J. Hasnip, K. Refson, M.I.J. Probert, J.R. Yates, S.J. Clark, C.J. Pickard, Density functional theory in the solid state, Philos. Trans. R. Soc. A Math. Phys. Eng. Sci. 372 (2014) 20130270. doi:10.1098/rsta.2013.0270.

[143] J.M. Martínez-Duart, R.J. Martín-Palma, F. Agulló-Rueda, Chapter 2 - Survey of Solid State Physics, in: J.M. Martínez-Duart, R.J. Martín-Palma, F.B.T.-N. for M. and O. Agulló-Rueda (Eds.), Eur. Mater. Res. Soc. Ser., Elsevier, Amsterdam, 2006: pp. 21–53. doi:https://doi.org/10.1016/B978-008044553-3/50005-9.

[144] S. Rahmanian Koshkaki, An overview of Density-Functional-Theory (DFT) for students, (2015).

[145] E.K.U. Gross, R.M. Dreizler, E.K.U. Gross, Density Functional Theory: An Approach to the Many- Body Problem, 1990. http://doi.wiley.com/10.1002/9780470447710%5Cnhttp://link.springer.com/10.1007/978-3-642-86105-5.

[146] P.E. Blöchl, Projector augmented-wave method, Phys. Rev. B. 50 (1994) 17953–17979. doi:10.1103/PhysRevB.50.17953.

[147] P.E. Blöchl, C.J. Först, J. Schimpl, Projector augmented wave method:ab initio molecular dynamics with full wave functions, Bull. Mater. Sci. 26 (2003) 33–41.

doi:10.1007/BF02712785.

[148] A. Hjorth Larsen, J. JØrgen Mortensen, J. Blomqvist, I.E. Castelli, R. Christensen, M. Dułak, J. Friis, M.N. Groves, B. Hammer, C. Hargus, E.D. Hermes, P.C. Jennings, P. Bjerre Jensen, J. Kermode, J.R. Kitchin, E. Leonhard Kolsbjerg, J. Kubal, K. Kaasbjerg, S. Lysgaard, J. Bergmann Maronsson, T. Maxson, T. Olsen, L. Pastewka, A. Peterson, C. Rostgaard, J. SchiØtz, O. Schütt, M. Strange, K.S. Thygesen, T. Vegge, L. Vilhelmsen, M. Walter, Z. Zeng, K.W. Jacobsen, The atomic simulation environment - A Python library for working with atoms, J. Phys. Condens. Matter. 29 (2017). doi:10.1088/1361-648X/aa680e.

[149] D. Wainstein, A. Kovalev, Fine determination of interatomic distances on surface using extended energy-loss fine structure (EELFS) data: Peculiarities of the technique, Surf. Interface Anal. 34 (2002) 230–233. doi:10.1002/sia.1289.

[150] W. Li, M. Zhao, X. Zhao, Y. Xia, Y. Mu, Hydrogen saturation stabilizes vacancy-induced ferromagnetic ordering in graphene, Phys. Chem. Chem. Phys. 12 (2010) 13699–13706. doi:10.1039/c003524f.

[151] S. Hariharan, M. Majumder, R. Edel, T. Grabnic, S.J. Sibener, W.L. Hase, Exploratory Direct Dynamics Simulations of 3O2 Reaction with Graphene at High Temperatures, J. Phys. Chem. C. 122 (2018) 29368–29379. doi:10.1021/acs.jpcc.8b10146.

[152] M. Králik, Adsorption, chemisorption, and catalysis, Chem. Pap. 68 (2014) 1625–1638. doi:10.2478/s11696-014-0624-9.

[153] Y. Wan, J. Wang, F. Huang, Y. Xue, N. Cai, J. Liu, W. Chen, F. Yu, Synergistic effect of

adsorption coupled with catalysis based on graphene-supported MOF hybrid aerogel for promoted removal of dyes, RSC Adv. 8 (2018) 34552–34559. doi:10.1039/C8RA05873C.

[154] A. Hassan, T. Tzedakis, Enhancement of the electrochemical activity of a commercial graphite felt for vanadium redox flow battery (VRFB), by chemical treatment with acidic solution of K2Cr2O7, J. Energy Storage. 26 (2019) 100967. doi:10.1016/j.est.2019.100967.

[155] G. Wei, W. Su, Z. Wei, X. Fan, J. Liu, C. Yan, Electrocatalytic effect of the edge planes sites at graphite electrode on the vanadium redox couples, Electrochim. Acta. 204 (2016) 263–269. doi:10.1016/j.electacta.2016.04.081.

[156] S. Yadav, J. Tam, C.V. Singh, A first principles study of hydrogen storage on lithium decorated two dimensional carbon allotropes, Int. J. Hydrogen Energy. 40 (2015) 6128–6136. doi:10.1016/j.ijhydene.2015.03.038.